WEAR BEHAVIOUR OF COMPOSITE COATINGS BY THERMAL SPRAY PROCESS FOR HIGH TEMPERATURE APPLICATIONS

Thesis Submitted

in Partial Fulfilment of the Requirements for the Degree of

DOCTOR OF PHILOSOPHY

in

Mechanical Engineering

Submitted by

Deepak Kumar
(Roll No.- 2K18/Ph.D./ME/07)

Under the Supervision of

Dr. Pushpendra Singh
(Associate Professor)
Department of Mechanical Engineering,
Delhi Technological University,
New Delhi, India

Dr. Qasim Murtaza
(Professor)
Department of Mechanical Engineering,
Delhi Technological University,
New Delhi, India

Dr. R.S. Walia
(Professor)
Department of Production and Industrial Engineering,
Punjab Engineering College,
Chandigarh, India

DEPARTMENT OF MECHANICAL ENGINEERING
DELHI TECHNOLOGICAL UNIVERSITY
(Formerly Delhi College of Engineering)
Main Bawana Road, Shahabad Daulatpur, New Delhi, Delhi 110042, India
December, 2023

CERTIFICATE

This is to certify that **Deepak Kumar (Roll no. 2K18/Ph.D./ME/07)** has carried out his research work presented within this thesis entitled **"Wear Behaviour of Composite Coatings by Thermal Spray Process for High Temperature Applications"** for the award of **Doctor of Philosophy** from Delhi Technological University, New Delhi, under our supervision. The thesis represents the results of the original research work conducted by the student himself. The thesis content is not utilized as a basis for conferring any other degrees, either to the student or to any individual affiliated with this University/Institution or any other one.

Signature	Signature	Signature
Dr. Pushpendra Singh (Associate Professor) Department of Mechanical Engineering, Delhi Technological University, New Delhi	**Prof. Qasim Murtaza** (Professor) Department of Mechanical Engineering, Delhi Technological University, New Delhi	**Dr R.S. Walia** **(**Professor) Department of Production and Industrial Engineering, Punjab Engineering College, Chandigarh

CANDIDATE'S DECLARATION

I, Deepak Kumar, Roll No. 2k18/Ph.D./ME/07, hereby declare that the thesis titled "**Wear Behaviour of Composite Coatings by Thermal Spray Process for High Temperature Applications**", which is submitted by me to the Department of Mechanical Engineering, Delhi Technological University, New Delhi in partial fulfilment of the requirement for the award of the degree of Doctor of Philosophy is original and not copied from any source without proper citation. This work has not previously formed the basis for the award of any Degree, Diploma Associateship, Fellowship or other similar title or recognition.

Place: New Delhi **Deepak Kumar**

Date: **(Roll No. 2K18/Ph.D./ME/07)**

ACKNOWLEDGEMENT

I would like to express my profound gratitude to my supervisors, Dr. Pushpendra Singh and Prof. Qasim Murtaza from the Department of Mechanical Engineering at Delhi Technological University, New Delhi, as well as Prof. R S Walia, Department of Production and Industrial Engineering at Punjab Engineering College, Chandigarh. Their invaluable guidance, unwavering inspiration, extensive suggestions, and consistent support have been instrumental throughout this research endeavour.

I am deeply grateful to Prof. S.K. Garg, Head, Department of Mechanical Engineering, Delhi Technological University, for his continued inspiration and support during this research work. I am very thankful to the SRC committee members. I want to thank Prof. Pradeep Kumar (Professor at IIT Roorkee and Ex-Vice Chancellor, DTU) and Dr. Mohit Tyagi for his invaluable moral support, constant motivation, and valuable feedback during my thesis work.

I want to thank my fellow lab mates Abdul, Sudeep, Rakesh, Ravi, Neeraj, and Yamika for helping and encouraging me throughout my research. A special thanks to my senior, Dr S K Singh, for his valuable time and critical comments from his experience that have helped me do my thesis on time. He enlightened me with a different approach to tackling the publication process when I was exhausted and stuck.

All my academic pursuits become a perceptible reality just because of my parent's Late Smt. Laxmi and Late Shri Jagdish Prasad, my elder brother Dr Manoj Kumar, and I dedicate this thesis to them. I want to express my deepest gratitude to my wife, Shrutika, for her unwavering mental and moral support during the ups and downs of my PhD journey. I also want to acknowledge my adorable son, OM, and his presence made the journey even more special and meaningful during my PhD work.

Deepak Kumar
(Roll No. 2K18/Ph.D./ME/07)

ABSTRACT

The aim of this research is to study the comparative wear behaviour of pure Al_2O_3 with varying TiO_2 content due to the high demand in the industry for high-temperature applications such as the automotive industry (piston ring and liner), petrochemicals industry (pump sleeves) and textile industry tools which require the hard bearing surface, abrasion resistance and particle corrosion at the higher temperature. In the present study, three coatings of Al_2O_3, Al_2O_3-13%(TiO_2) and Al_2O_3-40%(TiO_2) composite coatings were deposited by the thermally flame spray process. The comparative wear behaviour of the Al_2O_3-TiO_2 coatings has been studied under high temperatures of up to 400°C using a high-temperature tribometer at a constant load of 40N. Before the tribo-test, the coating morphology and elemental analysis were examined with the help of field emission scanning electron microscope (FESEM), elemental dispersion spectroscopy (EDS) and X-ray powder diffraction (XRD) techniques. The thermal behaviour and corrosion rate of the deposited coatings were examined. Before the experimentation, the mechanical properties of the coated samples, such as microhardness and surface roughness, have also been analysed and reported. The results reveal that the specific wear rate decreases with an increase in temperature for all the deposited coating except Al_2O_3 coating at 400°C. The overall friction coefficient of the coatings decreases with increasing temperature. The Al_2O_3-40%TiO_2 coating showed maximum sustainability against wear and a low coefficient of friction because of its low hardness and high adhesion properties. The examined worn surface validates the presence of brittle fracture and abrasive wear behaviour mechanism along with the oxidation wear, from room temperature to 400°C. The thermal conductivity of the deposited coating decreases with the increase in TiO_2 content. The Al_2O_3-40% TiO_2 coating has the lowest average thermal conductivity. The Al_2O_3-40% TiO_2 coating possesses a low corrosion rate (mmpy) compared to pure Al_2O_3 and Al_2O_3-13% TiO_2 coatings.

TABLE OF CONTENTS

LIST OF FIGURES

LIST OF TABLES

CHAPTER 1 INTRODUCTION

1.1 SURFACE ENGINEERING

Surface engineering is an interdisciplinary field that focuses on altering the surface properties of materials to attain specific desired properties such as improved performance, durability, and resistance to wear and corrosion. The surface of a material is the outermost layer that interacts with its environment, and its properties are crucial to the overall performance of the materials. Surface engineering techniques involve altering the surface and near-surface region of a material through various physical, chemical, and mechanical processes to improve its properties [1], [2].

Surface engineering finds diverse applications across a range of industries, including automotive, aerospace, biomedical, and energy. For instance, within the automotive sector, it plays a crucial role in enhancing the durability against wear, corrosion, and tribological stresses of crucial engine parts like pistons, bearings, and gears. In the aerospace industry, surface engineering enhances the fatigue and erosion resistance of aircraft components, such as turbine blades and structural materials [3]. In the biomedical industry, surface engineering is used to improve the biocompatibility and osseointegration of implants, such as dental implants, hip replacements, and spinal implants [4].

One of the main areas of application of surface engineering is in the field of tribology, which focuses on the investigation of friction, wear, and lubrication in surfaces that interact in relative motion. Tribological problems can lead to high friction, wear, and surface damage, resulting in increased energy consumption, reduced efficiency, and component failure[5]. Surface engineering techniques such as coating, surface texturing, and surface modification can enhance the tribological performance of components, reducing friction and wear and increasing their resistance to corrosion, fatigue, and other forms of degradation [6]. Some of the other processes involved in surface engineering [7] are shown in Figure 1.1.

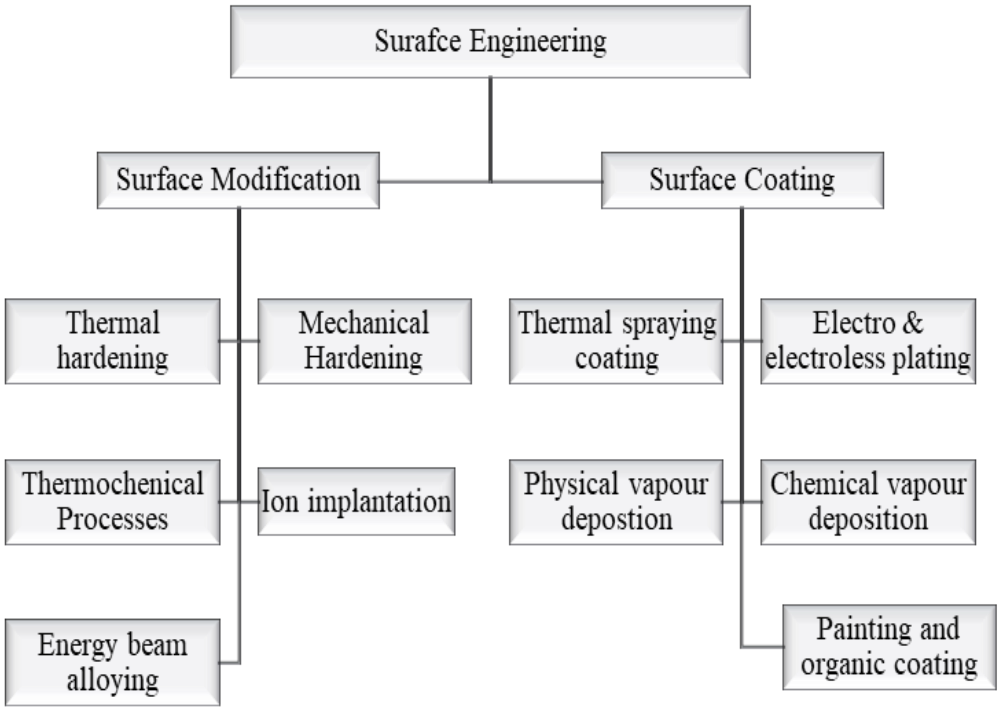

Figure 1.1 Processes of surface engineering

Coatings are one of the most common surface engineering techniques used to modify the surface properties of materials. Coatings can be applied to the surface of a material to enhance its properties, such as wear resistance, corrosion resistance, and hardness. Coatings can be deposited through various methods and are widely used for depositing thin films of materials onto the surface of a substrate. These techniques can produce coatings with excellent adhesion, uniformity, and thickness control [8].

Surface modification is another surface engineering technique that involves the modification of the surface chemistry of a material to enhance its characteristics. Surface modification can be achieved through various methods, including ion implantation, plasma treatment, and chemical modification. Ion implantation involves the bombardment of the surface of a material with high-energy ions, which can introduce new elements or modify the crystal structure of the materials. Plasma treatment involves exposing the surface of a material to a plasma form, which can change or modify the surface characteristics of the material. Chemical modification involves using chemicals to modify the surface of a material, such as by applying

functional groups or coating the surface with a thin film. Surface texturing is another surface modification technique of surface topography to improve the tribological performance of components. Surface texturing can reduce friction and wear by trapping lubricant between the contacting surfaces, reducing the contact area, and promoting hydrodynamic lubrication. Surface texturing can be achieved through various methods, including laser texturing, chemical etching, and micro-milling. Laser texturing is a popular technique that can produce precise and complex surface textures with high repeatability and accuracy [9].

Surface engineering can help to improve the efficiency, reliability, and lifespan of various mechanical and electrical systems, from automotive engines to biomedical implants. By optimizing the surface properties of materials, surface engineering can enhance the performance and durability of components, reduce energy consumption, and improve overall system performance. For example, in the locomotive industry, surface engineering can help to reduce friction and wear in engines, resulting in increased overall performance.

1.2 COATINGS

Coatings are an essential aspect of surface engineering, which is concerned with modifying the surface properties of base materials to improve their durability. Coatings involve depositing layers or layers of material onto the surface of a base material to enhance its properties. Coatings are commonly used to improve the tribological performance of components, but they also have other applications in surface engineering. One of the primary functions of coatings in surface engineering is to enhance the surface properties of materials. Coatings can modify the surface chemistry, morphology, and structure of materials to achieve desired properties such as improved adhesion, reduced friction, enhanced wear resistance, and increased hardness.

Coatings play a critical role in tribology, which is concerned with exploring the interaction between surfaces in relative motion, encompassing aspects of friction, wear, and lubrication.

Coatings are one of the most common techniques in surface engineering used to enhance the tribological performance of components, reduce friction and wear, and increase their resistance to corrosion, fatigue, and other forms of degradation. For example, in the automotive industry, coatings are applied to engine components such as pistons, bearings, and cylinders to reduce friction and improve fuel efficiency[10]. Coatings can also improve the electrical and thermal properties of materials. For example, the coating can be applied to electronic components to enhance conductivity or thermal barrier coatings to reduce heat transfer. Coatings can also provide a protective layer that enhances the corrosion resistance of materials. Corrosion can occur due to chemical reactions between the surface of the material and its environment. Coatings can provide a barrier that protects the material from the environment, preventing the occurrence of corrosion. For instance, coatings can be applied to offshore oil rigs, pipelines, and other structures exposed to harsh environments to prevent corrosion and prolong their lifespan [11].

1.3 COATING MATERIAL

Coating materials are a critical aspect of surface engineering that is used to modify the surface properties of materials to achieve desired characteristics. Coating materials are further categories into two sections, i.e., organic and inorganic. Organic coatings are composed of organic compounds, such as polymers, resins, and oils, and are commonly used for their decorative and protective properties. Inorganic coatings are composed of metallic and non-metallic materials, such as ceramics, metals, and oxides, and are typically used for their mechanical and chemical properties [12]. Coatings can be applied to a variety of materials, including different types of metals, ceramics, polymers, and composites. They can be used to improve their mechanical, chemical, electrical, and optical properties. The assortment of coating materials is based on the specific application and the desired properties. For example, coatings used in aerospace applications must withstand high temperatures, corrosion, and

wear while being lightweight and compatible with the materials they protect. Coatings used in biomedical applications must be biocompatible and able to adhere to the surface of the implant or device [13].

Ceramics are among the most popular coating materials that are used for high-temperature applications due to their excellent thermal stability, hardness, and wear resistance. Aluminium oxide (Al_2O_3) and zirconium oxide (ZrO_2) are two of the most commonly used ceramics for high-temperature applications. These materials have high melting points and can withstand extreme temperatures, making them ideal for gas turbines, aerospace engines, and other high-temperature applications due to their high-temperature stability, excellent wear resistance, and low thermal conductivity [14]–[16]. Zirconium oxide coatings are another popular choice for elevated-temperature mechanical applications due to their high melting point and excellent thermal shock resistance. These coatings are commonly used in gas turbines, where they provide protection against oxidation, corrosion, and erosion at high temperatures. Zirconium oxide coatings also have low thermal conductivity, which helps to reduce heat loss and increase efficiency [17]. Other ceramics, such as silicon carbide (SiC) and silicon nitride (Si_3N_4), are also used as coating materials in high-temperature applications due to their admirable thermal stability and are resistant to oxidation and corrosion at elevated temperatures. SiC coatings are commonly used in industrial furnaces, while Si3N4 coatings find their use in automotive engines and gas turbines [18]. Other coating materials include metals such as chromium, nickel, and titanium, which are also used due to their corrosion resistance, adhesion, and durability [19].

1.4 COATING TECHNIQUES AND THEIR CLASSIFICATION

The appropriate coating technique can significantly impact the properties and performance of a coating, making it critical to select the most appropriate method for the intended application. Coating techniques are the methods used to apply a coating material onto a substrate. These

techniques vary depending on the type of coating material, the substrate, and the intended application. Coatings can be applied using physical or chemical processes, and the choice of technique depends on the desired coating properties and the coating material's and substrate's limitations.

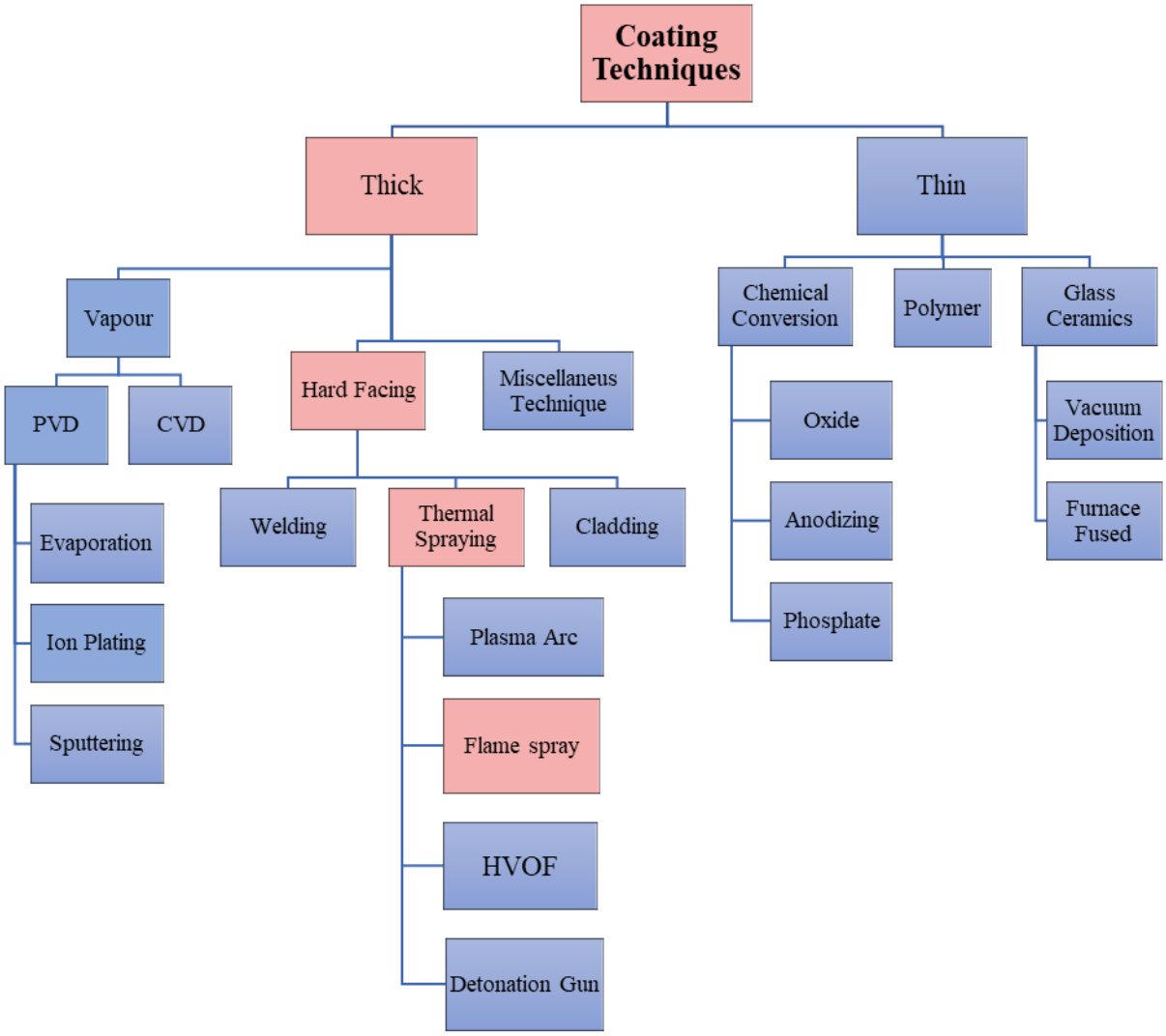

Figure 1.2 Coating Deposition Techniques

Coating techniques can be classified into two main categories: thin film deposition and thick film deposition. Thin film deposition techniques are used to apply coatings with a thickness of a few nanometres to a few micrometres. These coatings are typically used for functional purposes, such as reducing friction or enhancing corrosion resistance. Thick film deposition

techniques are used to apply coatings with a thickness of a few micrometres to several millimetres. Thick coatings are utilized to enhance various properties of materials, including wear and corrosion resistance[20]. In many industries, including automotive, aerospace, and manufacturing, thick coatings are crucial for ensuring optimal performance and longevity of components and products.

Thick coatings can be applied using various techniques, including thermal spraying, painting, and powder coating. Thermal spraying involves using a high-velocity stream of particles to deposit a coating onto a substrate. It is commonly used for functions requiring wear and corrosion resistance, such as gas turbines and aircraft engines. Figure 1.2 represents the flow chart of numerous coating techniques, wherein thermal spray coating and its types are broadly discussed [21].

1.4.1 THERMAL SPRAY COATING

Thermal spray processes involve heating a material near or slightly above its melting point and accelerating it in a gas stream toward a substrate to create a coating. As the material is heated and propelled, it breaks into droplets that hit the surface of the substrate and solidify, forming thin lamellar particles that adhere to the surface. As the material impacts the surface, it forms thin layers of solidified particles that interlock and overlap, creating a coating. This process is shown in Figure 1.3. Various other processes of thermal spray are shown in Figure 1.4. These processes offer several advantages, including:

Advantages:

- *Versatility*: Thermal spray processes can deposit various materials, including metals, ceramics, polymers, and composites, providing a wide range of coating options.
- *Customizability*: The thickness and composition of the coating can be tailored to meet specific requirements, such as wear resistance, corrosion protection, and thermal insulation.

- *Cost-effective*: Thermal spray processes can be cost-effective for high-volume production, as they can be automated and require minimal tooling.
- *Enhanced surface characteristics*: These coatings help to achieve or enhancement of surface *characteristics* such as hardness, adhesion, and lubricity, increasing durability and functionality.
- *Ability to repair*: These coatings can also be used to restore damaged or dented components, avoiding costly replacements.

However, thermal spray processes also have some limitations, including:

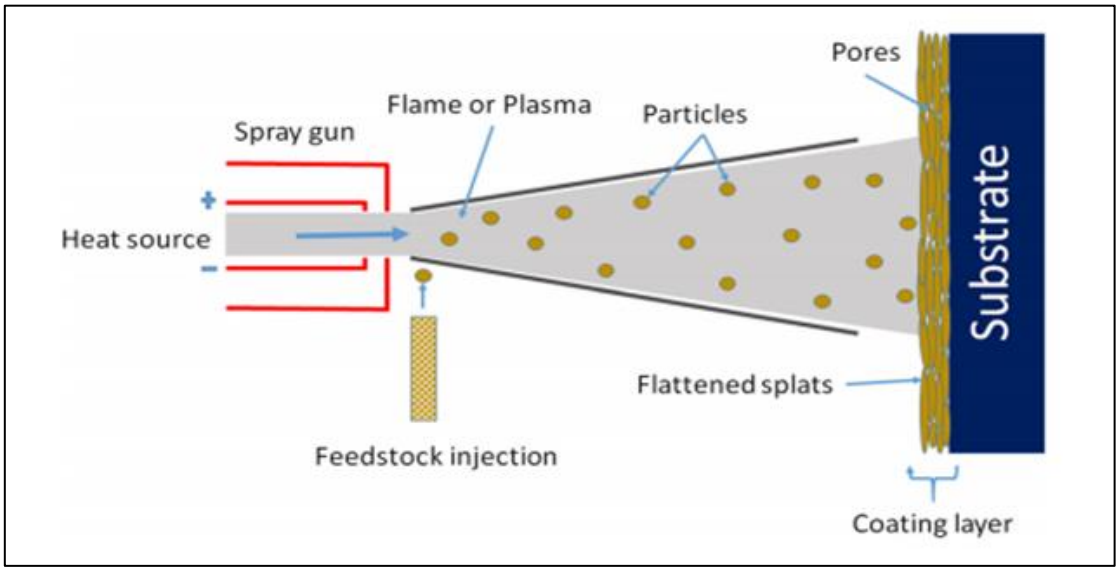

Figure 1.3 Thermal Spray Process[22]

Limitations:

- *Limited thickness*: The thickness of the coating is typically limited to a few millimetres, making it unsuitable for some applications that require thicker coatings.
- *Surface preparation*: The surface of the substrate must be prepared carefully before the coating process, which can be time-consuming and costly.
- *Post-processing*: The coating might need further post-treatments measures, such as grinding or polishing, to achieve the desired properties.

- *Environmental concerns*: The thermal spray process can generate hazardous materials and fumes, requiring proper handling and disposal.
- *Limited adhesion*: The adhesion between the coating and the substrate can be limited, which may affect the durability and performance of the coating. Spraying is a surface engineering process used to deposit coatings of various materials onto a substrate. The process involves heating the coating material in a high-temperature source and spraying it onto the substrate as fine particles, which then adhere and solidify onto the surface. This method can be used to yield coatings of different thicknesses and compositions, making it a versatile technique for various industrial applications.

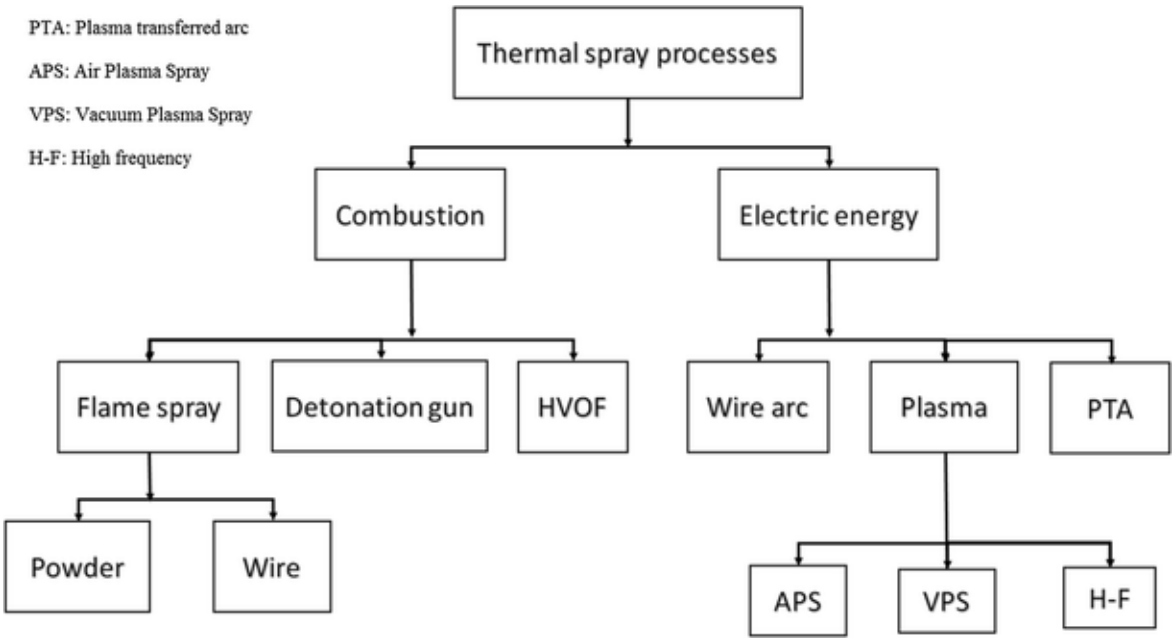

Figure 1.4 Thermal Spray Process [23]

1.4.1.1 Flame spray

The flame spray is a thermal spray process that uses fuel gas and oxygen to generate a high-temperature flame, which is used to melt and propel a powdered material onto a surface. The flame spray deposition technique involves using wire and powder as the coating material with a flame temperature range from 2500 °C to 3300 °C and a particle velocity of 40 m/s.

Combustible gases such as hydrogen, propane, natural gas, and acetylene are commonly used to produce heat and accelerate the atomization of particles during the flame spray process. In conventional flame spray guns, fuel combustion occurs externally at the nozzle's outer tip, and the fuel-air ratio is adjusted to achieve the desired flame spray temperature. This process can achieve a flame jet velocity of almost 100 m/s, particle speed of about 80 m/s, and particle temperature of approximately 2600 °C. An oxidizing or reducing flame can be achieved by adjusting the fuel-air ratio. Due to its flexibility, the flame spray procedure may be used to spray a wide variety of materials, including refractories and ceramics. Coatings produced by flame spray techniques have a highly porous and low deposition strength. The coatings' main characteristics are their lamellar structure, porosity, bond strength, surface roughness, and oxide content [24].

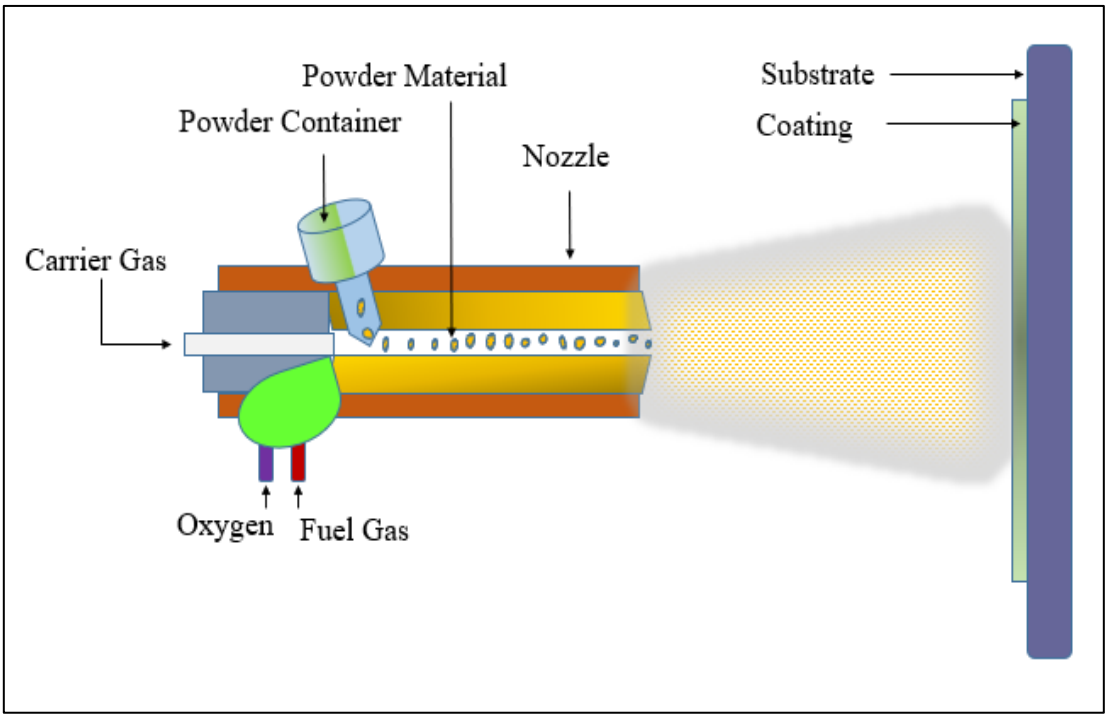

Figure 1.5 Flame spray process [25]

Optimizing parameters such as the spraying nozzle distance, gas flow rate, spraying conditions, flame temperature, and deposition time can successfully control the microstructure behaviour and syllable structure of the coatings, making the flame spray

process a cost-effective method for producing defect-free coatings. However, the flame spray process typically produces coarse structures with high porosity due to the low flame temperature and low spray velocity. Generally, different spraying parameters and coating materials achieve a lower coating density ranging from 85% to 98%. To improve the properties of the flame spray process, a spray and fuse technique is required, and fusion can be accomplished using a laser or furnace or by using a spraying torch without powder. The flame spray is shown in Figure 1.5, and it involves the following steps:

- *Preparation of the substrate*: The surface to be coated is prepared by cleaning and roughening it to confirm decent deposition adhesion.
- *Preparation of the powder*: The powder material is chosen based on the required properties of the coating and is usually a fine powder.
- *Combustion of gases*: A fuel gas, such as propane or acetylene, and oxygen are mixed and combusted in a gun, generating a high-temperature flame.
- *Melting of the powder*: The powder material is fed into the flame, which melts and is propelled towards the substrate.
- *Deposition of the coating*: The molten particles are deposited onto the substrate, rapidly solidifying and bonding to form the coating.

The flame spray process has several advantages, including:

i. Versatility: Flame spray can use different materials, including metals, ceramics, and polymers, allowing for customization of the coating properties.
ii. High deposition rates: The process can achieve high deposition rates, making it suitable for high-volume production.
iii. Cost-effective: The flame spray process is relatively simple and can be automated, making it a cost-effective method for large-scale production.

iv. Good adhesion: The high-velocity particles generated by the flame spray process can produce coatings with excellent adhesion to the substrate.

However, there are also some limitations to the flame spray process, including:

i. Limited uniformity: The particle size and velocity can affect the uniformity of the coating, leading to variations in thickness and properties.

ii. Rough surface: The surface finish of the coating may be rough, which may not be suitable for some applications.

iii. Porosity: The coatings formed by the flame spray process may have some degree of porosity, affecting their corrosion and wear resistance.

iv. Environmental concerns: The process can generate hazardous fumes and waste materials, requiring proper handling and disposal.

1.4.1.2 Detonation gun

The detonation gun process is a thermal spray process that uses a mixture of oxygen and fuel gases, such as acetylene, to propel powder particles onto a substrate. In this process, a spark ignites the mixture in a barrel, causing a high-temperature and high-pressure detonation wave to move down the barrel. The detonation wave heated the powder materials around their melting point or slightly high. It propelled them to velocities of nearly 700 m/s, with the possibility of achieving velocities of about 1000 m/s using the Super D-Gun process.

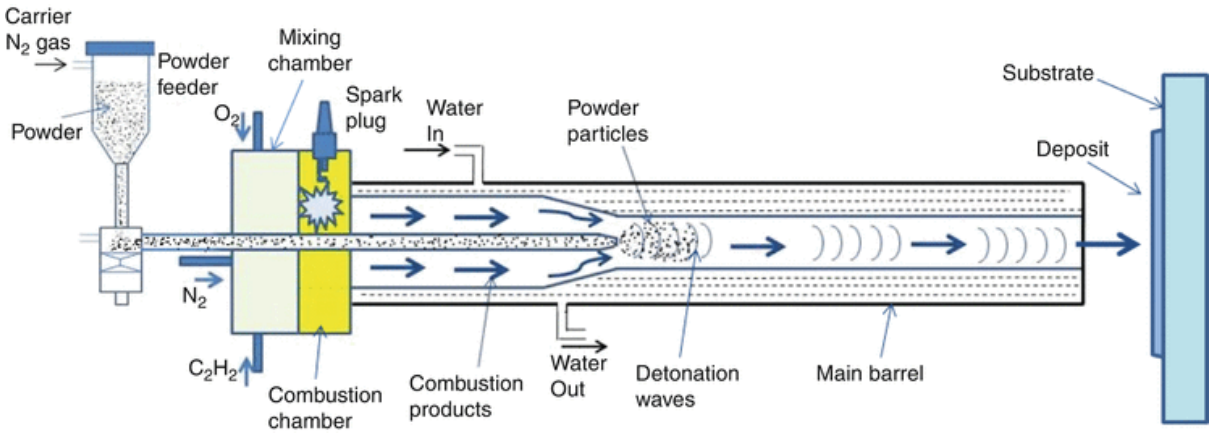

Figure 1.6 Detonation gun [26]

The detonation gun process, as shown in Figure 1.6, is a cyclic process, with the barrel being purged with nitrogen after each detonation and the process being repetitive up to around 10-12 times per second. The coating developed by detonation spray was a dense and adhesive layer having a thickness of about 2.5 cm and can be used to coat hard materials. It can produce less porous, low oxygen content, and good wear resistance coating at low load conditions. The commonly used materials for coating deposition are hard materials, copper, iron, etc. This process offers advantages such as high deposition efficiency, high coating quality, and the capability to apply numerous materials, including metals, ceramics, and composites. However, it also has limitations such as high capital investment, high operating costs, and limitations on the size and shape of the parts that can be coated.

1.4.1.3 HVOF

High-velocity oxy-fuel (HVOF) spray is a famous thermal spray coating method that can deposit a layer up to approximately 10 mm thick, with the highest deposition rate compared to other techniques. The high-velocity oxyfuel setup is shown in Figure 1.7. This technique supplies a large amount of fuel gas and air to the combustion chamber, where oxygen and the spraying fuel are ignited. The gases flow through a convergent-divergent nozzle at a speed greater than 1500m/s. The commonly used fuel gases are propylene, acetylene, LPG, hydrogen, and kerosene.

In contrast, a carrier gas such as argon, nitrogen, or helium feeds the coating powder from feedstock to the spraying nozzle. The powder particles impact the substrate with colossal force and have a spraying speed of 1000m/s at a temperature of 3300°C. The coatings produced have excellent cohesive and adhesive strength, low oxide content, and less porosity. The low particle temperature ensures less thermal stress and optimized HVOF deposition conditions can produce less than 1% porosity and more than 80MPa bond strength. HVOF can provide high bond strength, good surface finish, improved toughness, improved hardness, and higher

thickness of coatings by varying deposition parameters such as spray distance, powder feed rate, powder size, fuel rate velocity, deposition time, temperature, oxygen pressure, and jet velocity [27]. These features make HVOF a novel technique for generating sound coatings at a low cost. Following are some of the advantages of the HVOF system:

- Effective heating of sprayed particles
- Almost elimination of air mixing with sprayed particles
- High particle speeds result in low exposure time, which ultimately reduces particle oxidation
- Low particle temperature.

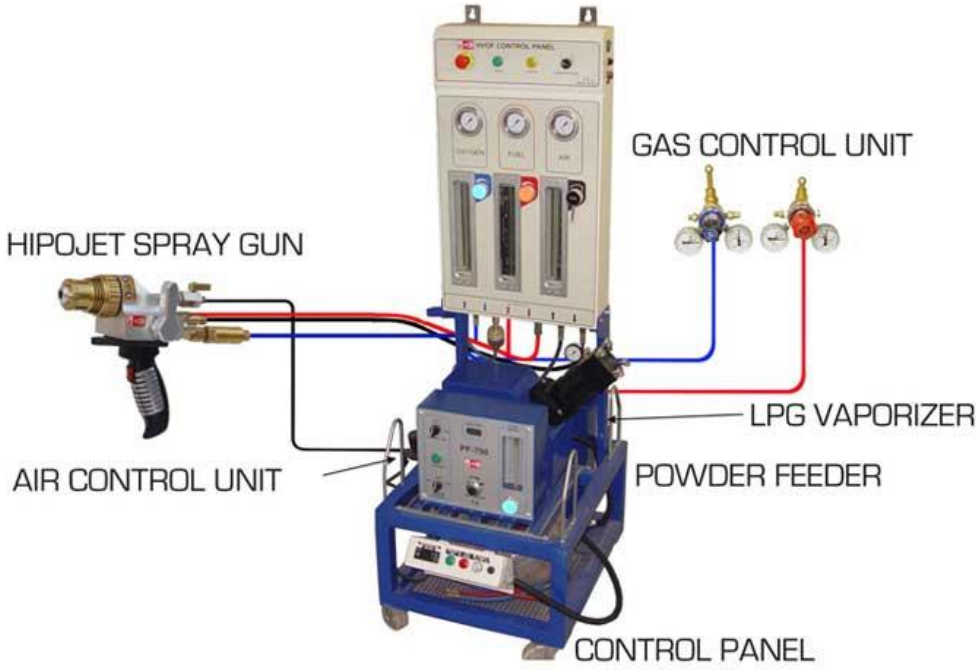

Figure 1.7 HVOF setup

1.4.1.4 Plasma Spray

A Plasma spray is a coating deposition technique that uses high DC voltage to generate plasma arcs that ionize gases such as helium, argon, and nitrogen. The resulting plasma jet temperature can reach 10,000K due to the release of significant heat from the ions combined with free electrons. A convergent-divergent nozzle obtains the desired plasma jet with supersonic velocity. Typically, tungsten-doped inert elements are used for plasma electrodes.

Powder particles are introduced axially or radially into the plasma jet, heated, and then propelled onto the substrate material with high velocity to provide the coating [28].

Plasma spray can produce coatings with high bond strength, good surface finish, improved toughness, improved hardness, and greater thickness by adjusting the deposition parameters, such as electrodes, spray distance, temperature, and so on. Optimized spraying parameters can achieve low porosity (less than 1%) compared to HVOF spray and detonation gun. Due to the high working temperature, plasma spray can deposit almost all liquid phase materials with less distortion, making it a valuable and versatile coating deposition technique. Metals, alloys, carbides, refractory oxides, and ceramics are widely used materials. According to ASTM C-633 standards, the tested bond strength of plasma spray ranges from 34 to 69 MPa. Compared to other thermal spray techniques, plasma jet spray experiences less in-flight oxidation due to the use of inert gases. However, some in-flight particles may still get oxidized and trapped in splats. To minimize the inclusion of oxide, optimization of spraying distance, particle temperature, and particle velocity is necessary. The systematic illustration of the plasma spray process is shown in Figure 1.8.

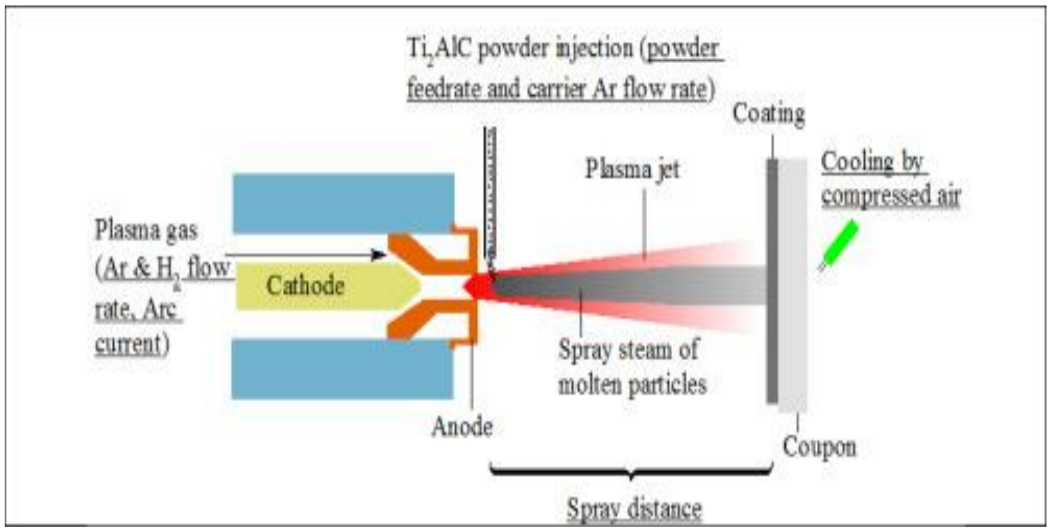

Figure 1.8 Plasma spray coating [29]

1.5 TYPES OF WEAR IN THE COATING

Wear in coatings refers to the loss or removal of material from the surface of a coated component due to the interaction with the environment or contact with another surface. Coatings are applied to surfaces to protect them from wear, but they can also experience wear. Wear can occur due to various factors such as sliding, rolling, impact, abrasion, erosion, and corrosion. The wear mechanism depends on the nature of the contact and the properties of the coating and substrate materials. Several types of wear can occur in coatings, mainly including the following:

a) Abrasive Wear

It is a type of wear mechanism that occurs due to the movement of hard particles over a surface, resulting in the gradual removal of material shown in Figure 1.9. It is one of the most common types of wear and can be found in many industrial applications, such as mining, cutting tools, and machinery components. The abrasive wear process involves the removal of material from a surface due to hard particles, such as sand, grit, or other abrasive substances.

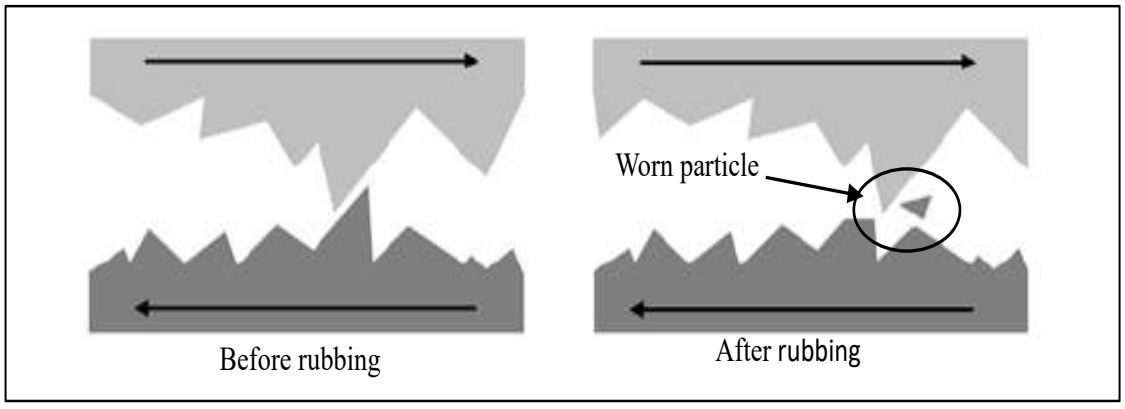

Figure 1.9 Abrasion wear [30]

The particles can be present in a fluid, such as water or oil, or as solid debris on the surface. As the particles move over the surface, they create scratches and grooves, gradually removing the surface material. The severity of abrasive wear is determined by several factors, including the size, shape, hardness, and concentration of the abrasive particles, as well as the velocity

and pressure of the particle stream. The harder and sharper the particles, the more severe the wear will likely be. The wear mechanism of abrasive is challenging to control and prevent as it doesn't describe the mechanism precisely, and all the wear mechanism co-occurs with different characteristics. The various abrasive wear mechanism involved is grain pull-out, fracture, cutting, and fatigue. Ploughing wear occurs when grooves are formed and materials are dispatched from the materials. Fragmentation occurs when the material is removed from the surface by cutting action and due to an indenting abrasive localised fracture. Material is imparted from the material's surface in the form of microchips, small debris with less or no material dislocating to the next side of the grooves.

b) Adhesive Wear

Adhesive wear is a common mechanism of wear that happens when two bodies in relative motion adhere together and then separate, causing the material to be relocated from one surface to the other. During the adhesive wear process, the contacting surfaces become welded together at the contact point. As the surfaces continue to slide against each other, the welded area is sheared off, and material is relocated from one surface to another, as shown in Figure 1.10. This can enhance the growth of small cracks, which can propagate and lead to more severe wear. Adhesive wear can be minimized by using lubrication, reducing contact pressure, or improving the surface finish of the contacting surfaces.

The adhesive wear mechanism involves initial surface contact, plastic deformation, and material transfer. During the initial surface contact, the asperities or roughness on the surface come into contact with each other. The high pressure and friction generated by the contact cause the surfaces to undergo plastic deformation. This can lead to small cracks or voids on the surface. The material from one surface is transferred to the other during the material transfer stage. The transferred material can then act as an abrasive and cause further wear on

the opposing surface. This cycle can continue and lead to further material transfer and increased wear.

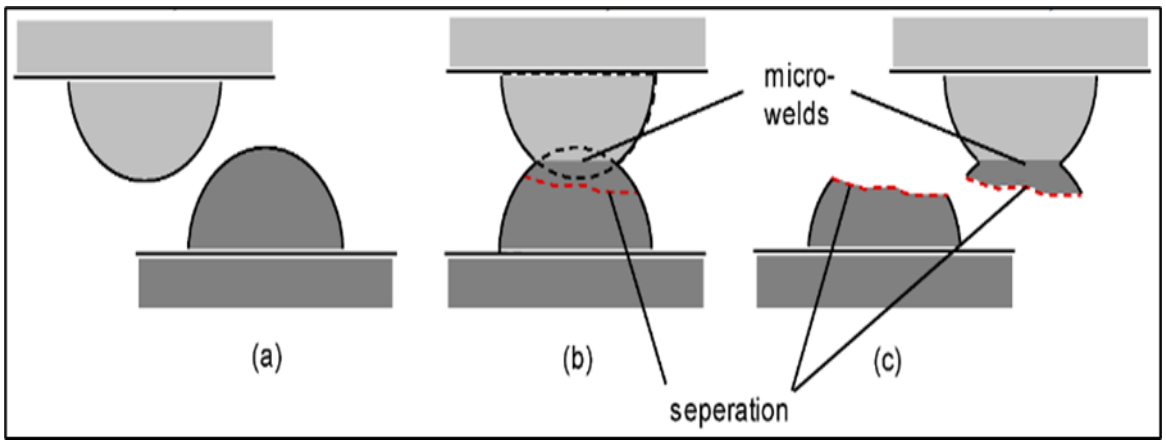

Figure 1.10 Adhesion wear (a) before contact, (b) during contact and (c) after contact [31]

c) Erosion Wear

Erosion wear is the material loss from a surface due to the impact and flow of solid particles, liquid droplets, or gas molecules. It is a complex process in various industrial, natural, and biological systems, such as pumps, valves, turbines, pipes, propellers, beaches, cliffs, and teeth.

The mechanism of erosion wear involves three main stages: initiation, propagation, and removal. In the initiation stage, the impacting particles or droplets strike the surface with a certain velocity and angle, causing local deformation, stress concentration, and material displacement. This can result in the formation of microcracks, voids, or pits, depending on the properties of the surface and the particles, as shown in Figure 1.11. The initiation stage is influenced by factors such as the particles' size, shape, hardness, velocity, concentration, surface roughness, hardness, and strength.

In the propagation stage, the microcracks or pits created in the initiation stage act as stress concentrators and can lead to the formation of larger cracks or grooves under repeated impact or flow cycles. The propagation stage is influenced by factors such as the frequency, duration,

and intensity of the impact or flow cycles and the properties of the surface and the particles. In the removal stage, the worn material is detached from the surface and transported away by the impacting particles. The removal stage is influenced by factors such as the adhesion, cohesion, and surface energy of the material, as well as the properties of the particles or fluid.

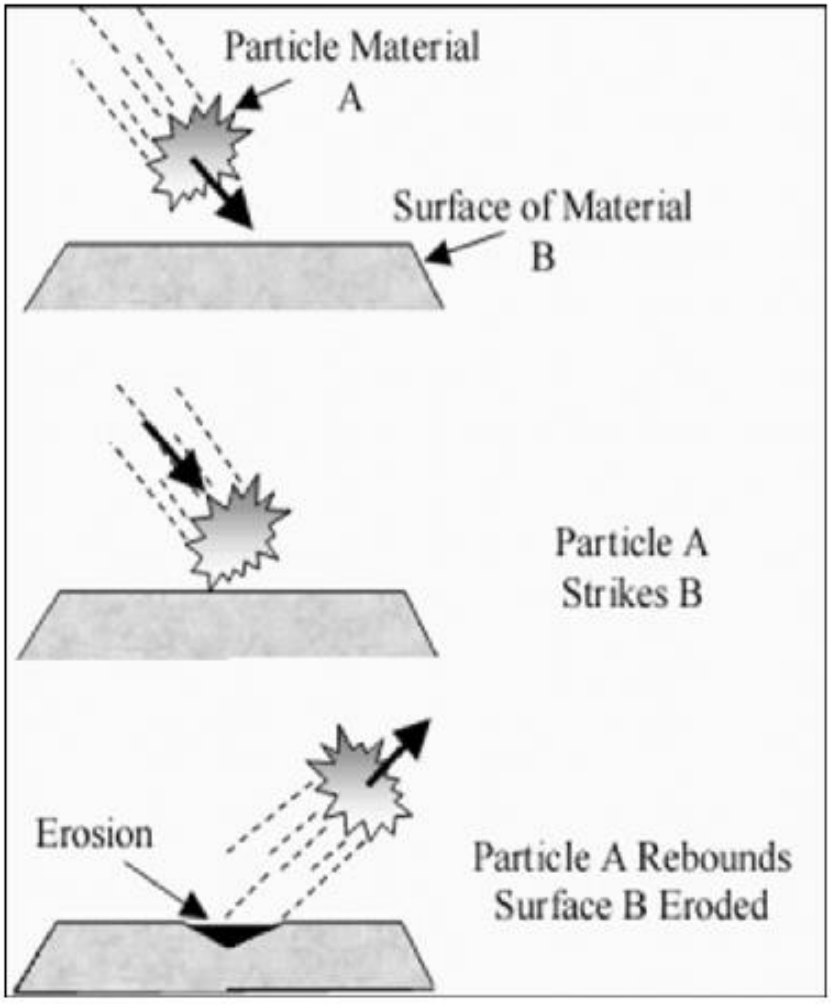

Figure 1.11 Erosion wear [32]

d) Fretting Wear

Fretting wear occurs at the interface between two surfaces in contact under small-amplitude oscillatory motion or vibration. It is a common problem in many engineering applications, such as bearings, gears, connectors, and biomedical implants.

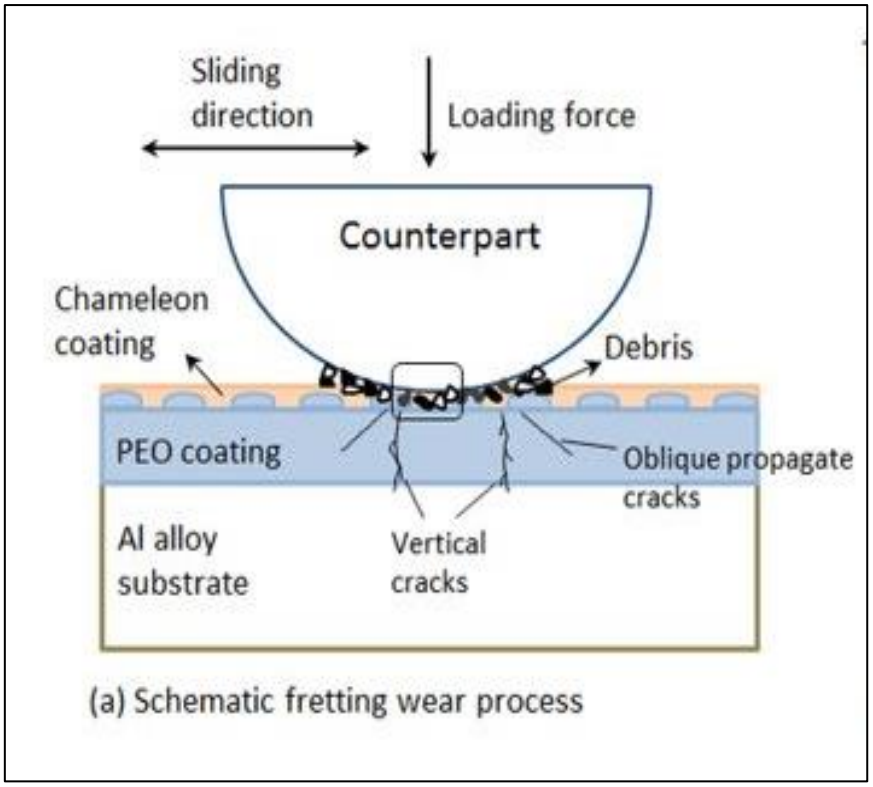

Figure 1.12 Fretting wear [33]

The mechanism of fretting wear involves three main stages: initial contact, fretting cycle, and wear debris accumulation. In the initial contact stage, the surfaces come into contact with each other and form micro-scale junctions due to the roughness and asperities of the surfaces. In the fretting cycle stage, the relative motion between the surfaces causes the micro-junctions to break and re-form cyclically, generating frictional forces, asperity deformation, and microcrack formation. This cyclic process can lead to the accumulation of wear debris, such as oxide particles and debris from the surface layers, as shown in Figure 1.12. Fretting wear is influenced by many factors, such as the amplitude and frequency of the oscillatory motion, the expected load and contact pressure, the material properties and surface roughness of the contacting surfaces, and the environment, such as temperature and humidity. The severity of fretting wear can vary from mild surface damage to catastrophic failure, depending on the application and the conditions.

e) Fatigue Wear

This type of wear occurs due to the repeated application of cyclic stresses or strains on a material, leading to progressive damage and failure over time. It is a common phenomenon in many engineering applications, such as aerospace, automotive, and structural engineering, where materials are subjected to cyclic loading or vibration.

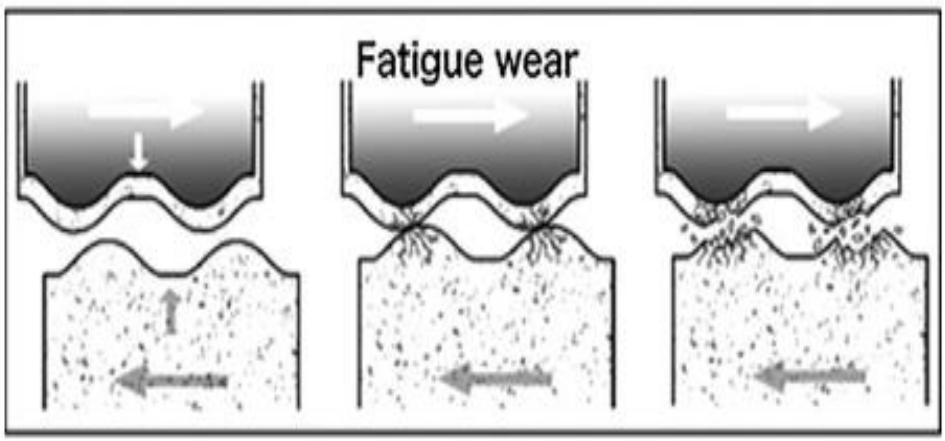

Figure 1.13 Fatigue wear [34]

The fatigue wear mechanism involves three main stages: crack initial formation, propagation, and final failure. During the crack initiation stage, small cracks or microcracks are formed at the surface of the material due to the cyclic loading. Many factors, such as stress amplitude, stress concentration, material properties, and surface condition, influence the formation of these cracks. In the crack propagation stage, the small cracks or microcracks continue to grow and link up with each other under cyclic loading, leading to the formation of larger cracks or fractures. This stage is characterized by the gradual increase in crack length and depth and the changes in surface topography and material properties. In the final failure stage, the material cannot withstand the applied cyclic loading anymore, and the crack grows rapidly until the material fractures, as shown in Figure 1.13. This stage is influenced by many factors, such as the stress concentration, crack size and orientation, and the properties of the surrounding material.

1.6 THERMAL BEHAVIOUR OF COATINGS

The thermal behaviour of the materials is the capability to conduct heat through it. It measures how efficiently a material can transfer heat under steady-state conditions and is typically expressed in watts per meter-kelvin. In essence, thermal conductivity is a critical characteristic that defines a material's thermal behaviour. In terms of coating, it is an important property that determines the ability of a coating material to transfer heat. A high thermal conductivity coating can quickly and efficiently dissipate heat, while a low thermal conductivity coating may trap heat and cause damage to the substrate or underlying material [35]. Confirming that the coating material used has an appropriate thermal conductivity for its intended application is crucial. Following are some detailed explanations based on the requirement of thermal conductivity in different scenarios:

1. **Insulation and Protection**: In certain applications, such as aerospace or high-temperature industrial equipment, the goal is to protect underlying components from excessive heat. Coatings with low thermal conductivity act as insulators and sinks the rate of heat transfer from the hot to the cooler environment. This helps maintain lower temperatures on the protected side and prevents potential damage to the substrate. Thermal barrier coatings (TBCs) used in aircraft engines are a prime example of such coatings, as they insulate turbine blades from the extreme heat generated during operation.

2. **Efficient Heat Transfer and Dissipation**: On the other hand, there are applications where efficient heat transfer and dissipation are essential. For example, in electronics and semiconductor devices, excess heat can degrade performance and reduce the lifespan of the components. Coatings with higher thermal conductivity can facilitate the rapid transfer of heat away from the sensitive electronics, ensuring better thermal management and improving the reliability of the devices. Heat sinks in computers and electronic devices often use coatings with high thermal conductivity to enhance heat dissipation.

3. **Energy Efficiency**: In building and construction applications, coatings are used to improve energy efficiency. Low thermal conductivity coatings can reduce heat transfer through walls and roofs, helping to maintain a stable indoor temperature and reducing the need for heating and cooling systems. This leads to energy savings and increased comfort within buildings.

4. **Thermal Therapies and Processing**: In medical applications, coatings used in thermal therapies or medical devices must be carefully designed to achieve specific thermal conductivity properties. For instance, coatings with tailored thermal conductivity can help deliver heat to targeted tissues in hyperthermia cancer treatment while minimizing heat transfer to healthy surrounding tissues.

5. **Solar Energy Conversion**: Coatings in solar panels are designed to capture and convert sunlight into electricity. Depending on the specific design and application, coatings with optimal thermal conductivity can help maximize the absorption of sunlight and improve the overall efficiency of energy conversion.

6. **Food Processing**: In the food industry, coatings on cooking surfaces or food processing equipment may have specific thermal conductivity properties to facilitate the cooking or processing of food items.

Ceramic coatings are used in various applications due to their unique properties, such as high-temperature resistance, wear resistance, and excellent thermal stability. The thermal conductivity of ceramic coatings is an important property that influences their performance in various applications.

1.6.1 FACTORS AFFECTING THERMAL CONDUCTIVITY

Various factors affecting the thermal conductivity of ceramic coatings are listed below [36]–[38]:

1. ***Composition of the ceramic material:*** The thermal conductivity of ceramic coatings depends on the composition and type of ceramic material used. For example, zirconia-based coatings have higher thermal conductivity than alumina-based coatings due to their crystal structure.

2. ***Thickness of the coating:*** The thickness of the ceramic coating can also influence its thermal conductivity. Thicker coatings generally have reduced thermal conductivity due to the growth in the number of boundaries that hinder heat transfer.

3. ***Temperature:*** The thermal conductivity of ceramic coatings is highly temperature-dependent. At high temperatures, this can decrease due to the surge in the phonon scattering and lattice defects.

4. ***Spray parameters:*** The thermal conductivity of thermally sprayed ceramic coatings can be influenced by spray parameters such as spray distance, spray angle, and powder feed rate. For example, increasing the spray distance can lead to increased porosity and reduced thermal conductivity.

5. ***Coating microstructure:*** The microstructure of the coating, such as its porosity and grain size, can significantly affect its thermal conductivity. Increased porosity and reduced grain size can result in decreased thermal conductivity. The presence of pores in ceramic coatings can significantly reduce their thermal conductivity as they act as barriers to heat transfer. Therefore, reducing the porosity of the coating can increase its thermal conductivity.

6. ***Composition of the ceramic material:*** Similar to non-thermally sprayed coatings, the composition of the ceramic material used in thermally sprayed coatings can also affect its thermal conductivity. For example, zirconia-based coatings have higher thermal conductivity than alumina-based coatings.

7. ***Substrate material:*** The substrate material on which the ceramic coating is applied can also affect the thermal conductivity of the coating. Substrates with high thermal conductivity, such as metals, can improve heat transfer through the coating.

1.6.2 PRINCIPAL AND MEASUREMENT TECHNIQUE

Heat transfer phenomena occur in ways of radiation, conduction and convection. In solids, thermal conduction is generally the primary heat transfer mode [39]. Thermal conductivity is the heat transfer rate through a unit area per unit of time with a one-degree Celsius temperature gradient. Heat transfer in solids occurs due to atomic collision and vibration and the availability of free electrons [40], where K_p and K_e are thermal conductivity due to metal vibrations and electrons, respectively.

$$K = K_p + K_e \quad (1)$$

➢ ***Contribution of metal vibration in thermal conductivity***

- The initial transmission of thermal energy occurs at the surface atoms of the specimen.
- The transmission process imparts vibrational energy to the surface atoms.
- Then, this energy at the surface will be transferred to the nearby adjacent atom with the speed of a wave.
- This way, the thermal energy will be diffused into the sample.
- The thermal energy will be transported to the crystal through a common vibrational or phonon mode.
- Finally, when this heat passing through the body reaches the other opposite surface of the body about which the potential gradient has been applied, the heat will acquire the mode of conduction if it needs to be transferred to the solid or will acquire the mode of Radiation or the Convection if it needed to be transferred to the Environment.

Some other parameters are there which affect the vibration and also, therefore, the thermal conductivity. Imperfections in the crystal, such as displacements or grain boundaries,

would affect the degree of vibrations, negatively affecting the thermal conductivity value. Other factors, such as hardness, crystal structure, and interatomic interactions, also affect the degree and level of vibration or phonon transfer.

- ***Contribution of electrons***

Metals are very desired materials because of their high value of thermal conductivity, especially copper (K nearly equal to 380-400 W/m-k), and they are widely used in applications where good thermal conductivity is required. In the case of metal, thermal conductivity can be considered solely due to the electron movement due to the electrical conductivity of heat. The thermal conductivity due to phonon can be considered nearly null.

1.7 CORROSION

Corrosion is a natural chemical process that occurs when metals come into contact with corrosive environments such as seawater, industrial chemicals, or atmospheric water vapour. Unfortunately, corrosion is a process that is rarely desirable and can have significant safety and economic implications. The impact of corrosion is widespread, affecting sectors such as infrastructure, manufacturing, utilities, government, and transportation. The full extent of the economic cost of corrosion is difficult to determine, as indirect costs such as lost productivity, plant downtime, or the impact of events such as power outages are often felt throughout society [41], [42].

The issue of metal and alloy corrosion has been a long-standing challenge in the industrial sector and continues to be a major problem today. The costs incurred due to corrosion are significant, often amounting to billions of dollars for developed nations. The oil and gas industry is particularly vulnerable to corrosion, as equipment and devices are constantly exposed to corrosive environments, resulting in substantial costs for this sector. Therefore,

improving the corrosion resistance of pipelines that transport crude oil and other petroleum products can significantly reduce the costs associated with inspection and maintenance [43], [44]. Therefore, it is essential to take anticipatory actions to minimise corrosion occurrence and its effects.

1.7.1 BASIC CONCEPT OF CORROSION

Corrosion can be classified into various types, including low and high temperatures and wet and dry corrosion [45]. Carbon and low-alloy steels are commonly used in various industries due to their cost-effectiveness. However, their corrosion resistance is limited in certain environmental conditions. Additionally, these steels may have diverse structures, affecting their mechanical properties and corrosion resistance in specific environments.

The corrosion mechanism incorporates an oxidation process (anode) alongside a reduction process (cathode) taking place on the corroding material's surface. The oxidation reaction produces metal ions and electrons, which are subsequently utilized within the reduction reaction. Various cathodic reactions (equation 2-4) can occur during metallic corrosion, and these are frequently encountered [46]. The most common are:

$2H^+ + 2e$ ----- H_2 [Hydrogen evolution] (2)

$O_2 + 4H^+ + 4e$ ------$2H_2O$ [Oxygen reduction (acid solution)] (3)

$O_2 + 2H_2O + 4e$ ----- OH [Oxygen reduction (neutral/basic solution)] (4)

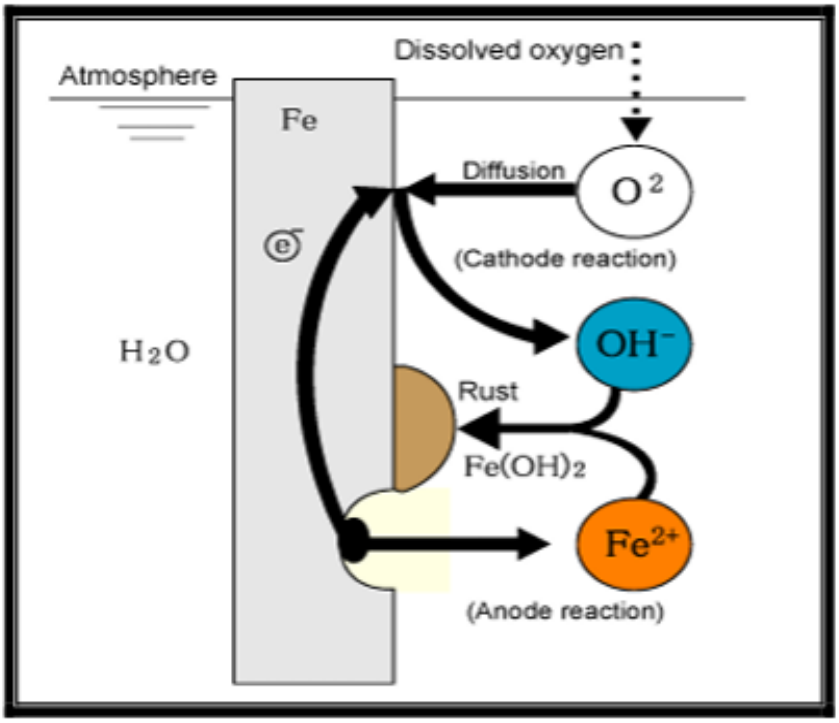

Figure 1.14 A schematic of the electrochemical mechanism of iron corrosion

In environments that contain water, which encompasses airborne moisture, electrons are utilized as they facilitate the conversion of oxygen and water into hydroxide-ions. For iron and numerous iron alloys, the resultant hydroxide-ions react with iron ions to create ferrous hydroxide. Consequent reactions lead to the formation of a mixture of magnetite (Fe_3O_4) and hematite (Fe_2O_3), commonly known as rust. This is schematically demonstrated in Figure 1.14.

1.7.2 TYPES OF CORROSION

The different types of corrosion, according to the American Society of Metals (ASM), are given below. These are the main types of corrosion as described by the ASM Handbook[47]. It's important to note that multiple factors can interact to influence the corrosion behaviour of a specific material in a given environment. Understanding the type of corrosion is crucial for implementing appropriate preventive measures, selecting suitable materials, and designing corrosion-resistant systems.

- **Uniform Corrosion:**

The uniform corrosion is the most common and recognizable type of corrosion. It occurs when a metal corrodes uniformly over its entire exposed surface. The corrosion rate is relatively constant, resulting in a gradual material loss. Uniform corrosion is typically caused by direct contact with a corrosive environment, such as moisture, acids, or salts. Factors that affect uniform corrosion include temperature, pH level, concentration of corrosive agents, and the presence of oxygen.

- **Galvanic Corrosion:**

Galvanic corrosion takes place when distinct metals or alloys possessing varying electrochemical potentials are linked electrically within an electrolyte's presence. The more active metal (with a higher potential) acts as an ‘anode’ and corrodes preferentially, while the less active metal acts as a ‘cathode’. The electrochemical potential difference between the metals drives the corrosion process. Galvanic corrosion can be accelerated when the electrolyte, such as water or an aqueous solution, facilitates the ion transfer between the anode and cathode.

- **Pitting Corrosion:**

Pitting corrosion is a type of localized corrosion distinguished by the development of minor cavities on the metal. This may occur when a minor area on the metal is subjected to a more aggressive environment or when the passive layer protecting the metal is locally damaged. Pitting corrosion can initiate due to the existence of chloride ions, crevices, or impurities on the surface. Once initiated, the pits can penetrate deeply into the metal, leading to structural failures, even if the corrosion rate is low.

- **Crevice Corrosion:**

Crevice corrosion emerges within constrained areas or gaps where stationary electrolytes are present. These include gaps, joints, seals, under deposits, and similar areas. Lack of proper oxygen circulation can create a differential concentration of chemicals, resulting in accelerated corrosion. Crevice corrosion is commonly encountered in crevices formed between two metal surfaces or between a metal and a non-metallic material. Factors that influence crevice corrosion include crevice geometry, the presence of chlorides, and environmental conditions.

- **Intergranular Corrosion:**

Intergranular corrosion is a selective attack along the grain interfaces of a metal. It occurs due to impurities, segregation of alloying elements, or heat treatments that can lead to the depletion of some aspects along the grain boundaries, making them more susceptible to corrosion. Intergranular corrosion can cause structural weakening and failure in metals, especially in stainless steels and other alloyed materials. It is often associated with sensitization, a condition in which the chromium-depleted regions near grain boundaries become susceptible to corrosion.

- **Stress Corrosion Cracking:**

This is a hazardous form of corrosion that occurs under the simultaneous influence of a corrosive environment and tensile stress. It typically manifests as cracks propagating through the material, leading to sudden failure. SCC can occur in various materials, such as metals, polymers, and ceramics. It is often associated with environments containing chlorides, caustic solutions, or high temperatures. Combining tensile stress and corrosive agents can accelerate crack initiation and propagation.

- **Erosion-Corrosion:**

Erosion-corrosion is a combined process involving both mechanical wear and corrosion. It occurs when a corrosive fluid impinges on a metal surface, causing physical erosion and chemical degradation. Erosion-corrosion is frequently observed in systems with high fluid velocities, such as pipelines, pumps, and turbines. The combined action of fluid flow and the corrosive nature of the environment can result in accelerated material loss and surface degradation.

- **Fretting Corrosion:**

Fretting corrosion categorises a corrosion type transpiring at the junction of two contacting surfaces experiencing minor relative motion due to vibration or mechanical loading. The repeated micro-motion causes the removal of the protective oxide layers, leading to localized corrosion. It is frequently noted in scenarios involving bolted joints, electrical connections, and alike applications with slight relative motion between surfaces.

- **Microbiologically Influenced Corrosion (MIC):**

This is caused or accelerated by the presence and activity of microorganisms, such as bacteria, fungi, and algae. These microorganisms can create localized electrochemical cells, produce corrosive byproducts, or induce the formation of biofilms that protect and concentrate corrosive species. MIC can occur in various environments, including aqueous systems, soil, and industrial settings.

- **High-Temperature Corrosion:**

This is referring to corrosion processes that occur at elevated temperatures, typically above 400°C (750°F). It encompasses various types of corrosion, including oxidation, sulfidation, carburization, and metal dusting. High-temperature corrosion mechanisms involve the interaction between the metal and the surrounding environment, which can consist of

gases, molten salts, or other reactive species. Factors influencing high-temperature corrosion include temperature, composition of the environment, and the presence of impurities or contaminants.

1.7.3 ELECTROCHEMICAL CORROSION MEASUREMENT METHOD

There are several electrochemical corrosion test methods commonly used to assess the corrosion behaviour and performance of materials. These methods involve measuring various electrochemical parameters and corrosion rates under controlled conditions [48]. Here are some widely used electrochemical corrosion test methods:

- **Potentiodynamic Polarization:** Potentiodynamic polarization testing involves applying a potential controlled sweep to the material while measuring the resulting current. The polarization curve obtained provides information about the corrosion potential, corrosion current density, and the breakdown potential of passivity. This test helps determine the corrosion resistance, the tendency of a material to undergo localized corrosion or pitting, and the evaluation of protective coatings.
- **Electrochemical Impedance Spectroscopy (EIS):** EIS is a powerful and versatile electrochemical technique used to measure the impedance response of a material/electrolyte interface to an applied small-amplitude AC signal over a range of frequencies. By analyzing the impedance spectra, information about the corrosion resistance, polarization resistance, capacitance, and other electrochemical parameters can be obtained. EIS is widely used for studying corrosion mechanisms, assessing coating performance, and monitoring the degradation of materials over time.
- **Galvanostatic and Potentiostatic Techniques:** Galvanostatic and potentiostatic techniques involve applying a constant current (galvanostatic) or a constant potential (potentiostatic) to the material and monitoring the resulting potential or current. These techniques are helpful for studying localized corrosion, pitting, and stress corrosion

cracking. Critical parameters such as corrosion potential, corrosion rate, and the onset of localized corrosion can be determined by analysing the current or potential transients.

- **Linear Polarization Resistance (LPR):** This type of testing involves applying a small polarization to the material and measuring the resulting current response. The polarization resistance can be calculated from the linear portion of the polarization curve, providing an estimation of the corrosion rate and corrosion resistance of the material. LPR is a simple and rapid technique used for corrosion rate monitoring, corrosion inhibitor evaluation, and material selection.
- **Salt Spray (Fog) Testing:** Salt spray testing is an augmented corrosion assessment method used to estimate the corrosion resistance of materials, particularly coatings and surface treatments. It involves subjecting the material to a highly corrosive environment, typically a saltwater mist, for a specified period. The test evaluates the material's resistance to corrosion by observing the extent and nature of corrosion, such as the formation of rust, blisters, or other visible signs of degradation.
- **Electrochemical Noise Analysis (ENA):** ENA is a non-destructive electrochemical technique that monitors the random fluctuations in the current or potential of a corroding system over time. These fluctuations contain valuable information about the corrosion process, including the initiation and propagation of corrosion events. ENA can provide insights into localized corrosion, stress corrosion cracking, and other corrosion phenomena.

These electrochemical corrosion test methods provide valuable information about the corrosion behaviour, performance, and degradation mechanisms of materials. This testing is broadly used in numerous industries, including aerospace, automotive, oil and gas, and corrosion research, to evaluate materials and coatings, assess the performance of corrosion inhibitors, and guide material selection for specific environments.

1.8 INDUSTRIAL APPLICATIONS

Several industrial sectors require materials with high-temperature wear and friction resistance, excellent thermal conductivity, and superior corrosion resistance properties to ensure optimal performance and durability in their operations. Some of the main sectors that require these properties are as follows:

- **Aerospace and Aviation:**

Gas Turbine Engines:

The aerospace industry heavily relies on gas turbine engines for aircraft propulsion. Coatings with high-temperature wear resistance, low friction, and excellent thermal conductivity are applied to turbine components to withstand extreme temperatures and stresses during flight. These coatings enhance engine efficiency and extend the service life of critical components[49].

Aircraft Structures:

Aircraft components, such as landing gear, engine mounts, and wing structures, require coatings with superior wear resistance and corrosion resistance to withstand the demanding conditions of flight, as well as exposure to harsh environmental factors. For example, landing gear components require coatings that can endure mechanical stresses during takeoffs, landings and also resist corrosion from exposure to varying weather conditions and runway de-icing agents[50].

- **Power Generation:**

Steam Turbines:

In power plants, steam turbines convert thermal energy into mechanical energy to generate electricity. Coatings with high-temperature wear resistance and friction resistance are applied

to turbine blades and rotors to minimize erosion and wear, ensuring long-term reliability and efficiency[51].

Boilers and Heat Exchangers:

Components in boilers and heat exchangers are exposed to high temperatures and corrosive environments. Coatings with excellent thermal conductivity and superior corrosion resistance protect these components, extending their lifespan and maintaining system efficiency.

- **Oil and Gas Industry**[52]**:**

Drilling and Exploration Equipment:

Drilling equipment used in oil and gas exploration faces challenging conditions, including abrasive wear and exposure to corrosive fluids. Coatings with high-temperature wear and corrosion resistance are applied to extend the life of drilling tools and enhance drilling efficiency.

Pipelines and Storage Tanks:

Oil and gas pipelines and storage tanks require coatings with excellent corrosion resistance to protect against the corrosive nature of petroleum products and natural gas.

- **Automotive Industry:**

Engine Components:

High-performance engines demand coatings with high-temperature wear resistance and low friction for critical components such as pistons, cylinder liners, and camshafts. These coatings improve engine efficiency, reduce fuel consumption, and enhance overall performance[53].

Exhaust Systems:

Coatings with high-temperature corrosion resistance are applied to exhaust systems to protect them from the corrosive effects of combustion by-products and condensation[54].

- **Metallurgical and Manufacturing Industries:**

Industrial Furnaces: Furnace linings require coatings with high-temperature wear resistance and thermal conductivity to withstand extreme conditions during metal smelting and heat treatment processes[55].

Cutting Tools:

Industrial cutting tools, such as drills and milling cutters, need coatings with high-temperature wear resistance and low friction to improve tool life and machining efficiency[56].

- **Electronics and Semiconductors:**

Semiconductor Manufacturing:

In semiconductor fabrication equipment, coatings with high-temperature wear resistance and low friction are utilised in wafer handling components and vacuum chambers to ensure precise and reliable operations[57].

- **Marine and Offshore Structures:**

Marine Equipment:

Ships, offshore platforms, and marine structures are exposed to harsh marine environments. Coatings with high-temperature wear resistance and corrosion resistance protect against seawater, salt spray, and the corrosive effects of marine environments, ensuring the structural integrity and longevity of marine equipment[58], [59].

Numerous research studies have been conducted to investigate the deposition process, properties, and performance of surface coatings. In particular, there has been a significant focus on comparing the friction and wear behaviour of hard coating materials that have been deposited through thermal spraying techniques. Various researchers have also examined the thermal conductivity and corrosion behaviour of thermally sprayed coatings. To classify the vast body of previous findings and establish a relationship between them, efforts have been made to analyse and synthesize the data as described below.

2.1 WEAR BEHAVIOUR OF THERMALLY SPRAYED CERAMIC COATINGS

The wear behaviour of thermal spray ceramic coatings has been extensively studied in the literature due to their excellent wear resistance properties. Many researchers have investigated the deposition process, microstructure, and mechanical & tribological properties of thermal spray ceramic coatings.

Singh et al. studied the influence of thermal spray parameters on the wear resistance of alumina coatings. The authors found that the coating microstructure, including porosity and grain size, had an imperative effect on the wear behaviour of the coatings. The coatings with lower porosity and smaller grain sizes exhibited higher wear resistance [60].

Habib et al. examined the porosity, phases, mechanical characteristics, and resistance to abrasive wear resistance of ceramic layers consisting of Al_2O_3/TiO_2 applied by the flame spray method. The percentage of titania strongly influences the porosity of the coatings, with higher titania content resulting in reduced porosity. The crystal phases of the deposition vary based on the powder characteristics and deposition process used. Hardness is primarily influenced

by the titania content, while toughness depends on factors such as porous structure and hardness. The resistance to abrasive wear is mainly determined by the coating's hardness [61].

Girolamo et al. explored the fabrication of alumina-based coatings for industrial applications, protecting against high temperature, wear, corrosion, and erosion. The coatings were produced by thermal spraying using pure Al_2O_3 and Al_2O_3-3 wt% TiO_2 powders. XRD analysis revealed predominant γ- Al_2O_3 and α- Al_2O_3 phases in the coatings, with the γ phase transforming to α phase after heat treatment. SEM and EDS analysis displayed TiO_2-rich splats in the microstructure micrographs. The alumina coatings revealed higher microhardness (12.8 GPa) and similar porosity compared to alumina-titania coatings. Both coatings show promise for high-temperature anti-wear applications due to their improved mechanical properties [62].

Aruna et al. examined the impact of crucial plasma spray parameters on the microstructure, microhardness, as well as wear and corrosion resistance of alumina coatings produced through plasma spraying. They found that the alumina powders, prepared through chemical precipitation without spray drying, exhibit γ- and α-forms. Varying critical plasma spray parameters (CPSP) affects crystallographic forms, microstructure, hardness, surface roughness, and wear properties. CPSP of 825 yields alumina coatings with superior wear and corrosion resistance. Coatings withstand 700 thermal cycles at lower and moderate [63].

Grewal et al. investigated Ni-Al2O3 composite coatings produced via High-Velocity Flame Spray (HVFS). Alumina content strongly influenced microstructural properties, including splat size, porosity, un-melted particles, and surface roughness. Microhardness increased with higher alumina fraction, reaching at 1158 HV with 60 wt.% alumina blending. Cracking and spallation were identified as the main mechanisms causing coating failure. [64].

Various research on Al_2O_3 sprayed by high-velocity flame spraying has demonstrated that these coatings demonstrate increased density, enhanced adhesion, and a finer microstructure

characterized by small lamellae when contrasted with traditional approaches [65]–[67]. Suspension HVOF spraying also offers the advantage of preserving the original crystal phases, which is particularly significant for Al_2O_3. During spraying, Al_2O_3 has a tendency to transmute from the initial stable α-phases to the metastable γ-phases, which possess lower corrosion resistance [68].

Wahab et al. examined for the purpose of understanding how micro-grooves influence the tribological performance of a plasma-sprayed Al_2O_3–13%TiO_2 coating. A surface profile featuring uneven depths and a micro-groove pattern was effectively generated through laser technology. The coatings showed a gradual decrease in wear rate, with slight friction coefficient reduction, due to wear debris entrapment. The composite surfaces led to wear rate reductions of up to 44.7% and 61.5% under 10 N and 20 N loads, respectively. [69].

Zuo et al. examined the ceramic coatings of Al_2O_3-13 wt% TiO_2 produced through atmospheric plasma spraying (APS) onto resin-based composites. A comprehensive investigation of the mechanical and tribological properties was conducted. The findings indicate that optimal hardness and bonding strength of the coatings are achieved at a spraying current of 650 A. The coatings maintain a consistent friction coefficient of 0.2 throughout the period of steady wear. Optimal wear resistance is noted within the spraying current range spanning from 600 A to 650 A [70].

Mehar et al. investigated and explored the impact of incorporating 20 wt. % Y_2O_3 into the Al_2O_3-13 wt.% TiO_2 coating, leading to enhanced densification, stabilization of the α alumina phase, and improved fracture toughness. The presence of Y_2O_3 also contributed to the stabilization of the α alumina phase under severe wear conditions, as confirmed by XRD and XPS analysis. The Al_2O_3-13TiO_2-20Y_2O_3 deposited coating exhibited a lesser friction coefficient and wear rate than the Al_2O_3-13 wt.% TiO_2 coating. This can be attributed to the

combined influence of the α-alumina phase and the development of the (Ti_2O_3) oxide phase of titanium. The use of friction energy maps helped to understand the different wear rates and identify diverse wear-out regimes and degradation modes of the coatings [71].

Samad et al. investigated the deposition of various alumina-based coatings containing different titania, zirconia, and chromia compositions using atmospheric plasma spraying (APS) and high-power plasma spraying (HPPS). The results showed that APS coatings exhibited coarser microstructure and higher porosity compared to HPPS coatings. Among the coatings, the Al_2O_3-40 wt.% ZrO_2 coating, deposited using agglomerated and sintered powder, demonstrated the best wear and friction behaviour [72].

Rico et al. examined to contrast the mechanical properties and high-temperature wear performance of nanostructured Al_2O_3–13%TiO_2 coatings with traditional coatings. Wear rates and friction coefficients were assessed using a Pin-on-disc apparatus, with both specimens comprising Al_2O_3–13%TiO_2. The trials were carried out across varying loads and unlubricated circumstances without the removal of wear debris. The nanostructured coatings displayed slightly higher mechanical properties and demonstrated significantly improved wear behaviour across all test conditions [73].

Nanostructured and conventional Al_2O_3-3wt.% TiO_2 coatings were evaluated against a silicon nitride ball at temperatures ranging from room temperature (25 °C) to 500 °C. The friction coefficients exhibited similarity for both coatings, spanning the range of 0.75 to 0.10. Wear rates demonstrated an increment with rising temperature in both cases. Elevated temperatures prompted brittle fractures on the worn surfaces of both coatings and the extent of damage escalated with increasing temperature. However, except at room temperature, the nanostructured coating exhibited superior wear resistance compared to the conventional

coating. The enhanced wear resistance properties of the nanostructured coating were attributed to its unique microstructural characteristics [74].

In summary, extensive research has been conducted on thermal spray ceramic coatings, focusing on their wear behaviour and properties. Factors such as microstructure, porosity, grain size, and composition significantly influence the wear resistance of these coatings. Various deposition processes have been explored, including thermal and plasma spraying. Different ceramic compositions, such as alumina, alumina-titania, and alumina-yttria, have been investigated, demonstrating improved mechanical properties and wear resistance. Thermal-sprayed coatings have shown enhanced wear resistance compared to conventional coatings, especially at high temperatures. Overall, thermal spray ceramic coatings hold promise for high-temperature anti-wear applications in various industries.

2.2 THERMAL BEHAVIOUR OF CERAMIC COATINGS

Thermal conductivity is a crucial property affecting the performance of thermal barrier coatings (TBCs). Numerous studies have examined factors influencing the thermal conductivity of TBCs.

Shen et al. examined the influence of coating thickness on the thermal conductivity of alumina coatings and alumina-coated aluminium substrates, both fabricated using the plasma spraying technique. The results revealed a slight increase in thermal conductivity from 1.8 W/mK to 2.6 W/mK as the coating thickness increased. The variation in grain size within the coating's gradient structure was identified as a potential factor contributing to this slight change. In the case of alumina-coated substrates with a constant substrate thickness, the augmentation in coating thickness exerted a more pronounced influence on the composite materials' equivalent thermal conductivity, as opposed to the effective thermal conductivity of the coatings independently. [75].

Ganvir et al. examined suspension plasma-sprayed thermal barrier coatings (TBCs) manufactured using axial injection with varied process parameters. The focus was on understanding the impact of coating microstructure on thermal properties. The findings revealed that the thermal properties of the coatings were significantly influenced by microstructural characteristics, particularly parameters like porosity, column density, and crystallite size, which played a crucial role in governing the thermal diffusivity and conductivity of the coating [76].

Wang et al. developed a finite element model to assess how pores and splat interfaces influence thermal conductivity. They incorporated spherical pores in the model and estimated pore orientation and distribution. The findings indicated that the presence of pores led to a significant decrease of up to 55% in thermal conductivity, highlighting the influence of porosity levels on the overall heat transfer properties [77].

Cernuschi et al. developed a model to analyse the thermal conductivity of deposited coatings. They examined the shape, orientation, and porosity fractions of the pores and concluded that the porosity has varying effects on the thermal conductivity of the coating [78].

Wang et al. observed that the geometrical sizes of pores have a significant impact on the thermal conductivity of depositions. Their findings revealed that narrow oblate pores, characterized by low roundness as indicated by the circularity factor, show greater thermal resistance in comparison to spheroidal pores [79].

Nicholls et al. investigated the thermal conductivity of APS-based coatings, which exhibited low values in the 0.7–1.2 W/mK range. This was attributed to the existence of unmelted particles and structural anomalies, encompassing interlayer pores and microcracks, which arise due to the layered composition of the coatings [80].

Furthermore, **Raghavan et al.** [81] observed no alteration in thermal conductivity arising from grain boundaries in YSZ generated through APS employing nanocrystalline powder. **Markocsan et al.** [82] investigated various materials with 7-8YSZ, illustrating that planar pores induced a more substantial decrease in thermal conductivity compared to spherical pores. **Huang et al.** [83] reported the impact of pore shape on thermal conductivity in APS-manufactured TBCs. **Chen et al.** [84] studied the influence of porosity, grain boundary density, and m-ZrO2 changes on the thermal conductivity of 4YSZ coatings at different temperatures.

The impact of porosity on thermal conductivity has been extensively investigated by numerous researchers through theoretical calculations and experimental studies. These studies have highlighted that total porosity has a secondary impact. The dimensions, configuration, and spatial arrangement of pores significantly influence the characteristics of a coating [85]–[87].

In summary, the thermal conductivity of thermal barrier coatings (TBCs) is influenced by various factors. Coating thickness was found to have a slight affect on thermal conductivity, with an increase observed as thickness increased. The microstructural characteristics, such as porosity, column density, and crystallite size, significantly influenced the thermal properties of the coatings. Pores and their shape, orientation, and distribution were identified as essential factors impacting thermal conductivity. The presence of pores caused a reduction in thermal conductivity, with narrow oblate pores exhibiting higher thermal resistance. APS-based coatings showed low thermal conductivity due to the presence of unmelted particles and structural defects. Grain boundaries and variations in material composition also affected thermal conductivity. Overall, the size, shape, and spatial distribution of pores were found to play a primary role in determining the thermal properties of the coatings.

2.3 CORROSION BEHAVIOUR OF CERAMIC COATINGS

Ceramic coatings possess exceptional strength and excellent stability at high temperatures, making them an ideal choice for safeguarding steel against corrosion in diverse and challenging environments [88]. The corrosion behaviour of ceramic coatings has been extensively studied in the following to understand their effectiveness in protecting metallic substrates against corrosion.

Celik et al. examined the corrosion performance of ceramic, cermet, and metallic coatings applied onto AISI 304L steel substrates within H_2SO_4 solutions through the utilization of a plasma spray method. The study found that deposited coatings exhibited higher corrosion resistance compared to Cr_2C_3+NiCr, NiAl, and NiCrAl coatings. The corrosion resistance was strongly influenced by the porosity and type of coating. The findings highlight the importance of coating selection and porosity control to optimize the performance of components in corrosive environments frequently encountered in industrial applications[89].

Ameen et al. reported that both polymeric-based and ceramic-based coatings demonstrated protection against seawater and "produced water" attacks with varying resistance levels. PVA/PANI/FLG reduced corrosion rates by 52% in seawater and up to 86% in "produced water," while TiO_2/GO reduced rates by 94% in seawater and approximately 57% in "produced water." Porosity and coating capacitance are crucial factors affecting performance, as more pores expose the greater metal surface area to corrosion. Coatings with better pore resistance outperformed those with lower coating resistance in specific environments [90].

Andrei et al. studied the electrochemical tests that revealed the porous ceramic coating obtained through Plasma Electrolytic Oxidation (PEO) does not exacerbate corrosion behaviour in a 0.5 M NaCl aqueous electrolyte. The corrosion rate values indicate that the aluminium-based thin films provide a certain level of corrosion protection. These findings

demonstrate the feasibility of obtaining Al oxide ceramic coatings on 316L steel using PEO, made suitable for use in high-temperature conditions such as boilers, furnaces, and nuclear installations as structural materials [91].

Pal et al. investigated the electro-chemical corrosion behaviour of F304 steel substrate in FeCl3 solution at temperatures ranging from 5 °C to 50 °C over 24 hours. The results indicated lower corrosion resistance and abundant chloride ion dissolution around the pit surface. Material degradation was observed quicker at the pit bottom, making it vulnerable to new pits and cracks. These findings provide practical insights into the material behaviour at different temperatures, aiding the application of F304 SS, such as in gate valve disks.

Prabhu and Rao examined the electrochemical analysis using the Tafel polarization technique. They investigated the corrosion response of the 6063-aluminium alloy when exposed to different concentrations of phosphoric acid and sodium hydroxide solutions at varying temperatures. The findings demonstrated that the 6063- aluminium alloy experiences more corrosion in the sodium hydroxide medium compared to the phosphoric acid medium. Moreover, the corrosion rate of the 6063 aluminium alloy escalated with higher acid and alkali concentrations, as well as with increasing temperature [92].

Shen et al. investigated the corrosion resistance of uniform TiO_2 coatings on steels. The findings indicate that TiO_2 particle coatings, resembling ceramic protecting films, demonstrate outstanding corrosion resistance in a 0.5 mol L^{-1} NaCl solution. Moreover, applying a TiO2 nanoparticle coating on 316L stainless steel significantly improves corrosion protection, as evidenced by the positive shift in corrosion potential, a decrease in Icorr by three orders of magnitude, and an increase in significant corrosion resistance as compared to steels in the same environment [93].

The processing and hot corrosion behaviour of composite coatings deposited by the HVOF technique with different Al_2O_3 contents (10, 20, and 30 wt. %) were investigated. The high-temperature corrosion performance of both uncoated and coated specimens was evaluated in a high-temperature furnace at 900 °C for a duration of 50 hours. The results showed that the coating containing 30 wt.% Al_2O_3 revealed the highest hardness and demonstrated the best hot corrosion resistance among the tested compositions. The inclusion of Al_2O_3 and the formation of various protective oxides contributed to the improved corrosion resistance of the coatings compared to the uncoated grey cast iron substrate[94].

Wei et al. compared WC-CoCr and Al_2O_3-TiO_2 coatings deposited through HVOF and APS methods, respectively. Both coatings were tested for long-term corrosion resistance in a simulated seawater environment containing 3.5 wt% NaCl. The results showed that the Al_2O_3-TiO_2 coating exhibited more stable and superior corrosion resistance throughout the entire immersion process compared to the other coating [95].

Ceramic coatings have shown exceptional strength and stability at high temperatures, making them a preferred choice for corrosion protection in challenging environments. Various studies have investigated the corrosion behaviour of ceramic coatings, cermet coatings, and metallic coatings, revealing that certain compositions, such as Al_2O_3, Al_2O_3-TiO_2, ZrO_2+NiAl, and $MgZrO_3$+NiAl, offer higher corrosion resistance compared to others. Moreover, the inclusion of nano-Al_2O_3 and the formation of protective oxides play crucial roles in improving the corrosion resistance of coatings. In specific applications, polymeric-based and ceramic-based coatings have demonstrated varying levels of protection against corrosion, with pore resistance being a significant factor affecting performance. Additionally, some studies have explored the use of ceramic coatings for corrosion protection in aggressive environments, and positive results have been observed, indicating the potential for practical applications in various industries.

2.4 RESEARCH GAPS

Several significant research gaps have been identified after analysing the information presented in the literature review.

1. There are very few works of literature available for high-temperature application composite coatings deposited by the thermal spray process. The bonding mechanism of coating with the substrate is also lacking.
2. Coating characterization needs to be addressed. Coating thickness also needs to be analysed in detail with the substrate (FESEM and EDS of cross-section).
3. Friction and wear behaviour of a blend of materials such as metal and ceramics-based coating is not compared in different test environments.
4. The wear mechanism needs to be discussed in detail. There are very few papers that plot the wear map of the coating (commutative effect of all wear test parameters in pictorial form).
5. The study of the heat transfer phenomenon across the exposed surface is also missing. The measurement methods also need to be discussed in detail.
6. The comparison of the corrosion resistance of the coating with the substrate is still not accounted for in the recent literature.

2.5 RESEARCH OBJECTIVES

1. To synthesise composite coating such as Al_2O_3, Al_2O_3-13%(TiO_2) and Al_2O_3-40%(TiO_2) through a thermal spray process for high-temperature applications.
2. To characterize the developed coatings and rigid mechanical properties such as microhardness with the help of Scanning electron microscope (SEM), X-ray diffraction (XRD), Energy dispersive spectroscopy (EDS) and Vickers indentation micro-hardness.
3. To analyse the friction and wear behaviour of the coating in various conditions with the help of a pin-on-disk tribometer.

4. To study the wear mechanism with the help of FESEM.
5. To study the effect of selected coating on the heat transfer phenomenon across the exposed surface.
6. To study the corrosion behaviour of developed coating.

CHAPTER 3 MATERIALS AND METHODS

3.1 SUBSTRATE MATERIAL

Austenitic stainless steel of grade 304 is used for high temperature applications. It is extensively used for various high-temperature applications such as heat exchangers, boilers, and feedwater heaters, as well as aircraft and aerospace applications. Therefore, this steel was preferred as the substrate material in the present article. The chemical composition of the substrate is provided in Table 3.1. The circular plate diameter of 100 mm and thickness of 3 mm were taken from the selected substrate material.

Table 3.1 Nominal chemical composition of steel substrate grade 304 (wt %)

Grade	Cr	Ni	Mn	N max.	S max.	C max.	Si max.	P max.	Fe
304	18-20	8-10	2	.10	.03	.08	.75	.045	Balanced

3.2 COATING DEPOSITION

Commercially available Al_2O_3, Al_2O_3 -13% (TiO_2) and Al_2O_3 -40%(TiO_2) ceramic powders were used for comparison of wear behaviour at high temperatures in this article. The composition details of the composite powders are given in Table 3.2. The morphological study of powders was analyzed using a field emission scanning electron microscope (FESEM, Carl Zeiss, from Indian Instrumentation Centre in Indian Institute of Technology, Roorkee, India). The electron dispersion spectroscopy (EDS) analysis was studied to authenticate the presence of the desired element in the composite powders. The FESEM micrographs and EDS analysis of powders are shown in Figure 3.1. These ceramic powders were deposited on the given base material samples with the help of the flame spray process. The details of the coating parameters used for the deposition of the composite powders are given in Table 3.3, and the actual and schematic diagram of the thermally flame spray process is shown in Figure 3.2.

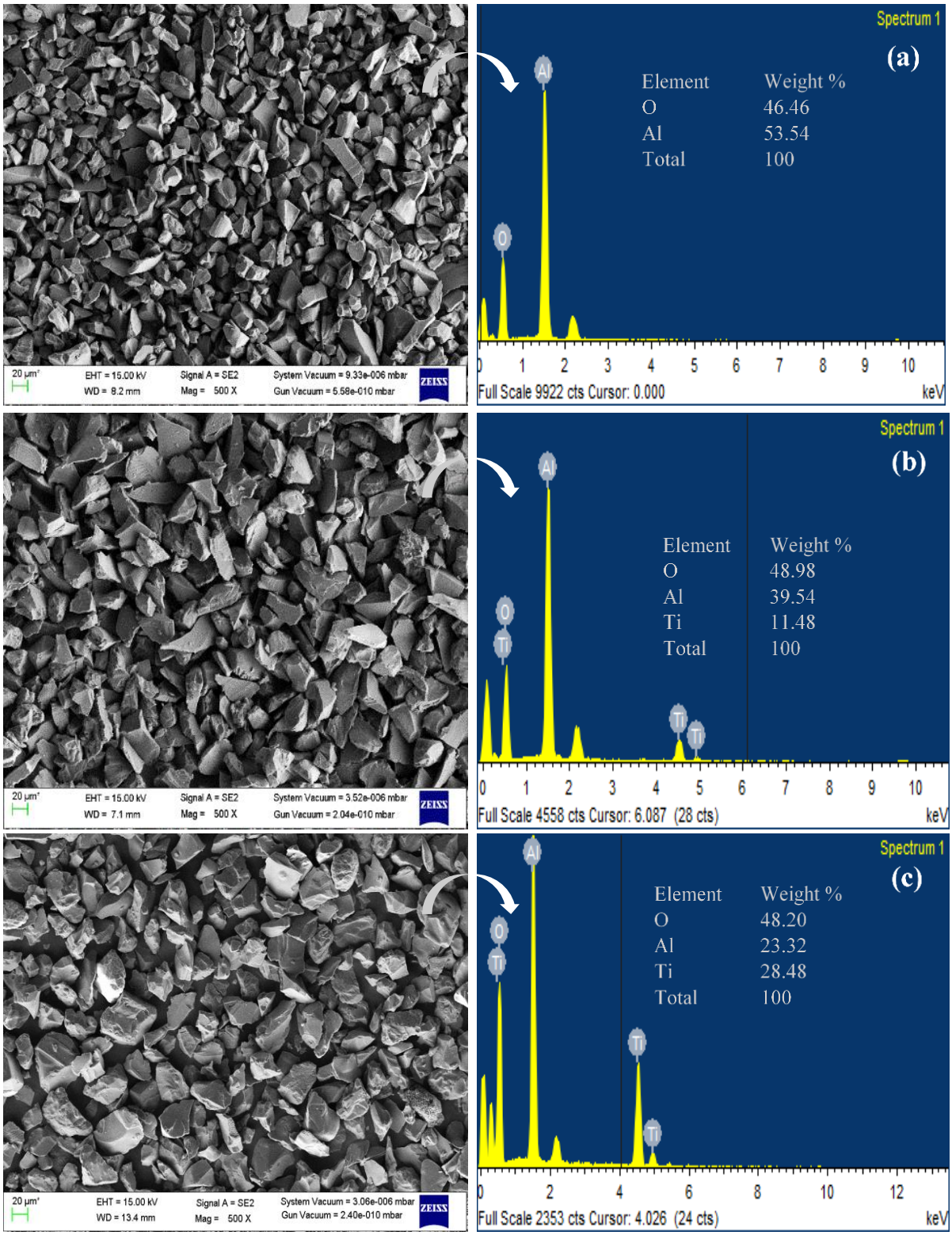

Figure 3.1 FESEM and EDS analysis of powders (a) Al_2O_3 (b) Al_2O_3 -13% (TiO_2) and (c) Al_2O_3 -40%(TiO_2)

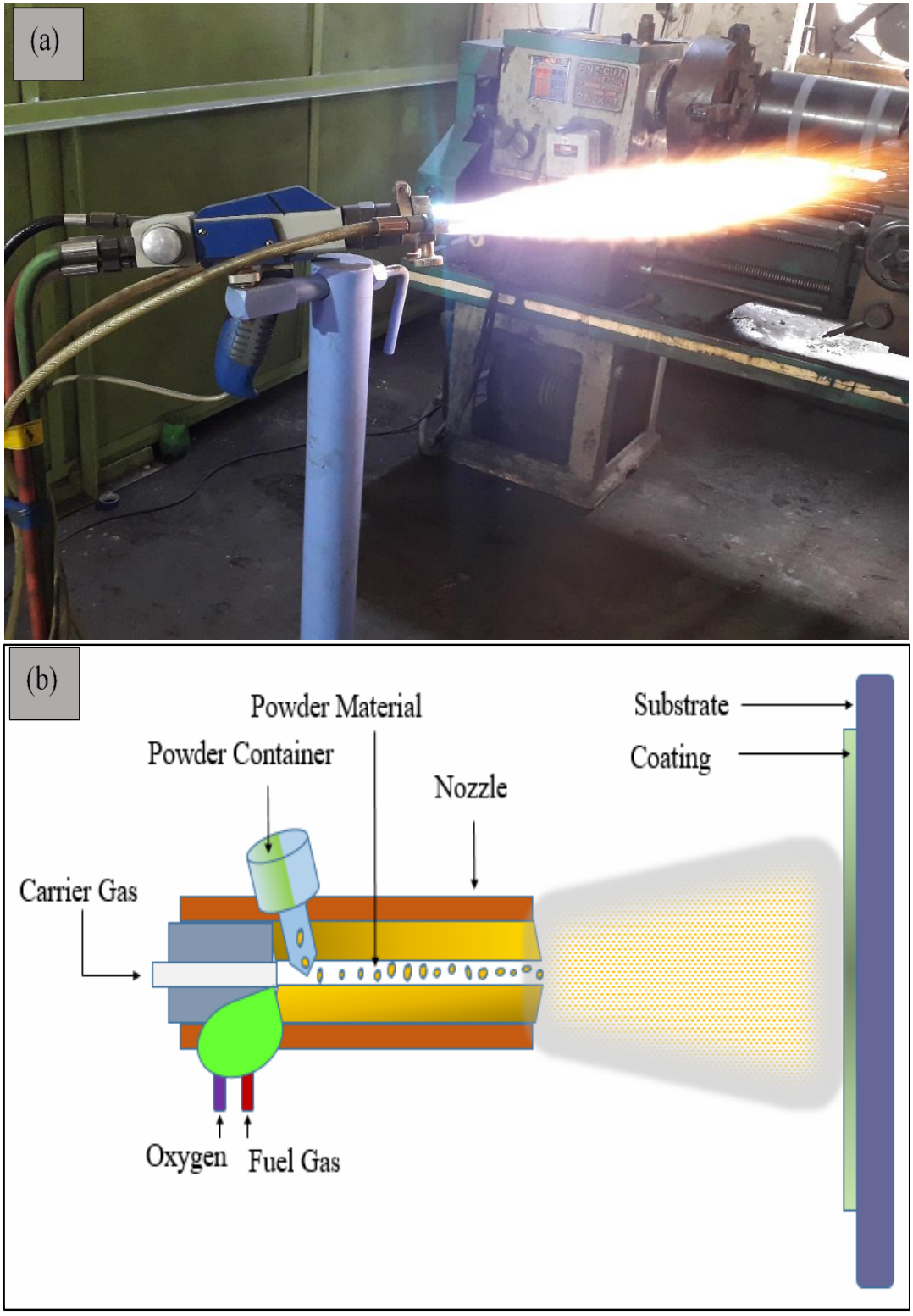

Figure 3.2 Thermally flame spray equipment: (a) actual image of the equipment (b) schematic diagram of equipment

Table 3.2 Composition details of composite powders

Composite Powders	Company	Morphology	Manufacturing Method	Particle Size (µm)
Al_2O_3	H.C. Strack	Irregular	Fused and irregular	-45+10
Al_2O_3-13%TiO_2	H.C. Strack	Mixed Ellipsoid/ elongated	Fused and irregular	-45+10
Al_2O_3-40%TiO_2	H.C. Strack	Angular	Fused and irregular	-45+10

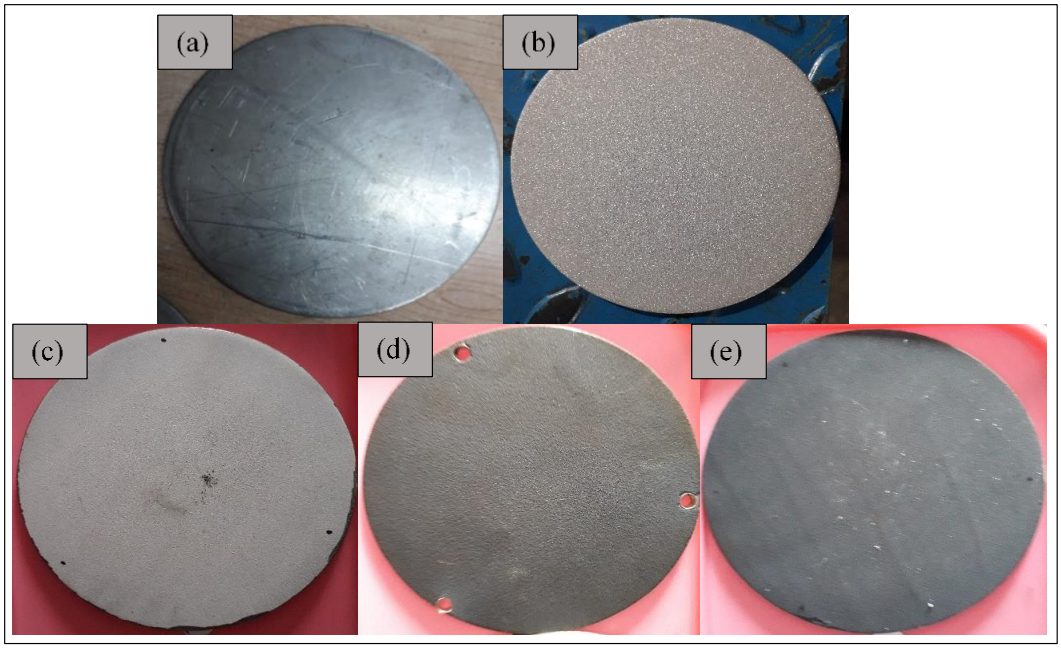

Figure 3.3 Images of the substrate (a) uncoated (b) after alumina grit blasted (c) Al_2O_3 coating (d) Al_2O_3 -13% coating and (e) Al_2O_3 -40% coating substrate

The substrate, before coating deposition, has been prepared for better adhesion of the materials. The base material was grit blasted on the exposed surface. Grit blasting is a process in which alumina particles are propelled by compressed air to the substrate. Alumina grit was used for grit blasting to increase the surface roughness and desired coating adhesion. The optical images of the unprepared substrate, after grit blasted substrate and coated samples, are shown in Figure 3.3.

Table 3.3 Coating parameter used for flame spray deposition

Oxygen flow rate	Acetylene Flow rate	Spraying distance	Nitrogen carrier flow rate	Oxygen Pressure	Acetylene Pressure	Nitrogen carrier pressure
45 NLPM	26 NLPM	75 mm	7 NPLM	2.4 bar	2.1 bar	4 bar

*NLPM- Normal litre per minute

3.3 CHARACTERIZATION AND ANALYSIS INSTRUMENTS

3.3.1 FESEM

Field Emission Scanning Electron Microscopy (FESEM) is a powerful imaging technique used to study the surface morphology of materials at very high resolution. This technique operates on the principles of electron microscopy, in which a beam of electrons is focused onto a sample surface to produce an image. However, FESEM uses a different electron source, enabling it to achieve much higher resolution than traditional scanning electron microscopes. FESEM is capable of producing images with resolutions as low as a few nanometres, allowing for the detailed examination of material surfaces at the atomic scale. It is particularly useful for studying the topography, composition, and structure of a wide range of materials, including metals, ceramics, polymers, and biological specimens.

The high-resolution images produced by FESEM can provide valuable insights into the properties and behaviour of materials, making it an essential tool for research and development in fields such as materials science, nanotechnology, and biotechnology. In addition to imaging, FESEM can also be used for elemental analysis, known as energy dispersive X-ray spectroscopy (EDS), allowing researchers to determine the chemical composition of materials at the nanoscale. Overall, FESEM is a powerful technique that has revolutionized the way scientists study materials. Its ability to produce high-resolution images and provide detailed information about the properties of materials has made it an indispensable tool in the fields of materials science, nanotechnology, and biotechnology. In

the present study, the morphological study of the powder, coated sample, and its cross-sectional area were analysed by FESEM before and after the friction and wear test. The FESEM, as shown in Figure 3.4, was available in the Indian Instrumentation Centre at the Indian Institute of Technology, Roorkee, India (Model- Carl Zeiss).

Figure 3.4 FESEM setup

3.3.2 XRD

XRD, or X-ray diffraction, is a powerful analytical technique used to study the crystal structure of materials. It works by exposing a sample to a beam of X-rays, which interact with the atoms in the sample and produce a diffraction pattern that can be analyzed to determine the sample's crystal structure.

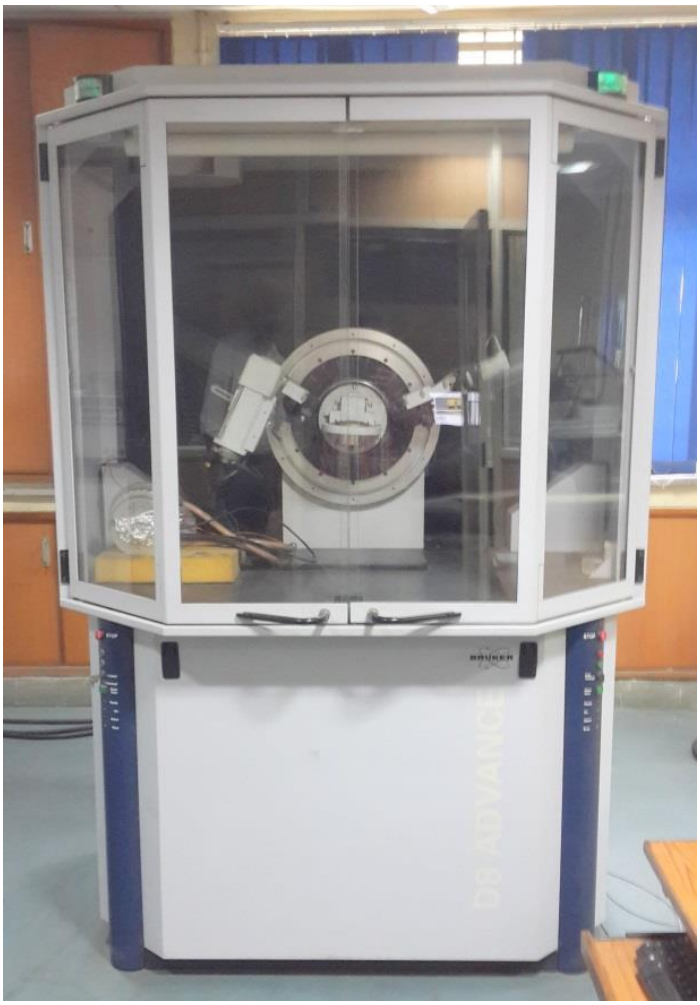

Figure 3.5 XRD Machine

XRD is widely used in a variety of scientific and industrial applications, including materials science, geology, chemistry, and biology. It can identify the composition and structure of a wide range of materials, including minerals, metals, ceramics, and polymers. One of the critical advantages of XRD is its ability to provide non-destructive analysis of materials, allowing scientists and researchers to study samples without altering their structure or

properties. XRD can also provide information on the size, shape, and orientation of crystals in a sample, which can be important for understanding the properties and behaviour of materials.

In addition to its analytical capabilities, XRD is relatively simple and straightforward, with many modern instruments offering automated data collection and analysis. This has made XRD a valuable tool for a wide range of scientific and industrial applications, from studying the structure of new materials to controlling the quality of industrial products. As shown in Figure 3.5, the XRD equipment used in this study is available at the Department of Physics, Delhi Technological University, New Delhi, India (model- Bruker D-8 Advance).

3.3.3 Vickers indentation micro-hardness setup

Vickers indentation micro-hardness is a method used to measure the hardness of a material. This method involves making an indentation on the surface of a sample using a Vickers indenter, which is a diamond pyramid with a square base. The indentation is then measured to determine its size, and the load used to make the indentation is recorded. Vickers micro-hardness testing is a popular technique used in materials science and engineering, as it can provide information on the mechanical properties of a wide range of materials, including metals, ceramics, polymers, and composites. The technique is particularly useful for studying the hardness of thin films and coatings, as well as for characterizing the mechanical properties of small or complex structures.

One of the main advantages of Vickers micro-hardness testing is its ability to provide accurate and precise measurements of hardness with high resolution and sensitivity. The Vickers indenter can produce indentations with a range of sizes, from a few microns up to several hundred microns, allowing for hardness measurements over a wide range of scales. Another advantage of Vickers micro-hardness testing is its non-destructive nature. Since the

indentation made by the Vickers indenter is very small, it typically does not cause damage to the material being tested. This makes Vickers micro-hardness testing a valuable tool for studying the properties of delicate or sensitive materials.

Figure 3.6 Vickers indentation micro-hardness tester setup

Overall, Vickers indentation micro-hardness testing is a powerful and widely used technique for studying the hardness and mechanical properties of materials, with applications ranging from fundamental research to industrial quality control. The Vickers indentation micro-hardness, as shown in Figure 3.6 (*model- DURAMIN-40 M1*) testing, was done in the Metal

Forming Lab, Department of Mechanical Engineering, Delhi Technological University, New Delhi, India.

3.3.4 Wear and friction setup

A high-temperature tribometer is an advanced testing instrument used to study the friction and wear properties of materials under high temperature and pressure conditions. This type of tribometer is specifically designed to simulate extreme operating conditions, such as those experienced in engines, turbines, and other high-temperature applications.

High-temperature tribometers typically consist of a testing apparatus that includes a heating element and a test specimen holder, as well as a load cell and a displacement sensor for measuring the frictional forces and wear of the test specimen. The test specimen is usually a small disc or cylinder made of the material being studied, which is placed in contact with a counter-surface, such as a ceramic or metal disk.

High-temperature tribometers are used in a wide range of industries, including aerospace, automotive, and energy production. They are beneficial for studying the tribological properties of high-performance materials, such as ceramics, composites, and alloys, under extreme temperature and pressure conditions. One of the critical advantages of high-temperature tribometers is their ability to provide accurate and reliable data on the wear and friction properties of materials at elevated temperatures. This information is critical for designing and optimizing components and systems for high-temperature applications and improving the performance and durability of materials and coatings.

In the present study, the friction and wear experimentations were carried out at a constant sliding velocity of 1 m/s and load 40N on a Ducom high-temperature tribometer (Delhi Technological University, New Delhi, India) according to ASTMG99 standard as shown in Figure 3.7. The high-temperature tribometer was manufactured by DUCOM Instruments Bangalore, India. The data acquisition system is connected through WINDUCOM 2010

software. Data acquisition consists of sensors for measuring frictional force, wear, temperature and speed, which are part of the testing unit. The disc speed has a proximity sensor with a range of 300-3000 rpm with the least count of 1 rpm. The frictional force has load cell-type sensors that have a range of 0 to 200 N with the least count of 0.1 N. The wear sensor has a range of 0-2000 microns with a least count of 1 micron. The disc temperature has a k-type thermocouple sensor range of up to 800 ^{o}C with the least count of 1 ^{o}C.

The coated steel plate was mounted on a high-temperature tribometer, and the pin of diameter 8 mm of material similar to base material was used as the counter body. The experiment parameters set for friction and wear test for a coated steel plate are given in Table 3.4. The acquisition system connected to the tribometer was used to feed the given parameters. The coefficient of friction and wear depth curve of the experimentation were taken with the system connected to the high-temperature tribometer, and specific wear rates were calculated using the Archands equation.

Archard's equation is a fundamental relationship in tribology that describes the rate of wear of a material due to sliding contact with another material. It was developed by British engineer Derek Henry Edward Archard in 1953 and is widely used in materials science and engineering to predict the wear behaviour of materials in a wide range of applications.

The equation states that the wear volume (V) of a material is directly proportional to the sliding distance (S), the normal load (P), and a material-specific constant known as the wear coefficient (K). Mathematically, the equation can be expressed as:

$$V = KPS/H \qquad (5)$$

Where, V is the wear volume, K is the wear coefficient, P is the normal load, S is the sliding distance and H is the hardness of material.

Table 3.4 Parameters set of friction and wear test for a coated steel plate

S.No.	Track Diameter (mm)	Speed (rpm)	Sliding Distance (m)	Temperature (°C)	Load (N)
1	20	955	1000	25	40
2	30	636	1000	100	40
3	40	477	1000	200	40
4	50	382	1000	400	40

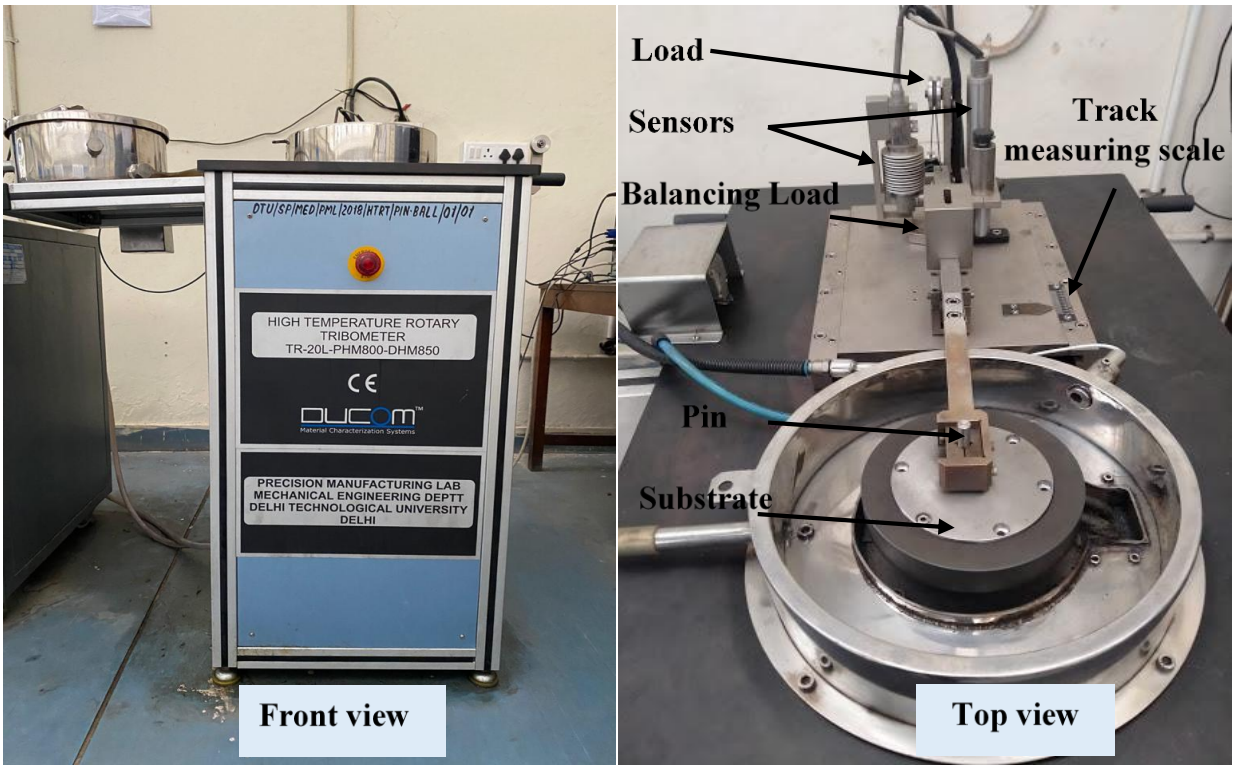

Figure 3.7 High-temperature tribometer setup

Archard's equation assumes that the wear occurs due to the formation and removal of micro-scale material particles or asperities from the surfaces in contact. The wear coefficient K is a material-specific constant that depends on factors such as the hardness, roughness, and composition of the materials in contact, as well as the environment and operating conditions. Archard's equation is a powerful tool for predicting wear in a wide range of tribological applications, from simple sliding contacts to complex systems such as bearings, gears, and cutting tools. It provides a quantitative framework for understanding the wear behaviour of

materials. It is widely used in research and industrial settings to optimize the performance and durability of components and systems.

3.3.5 Thermal conductivity setup

The thermal conductivity of a material is an important property that can impact its performance in various applications. It is defined as the ability of a material to conduct heat and is typically measured in units of watts per meter Kelvin (W/m-K). It is important to use a reliable and precise experimental setup to accurately measure the thermal conductivity of the coating material. The hot plate guarded setup is a commonly used method for measuring the thermal conductivity of materials. In this method, a thin sample of the material is placed

Figure 3.8 Hot plate guarded setup

between two flat plates, with one plate heated and the other cooled. The heat flow through the sample is measured, and the thermal conductivity is calculated from the temperature gradient across the sample.

The developed hot plate guarded setup, as shown in Figure 3.8, is available at Precision and Manufacturing Lab, Department of Mechanical Engineering, Delhi Technological University, New Delhi, India. The schematic diagram of the enclosed chamber of the hot-guarded setup is shown in Figure 3.9. It is a robust and reliable setup that was used to investigate the thermal conductivity of the deposited coating. This setup included a heater, sample plate, top lid, and electrical components. To conduct the experiment, the sample was placed on the heater and secured with the top lid to prevent any heat loss. The entire system was enclosed in an insulated chamber to shield it from any external factors. The current supply of the setup was switched on, and the voltage was adjusted using a variable autotransformer. This caused a fixed current value to flow through the ammeter, and the test piece heated up slowly.

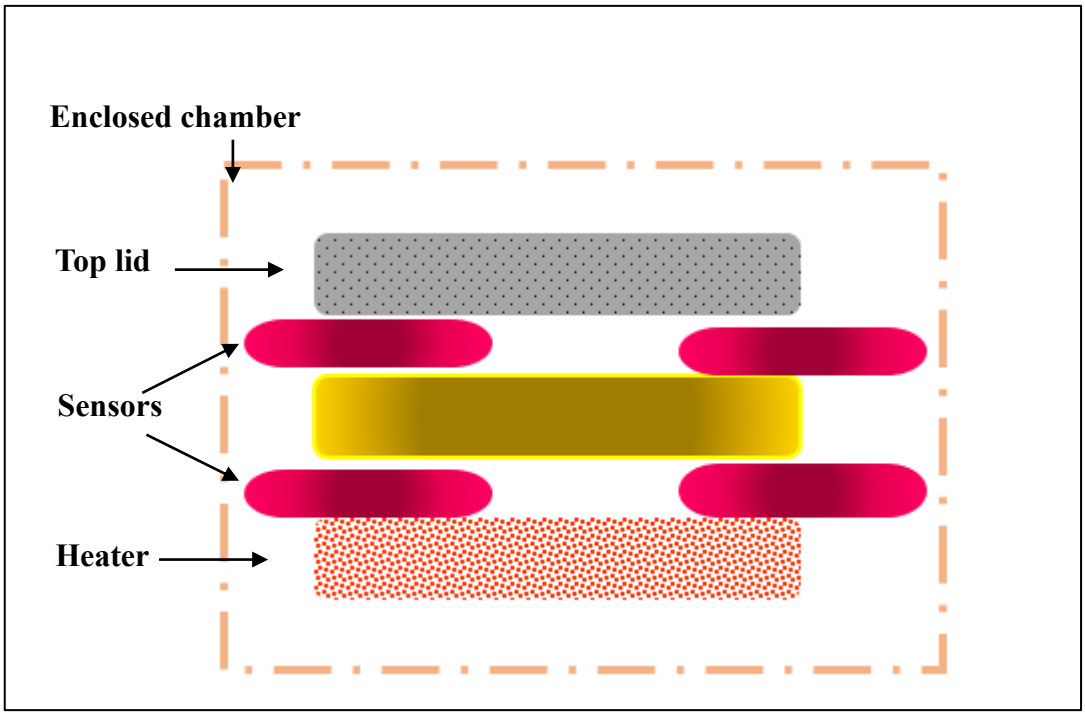

Figure 3.9 schematic diagram of enclosed chamber of hot guarded setup

During the initial stage, the temperature of the test piece was in an unsteady state, and it took about an hour to reach a steady state. Once the steady state was achieved, the temperature values were recorded from sensors placed at the bottom and top of the substrate. The

experiment was repeated three times to ensure the reliability of the data obtained from the setup. The recorded temperature values were then used to calculate the thermal conductivity of the coating material using Fourier's law of heat conduction. This law states that the heat flow through a material is directly proportional to the temperature gradient and the cross-sectional area of the material.

3.3.6 Electrochemical Corrosion Test

The electrochemical corrosion behaviour of Al_2O_3, Al_2O_3-13%(TiO_2) and Al_2O_3-40%(TiO_2) composite coatings were studied using Biologic Potentiostat (Model SP 100) setup in 3.5% NaCl aqueous solution available at Particulate Metallurgy Laboratory facility PEC Chandigarh, India. The corrosion behaviour of the coating samples was investigated using the potentiodynamic polarization technique employing three electrode configurations setup as shown in Figure 3.10. The configurable setup consists of a reference electrode considered saturated calomel, a counter electrode considered platinum mess (1 cm^2), and a working electrode considered a coating sample. Tafel plots were generated and analysed for corrosion rate using potentiostat by EC lab software.

Prior to conducting the electrochemical corrosion test, the individual samples underwent preparation. Initially, the coated sample was connected to low-resistance copper wire using a soldering process. Subsequently, the sample was mounted in epoxy resin from the backside while the coated side was left exposed to enable the electrochemical corrosion test to be performed. The exposed surface of the sample was manually polished with 1000-grit SiC emery paper to achieve the desired level of finish, thereby removing the epoxy on the exposed surface. Following this step, the samples were cleaned with acetone and distilled water. Finally, the prepared sample and electrodes were positioned appropriately in the glass cell in a manner such that the sample and electrodes were adequately immersed in the solution and faced each other at the same level to enable the measurement of the corrosion rate.

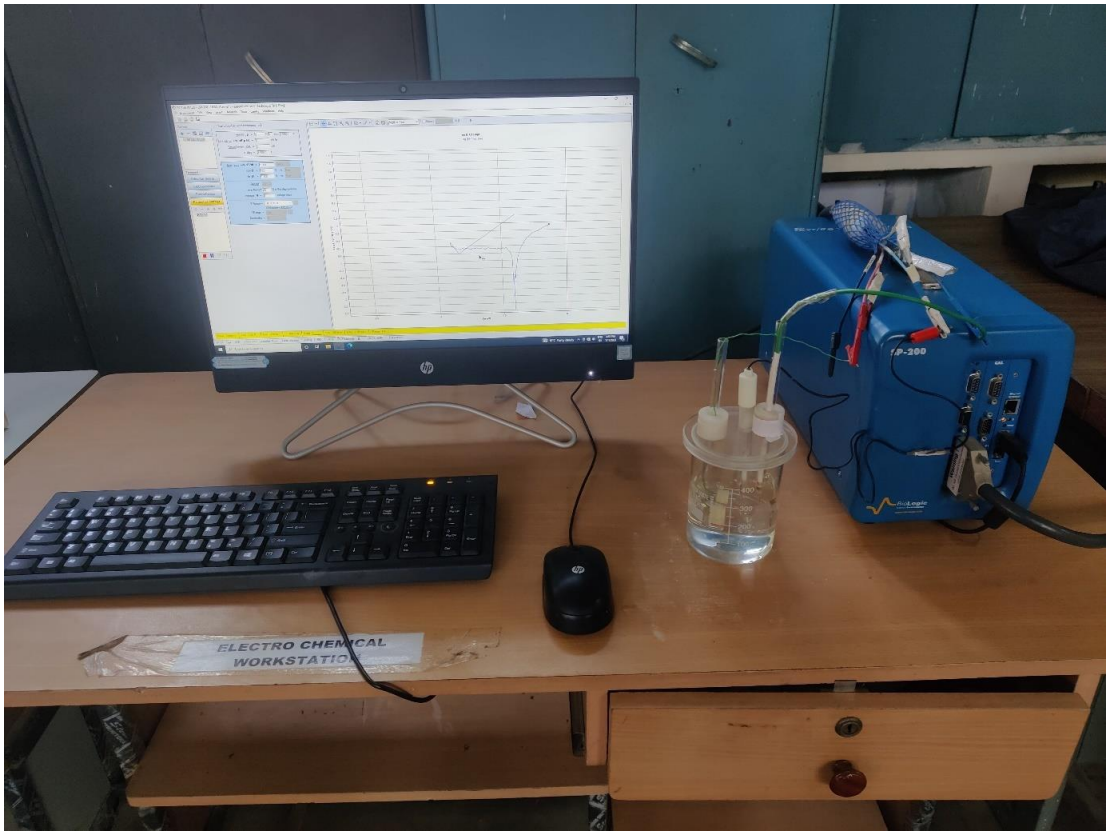

Figure 3.10 Electrochemical corrosion workstation

CHAPTER 4 RESULTS AND DISCUSSIONS

4.1 COATING CHARACTERIZATION

The morphology of the Al_2O_3, Al_2O_3-13%TiO_2 and Al_2O_3-40%TiO_2 composite coatings was examined with the help of the FESEM micrographs, as shown in Figure 4.1. The examination reveals that coatings possess laminar splats, minor micro-cracks and a partially melted region. Figures 4.1 (a) and (b) show a few pores, which are comparatively more than shown in Figure 4.1(c). Micro-pores and interconnected pores are evident as dark regions in the coatings in Figure 4.1 (b). The laminar cracks were generated on the coating surface due to the high-temperature flame, i.e., regions that were highly exposed to the heat generated by the flame spray torch. During the flame process, powder particles behave differently. Some power created a completely melted region, while some created a partially melted. This may be due to the distribution of the powder particles and also the temperature distribution in the flame spray torch.

In flame spray, the particles were melted due to high-temperature flames produced in the gun. These melted droplets accelerated and struck towards the substrate at high speed to form the micro-level laminar structured and dense coating. Due to the high speed of the flame and the distance between the substrate and the gun, some powder particles were not fully melted during the flying and created a partially melted region on the substrate (see Figure 4.1 a). Besides, a few micro-cracks and pores were also developed at the time of coating deposition. The cross-sectional images of the deposited coating were also taken with FESEM micrographs and element mapping, as shown in Figure 4.2. The thickness of the different deposited coating ranges from 148 to 152 μm, i.e., for Al_2O_3 coating is 148.8 μm, Al_2O_3-13% TiO_2 is 152.1 μm and Al_2O_3-40% TiO_2 is 151.19 μm.

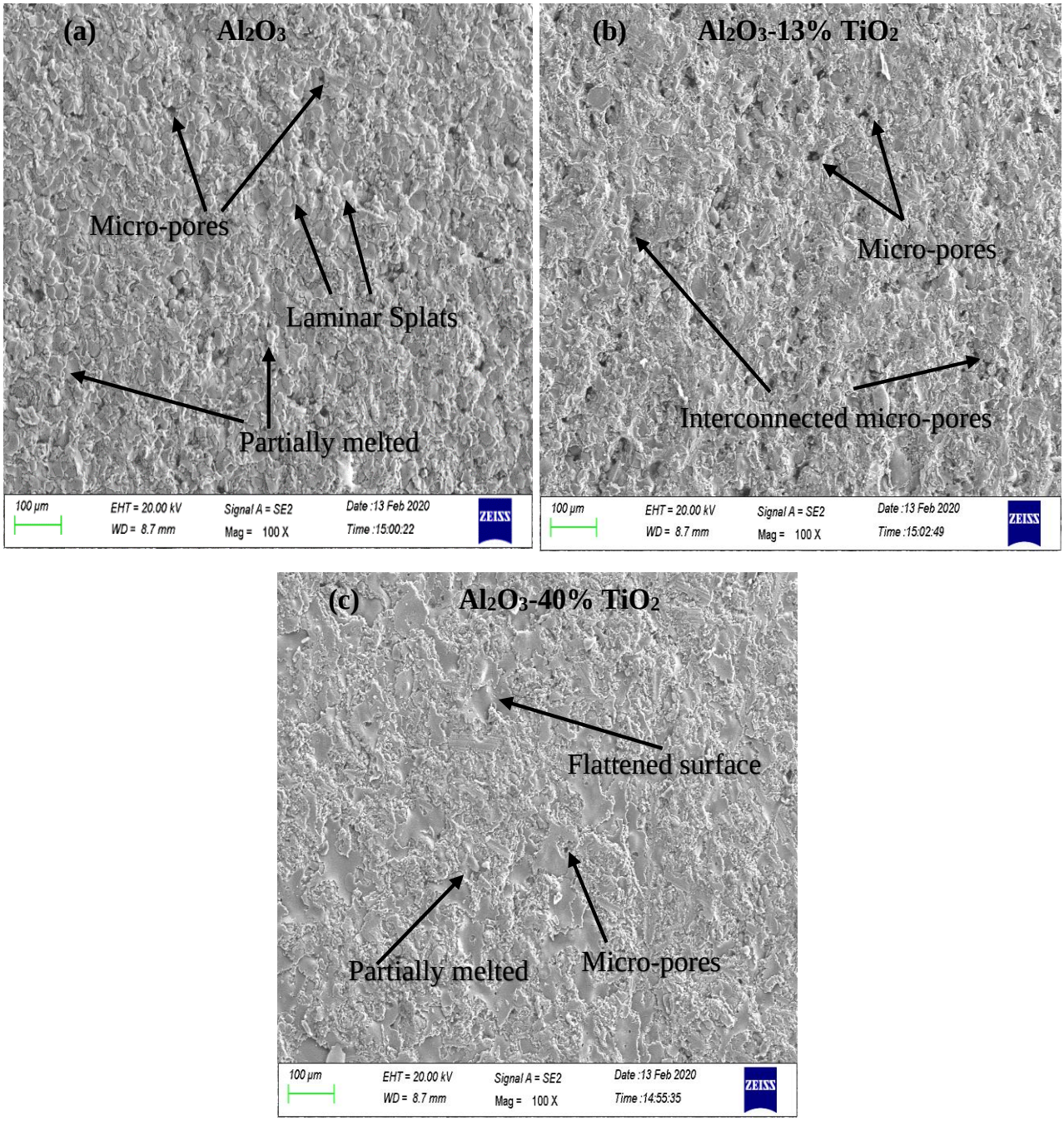

Figure 4.1 FESEM micrographs of coating characterizations: (a) Al_2O_3 coating, (b) Al_2O_3 - 13% (TiO_2) coating and (c) Al_2O_3 -40%(TiO_2) coating

The coatings' chemical composition was analysed using energy-dispersive X-ray spectroscopy (EDS), and the results are presented in Figure 4.3. The EDS spectra show the mass percentage of the different coating elements. The presence of aluminium, oxygen, and titanium was confirmed in all three coatings. The EDS analysis showed that the aluminium content was highest in the Al_2O_3 coating, with a mass percentage of 53.6%. The Al_2O_3-13%

TiO_2 and Al_2O_3-40% TiO_2 coatings had lower aluminium content, with 28.18% and 29.74% by weight, respectively. The oxygen content was found to be the highest in the Al_2O_3 and Al_2O_3-13% TiO_2 coatings, with 46.38% and 46.17% by weight, respectively. The Al_2O_3-40%TiO_2 coating had a slightly lower oxygen content of 42.87% by weight. The EDS analysis also revealed the presence of titanium in the Al_2O_3-13%TiO_2 and Al_2O_3-40%TiO_2 coatings. The mass percentage of titanium was found to be 25.65% and 27.39%, respectively, which indicates that the titanium content increased as the TiO_2 content in the coating composition increased. Moreover, the EDS analysis and elemental mapping revealed that the powder materials were evenly distributed on the surface of the deposited coatings, as shown in Figure 4.2. This even distribution is crucial in achieving the desired coating characteristics, including corrosion resistance and adhesion.

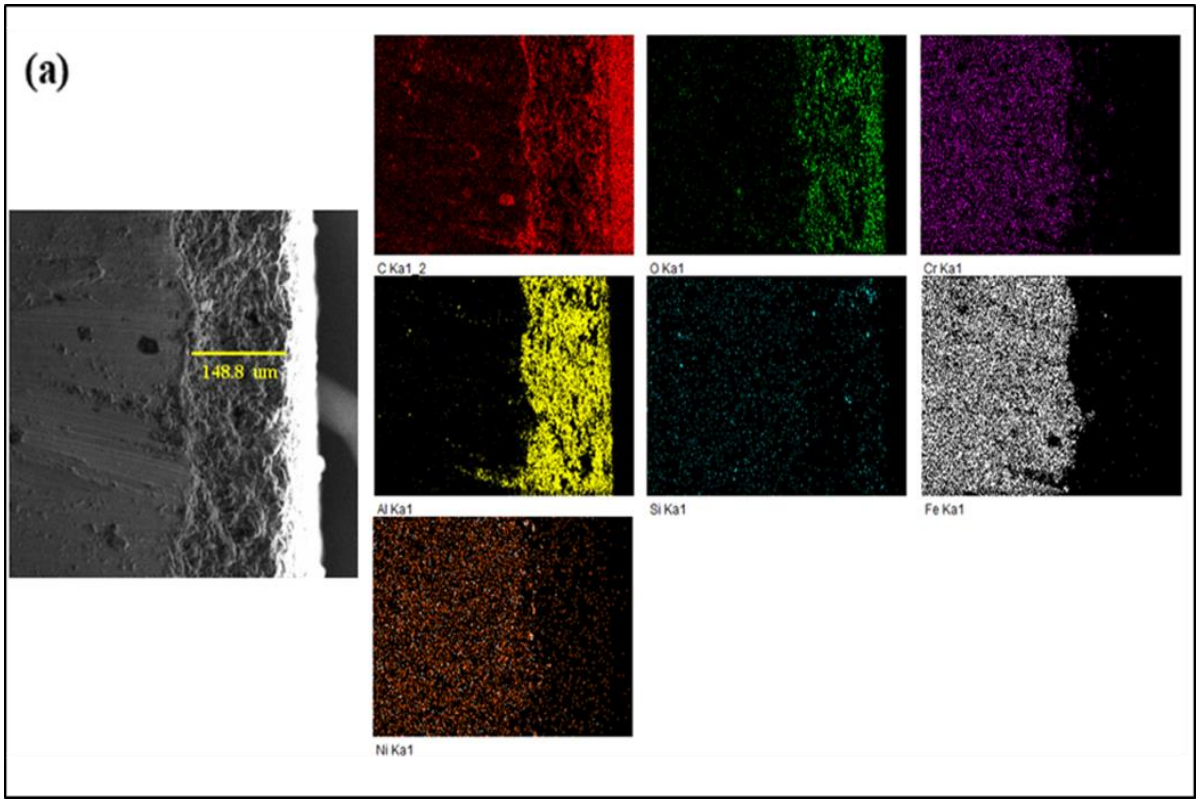

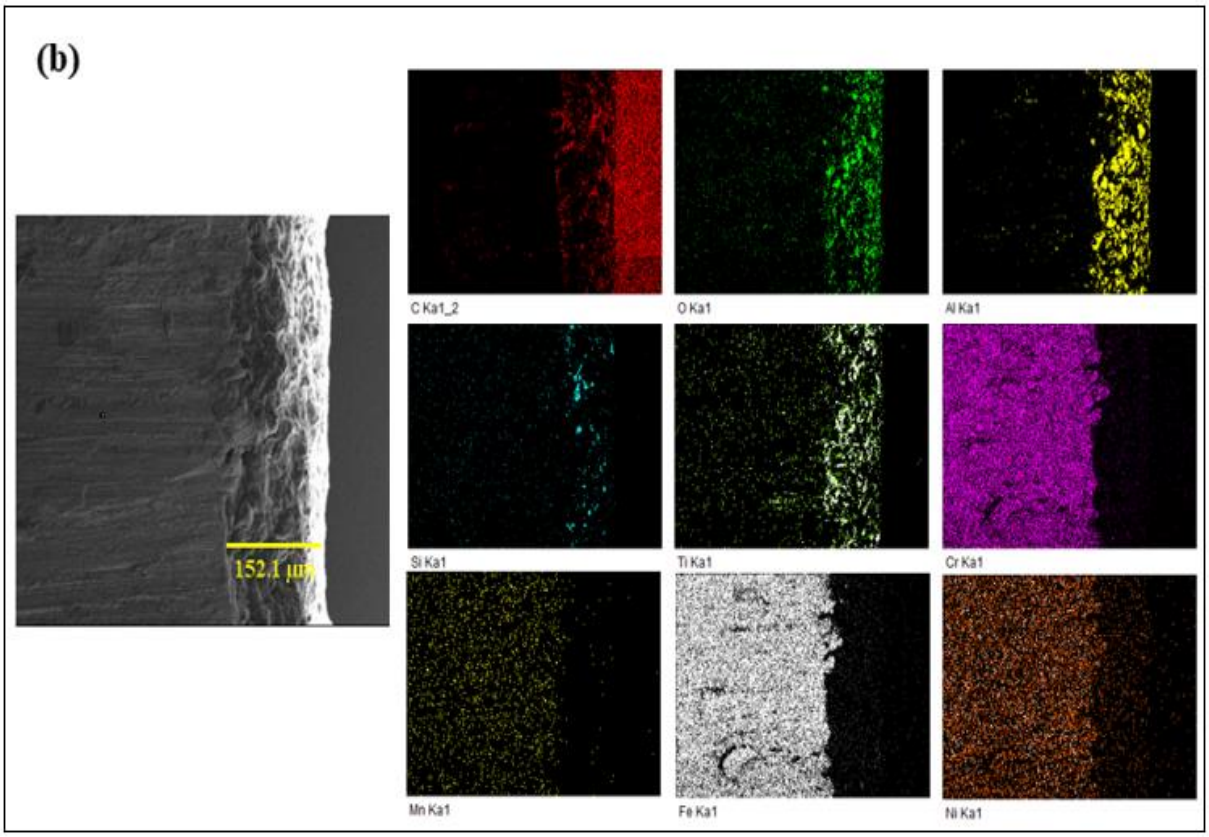

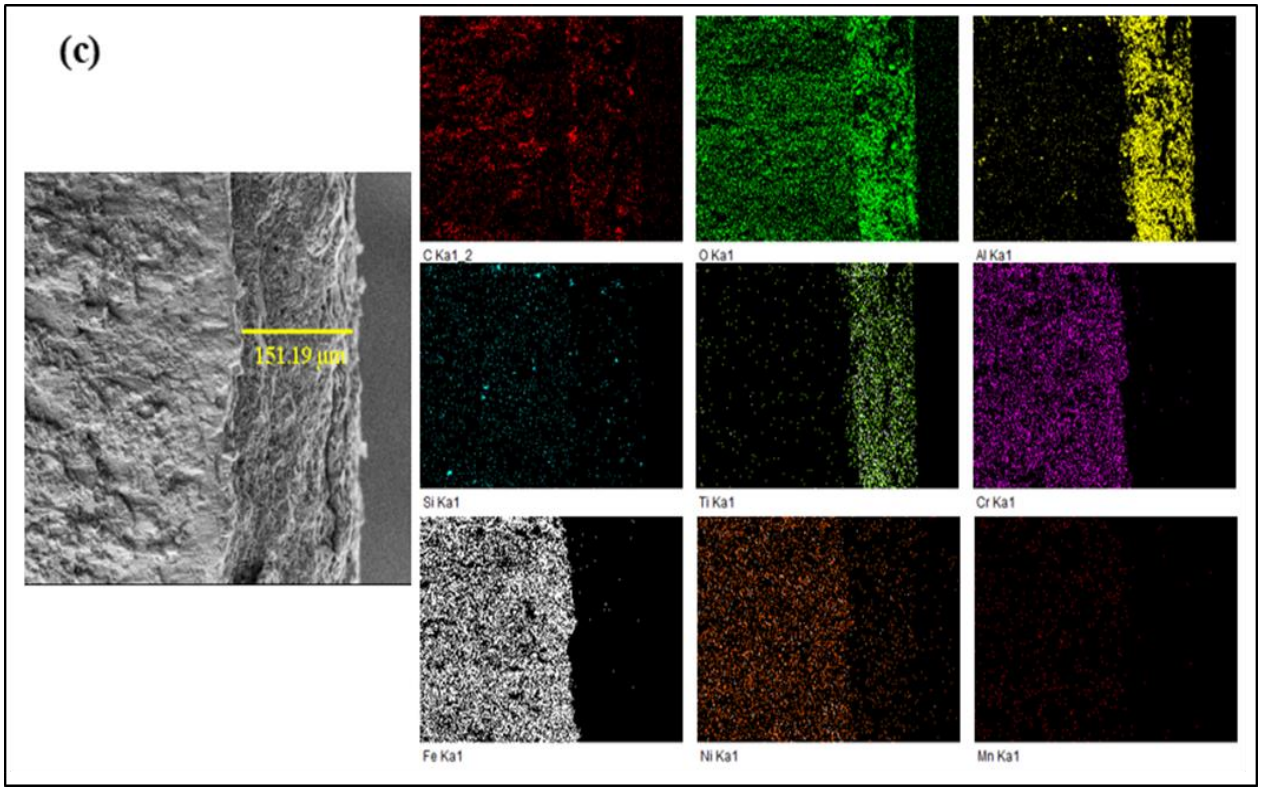

Figure 4.2 FESEM micrographs and element mapping micrographs of coating thickness (a) Al_2O_3, (b) Al_2O_3 -13% (TiO_2) and (c) Al_2O_3 -40%(TiO_2)

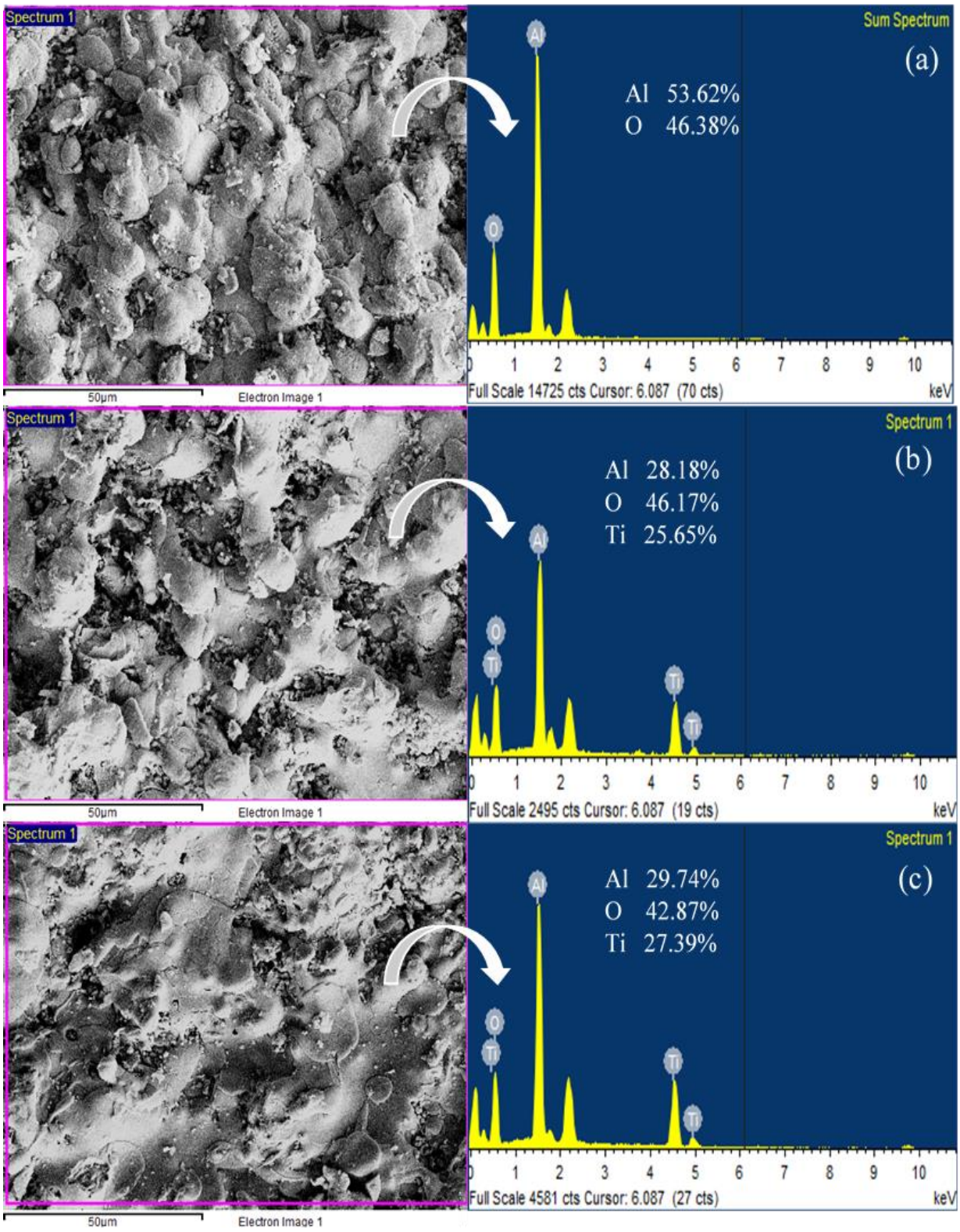

Figure 4.3 EDS analysis of the coatings (a) Al_2O_3 (b) Al_2O_3 -13% (TiO_2) and (c) Al_2O_3 - 40%(TiO_2)

Figure 4.4 presents the XRD pattern of the different coatings that were deposited. The XRD pattern analysis revealed the presence of different phases in the coatings. In the Al_2O_3 coating, both γ- Al_2O_3 and α- Al_2O_3 phases were detected in the deposited coating. The formation of α- Al_2O_3 phase was attributed to the partial melting of the powders during the flame spraying process, as previously confirmed in the microstructure analysis. In the case of the 13% TiO_2 coating, the XRD pattern showed the presence of rutile TiO_2 that reacted with Al_2O_3 to form Al_2TiO_5. This reaction occurred due to the high temperature during flame spraying, which facilitated the formation of the Al_2TiO_5 phase. The significance of the Al_2TiO_5 phase present in the coatings that it exhibits very low thermal expansion coefficient, high thermal shock resistance, high refractoriness and good corrosion resistance. These characteristics make the deposited coating suitable for high temperatures applications.

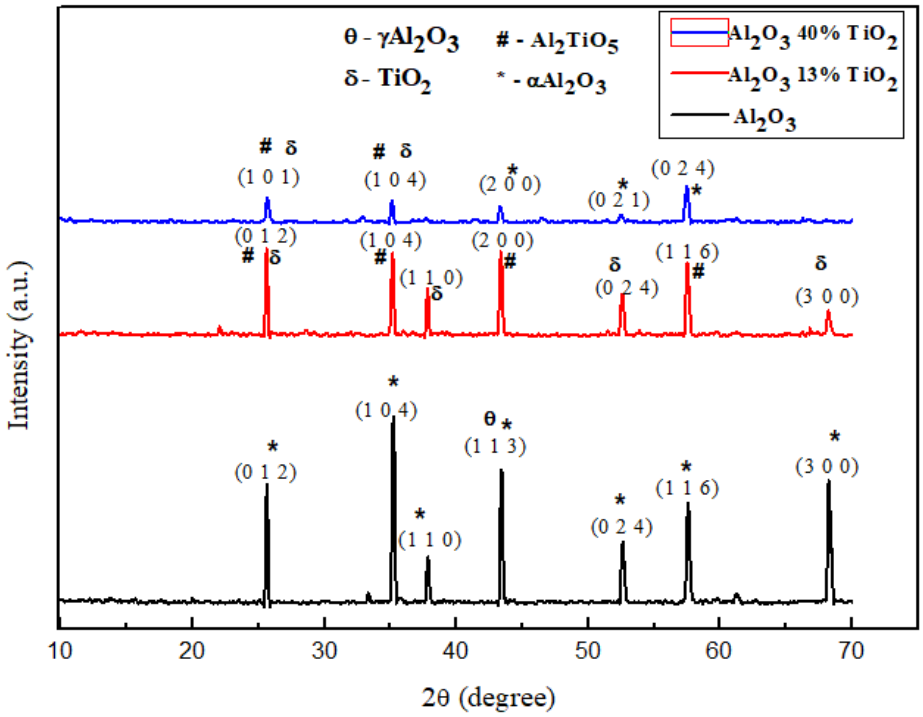

Figure 4.4 XRD pattern of the deposited coatings

In contrast, the XRD pattern of the 40% TiO_2 coating indicated the presence of a significant phase, rutile tialite Al_2TiO_5. The tialite phase was formed as a result of the reaction between the spraying flame of Al_2O_3 and TiO_2 particles. The XRD analysis provided helpful

information on the phase composition of the coatings. The presence of different phases in the coatings could affect the coatings' mechanical and corrosion properties. Therefore, the XRD analysis can help to optimize the coating parameters to obtain the desired phase composition and properties.

The microhardness value of the coatings was determined using a load of 300 g and a dwell time of 10 seconds. The measurements were taken at five different locations under the same conditions to obtain an accurate representation of the coating's hardness. Figure 4.5 shows the results of the microhardness measurements. The average microhardness values for the Al_2O_3 coating, Al_2O_3-13%TiO_2 coating, and Al_2O_3-40%TiO_2 coating were found to be 913.30 HV, 900.15 HV, and 742.17 HV, respectively. It was observed that the Al_2O_3 coating had the highest average microhardness value compared to the other coatings.

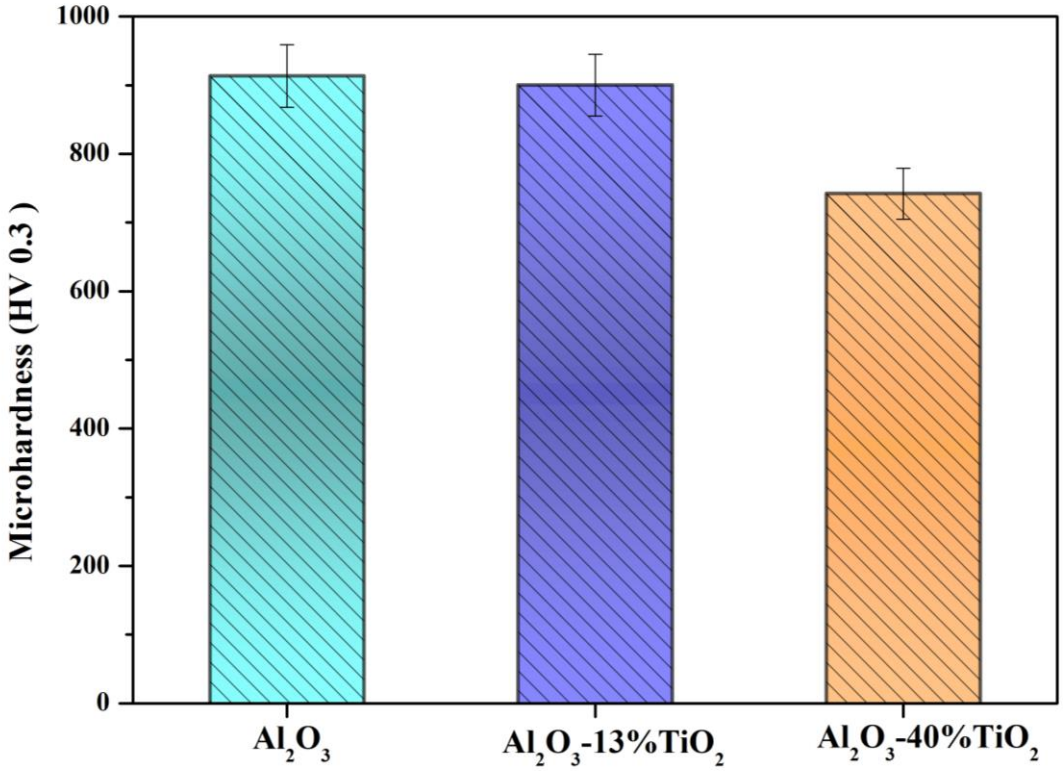

Figure 4.5 Microhardness graph of the deposited coatings

The microhardness of a material is a measure of its resistance to indentation or scratching. It is an essential mechanical property determining the material's ability to withstand wear and

deformation. The high microhardness value of the Al_2O_3+13%TiO_2 coating indicates that it has a higher resistance to wear and deformation compared to the other coatings. The addition of TiO_2 to the Al_2O_3 coating had a significant impact on the microhardness of the coating. The microhardness of the Al_2O_3-40%TiO_2 coating was found to be lower than that of the other coatings. This could be due to the fact that the addition of a large amount of TiO_2 to the coating composition may have resulted in the formation of a more brittle coating, which is more prone to cracking and deformation. The surface roughness of the deposited coatings was obtained. The measured values are 5.3 μm for Al_2O_3, 6.3 μm for Al_2O_3-13% TiO_2 and 6 μm for Al_2O_3-40% TiO_2.

4.2. WEAR BEHAVIOUR OF COATINGS

4.2.1 SPECIFIC WEAR RATE

The standard wear test equation for specific wear rate (also known as wear coefficient) is often used in categorizing the resistance to contact wear [96], [97]. Expression for calculating the wear coefficient is given in Equation 6.

$$K = \frac{V_w}{W * s} \qquad (6)$$

Where K - *S*pecific wear rate (mm^3/Nm)

V_w - Wear volume (mm^3)

W- Load (N)

s- Sliding distance (m)

These wear coefficients are reflected as system-dependent quantities, i.e. (i) contact materials, (ii) surroundings and systems and (iii) operational conditions[98]. Also, the wear behaviour of the coatings is subjective to various elements such as porosity, hardness and fracture toughness. Hardness and fracture toughness have an inverse correlation with wear rate, whereas porosity bears a direct correlation with wear rate [99].

The specific wear rate of the deposited Al_2O_3, Al_2O_3 -13%(TiO_2) and Al_2O_3 -40%(TiO_2) ceramic coatings are taken at different temperatures of 25 ^oC, 100 ^oC, 200 ^oC and 400 ^oC at constant load 40N, and sliding velocity 1m/s is illustrated in Figure 4.6. The measured value of specific wear rate for Al_2O_3 deposited coatings is $0.063684*10^{-3}$ mm^3/Nm at temperature 25^oC, $0.045265*10^{-3}$ mm^3/Nm at 100 ^oC, $0.034228*10^{-3}$ mm^3/Nm at 200 ^oC. But it slightly increases to $0.072183*10^{-3}$ mm^3/Nm at 400 ^oC. Whereas in Al_2O_3-13%TiO_2 coating, the obtained values are $0.040595 *10^{-3}$ mm^3/Nm, $0.030219 *10^{-3}$ mm^3/Nm, $0.024618 *10^{-3}$ mm^3/Nm and $0.026756*10^{-3}$ mm^3/Nm with different temperature of 25 ^oC, 100 ^oC, 200 ^oC and 400 ^oC respectively. In the case of Al_2O_3-40%TiO_2, the values are decreasing $0.034567*10^{-3}$ mm^3/Nm to $0.014581*10^{-3}$ mm^3/Nm with a temperature of 25 ^oC, 100 ^oC, 200 ^oC and 400 ^oC respectively. It is visible (Figure 4.6) that the specific wear rate is continuously decreasing with the successive rise in temperature except in the case of Al_2O_3 coating at 400 ^oC.

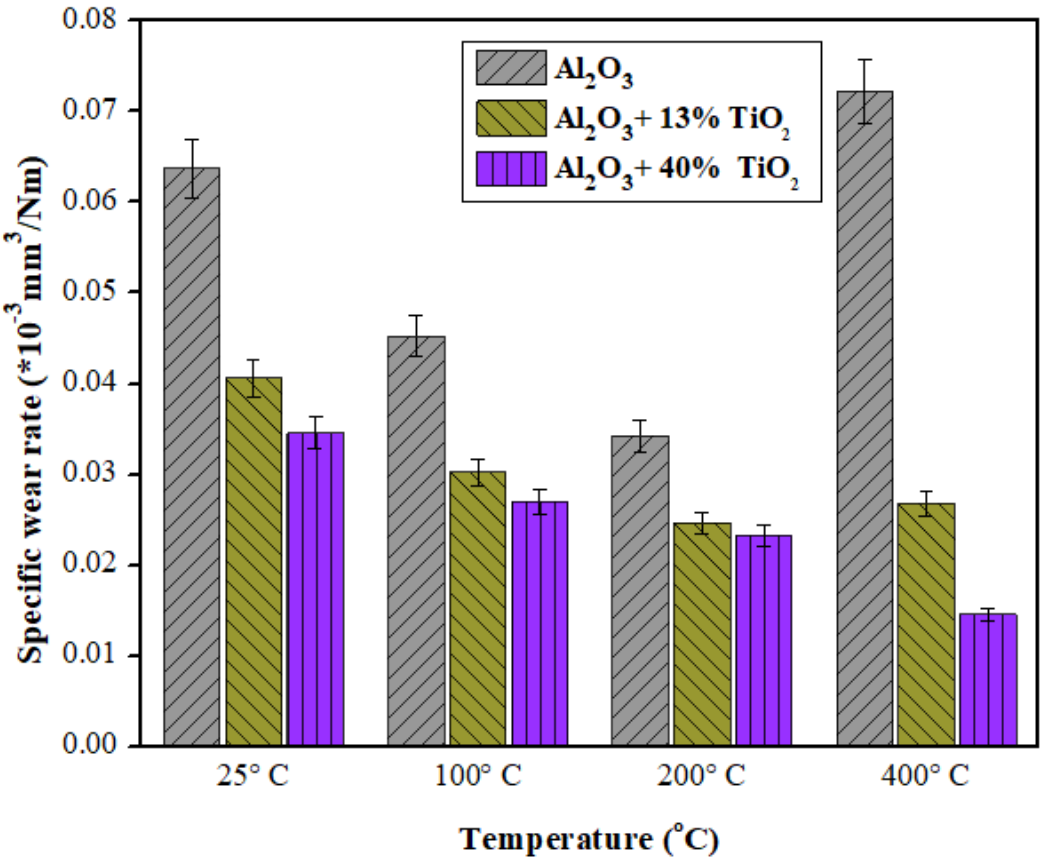

Figure 4.6 Specific wear rate at different temperatures

From the above discussion, For Al_2O_3 coating, it is clear that the wear coefficient decreases up to 200 °C and suddenly increases at 400 °C due to chippings or spalling from the substrate. From Figure 4.6, at 400 °C for Al_2O_3 deposited coating, the highest specific wear rate is observed, i.e., this $0.072183*10^{-3}$ mm^3/Nm. The wear properties depend upon the debris characteristics and the contact temperature. This effect could also be explained due to the deformation of the protective layer of the coating. The deposited coating has been plastically deformed and appears to be ploughed enough. This deformation and ploughing results in a large detachment from the substrate. Similar results were also reported about the specific wear rate of Al_2O_3 coatings rising when the temperature is raised to 400 ◦C [100]. Tetsuya Senda et al. [101] found that at elevated temperatures, the grain size has a significant impact on the wear resistance behaviour of alumina coating. The larger wear grooves of nanostructure coating also confirm the increase in wear rate at 25 °C, 100 °C, 200 °C and 400 °C, respectively.

All the even and compacted areas spread in the wear track are attained at 400 °C and 200 °C as well, but at room temperature, no traces of wear scars were observed. Therefore, this type of area in the wear scars increases with rising temperature, and it is called a tribolayer [102], [103].

For Al_2O_3-13%TiO_3, the decrease in the wear coefficient is observed with the increase in temperature of up to 200 ºC. However, at 400 ºC, Al_2O_3-13%TiO_3 coating shows a slightly increasing trend in specific wear rate, which is much lesser than pure Al_2O_3 coating at the same temperature. This is due to the less spalling/chilling formation in the Al_2O_3-13%TiO_3 coating on the substrate. In comparison, a similar specific wear rate trend was observed for Al_2O_3-40%TiO_3 coating till 200 ºC. However, at 400 ºC Al_2O_3-40%TiO_3 coating shows a gradually decreasing trend in specific wear rate. The addition of TiO_2 content in Al_2O_3 composite coating results in a drop in the hardness of the coating, which affects the material loss of the coating [104]. Subsequently, it results in added adhesive mode when compared with pure Al_2O_3. Hence, the adhesive wear mechanism is consistent and dominant as well[105].

4.2.2 COEFFICIENT OF FRICTION

The coefficient of friction of thermally sprayed deposited ceramic coatings can be effectively analyzed by subjecting it to the pin-on-disc test using a high temperature tribometer. To determine the coefficient of friction between the two surfaces, the following equation (7) is used[106]:

$$F = \mu N \qquad (7)$$

Where F represents the frictional force in Newton, μ denotes the coefficient of friction, and N represents the normal force, which is the applied load in each track or run of the test.

Figure 4.7 depicts the evolution of the coefficient of friction (COF) trend of Al_2O_3-based ceramic coatings at a constant load of 40 N under the influence of four levels of variable

temperatures (25 °C, 100 °C, 200 °C and 400 °C) for sliding distance of 1000m. It can be seen from Figure 4.7 that the COF of pure Al_2O_3-based coating decreases with increasing temperature from 25 °C to 200 °C. While COF was a maximum of 0.92 at the maximum operating temperature of 400 °C, this may be due to chippings or spalling of the coating from the substrate while rubbing or sliding.

For Al_2O_3-13%TiO_2 coating, the COF decreases with increasing temperature, i.e., the obtained values are 0.921, 0.795, 0.697 and 0.5863 with temperatures 25 °C, 100 °C, 200 °C and 400 °C respectively. Similar trends were also seen for Al_2O_3-40%TiO_2 coating, where COF ranges from 0.7284 to 0.3901 and temperature ranges from 25°C to 400°C, respectively. Hence, the coating Al_2O_3-40%TiO_2 has less coefficient of friction as compared to the other two coatings, i.e., Al_2O_3 and Al_2O_3-13%TiO_2.

The Al_2O_3-TiO_2 coatings and counter body react in a tribo-chemical nature, which is controlled and results in the reduction of the COF. The finding of a reduction in COF is due to the development of the oxide layer on the coating surface, which acts as a protective layer. Therefore, the sticking tendency of wear debris and material shear strength gets reduced with the increased operating temperature. So, the contact temperature produces softening and melting of the wear debris. These similar trends reported about the tribological properties of Al_2O_3-TiO_2 coatings are also highly determined by test environments, such as temperature and contact load [107], [108]. The wear of deposited Al_2O_3-TiO_2 coatings is decreased in the presence of absorbed environmental moisture[109]. The coefficient of friction decreases with the surge in the operating temperature due to the development of the tribo-layer at higher temperatures. Subsequently, the tribo-layer is dense and even; therefore, it has a significant role in the reduction of the coefficient of friction [110].

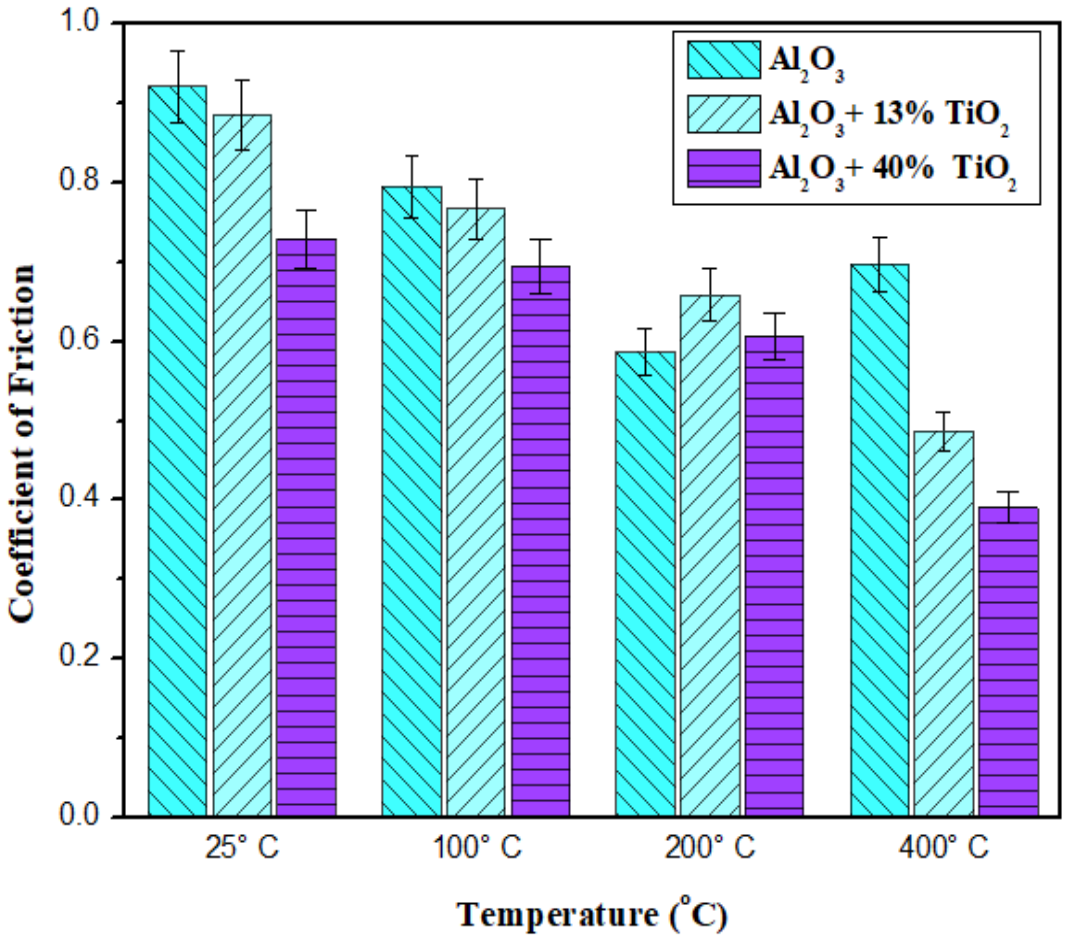

Figure 4.7 Coefficient of friction at different temperatures

4.2.3 WEAR MECHANISM

The wear behaviour of Al_2O_3-TiO_2 coatings was mainly affected by the microstructure, porosity, micro cracks and mechanical properties like fracture toughness and hardness. Figure 4.8 A, D, G, J reports the wear behaviours of the Al_2O_3-based ceramic coatings at the temperature of 25°C, 100°C, 200°C and 400°C respectively, with a constant load of 40N and sliding distance of 1000m. At 25°C, the Al_2O_3 coating shows abrasion wear due to more roughness and larger surface contact between the substrate and the counter body. While the temperature is increasing up to 200°C, the wear track is showing a decreasing trend. This is due to the fact of higher temperature stability of the coating at 200-300°C. Another evidence for the mild wear of the coating owing to the existence of oxygen in the wear track results in the oxidation of fine wear debris, their accumulation and subsequent development

of tribo-film. But at 400°C, Al_2O_3 coating showed poor wear resistance detachment of the coating particles from the substrate as there was a complete presence of Al_2O_3 content in the top layer of the deposited coating.

As per FESEM micrographs (Figure 4.8) of the coatings Al_2O_3-13% TiO_2 and Al_2O_3-40% TiO_2 at 200 and 400°C, ploughing and plastic deformation marks were observed on the worn surfaces along with areas of brittle fracture. The mechanism appears to be similar for all the wear surfaces. The major difference has been observed only in the brittle fracture areas caused due to ductility and cohesion of the coating.

Whereas wear mechanism in Al_2O_3 with varying percentages of TiO_2 coating wears scars, wear track with the flattened surface, minor cracks and severe abrasion, micro brittle fracture reported mainly by the researchers [111]. Oge et al. [112] observed the fatigue-induced surface cracks and consequent spallation arising due to the plastic deformation of the coating. While at high temperatures, Al_2O_3- TiO_2 shows a brittle fracture during sliding wear on the worn surface of the deposited coating at a temperature varying from 25 °C to 400 °C. This mainly occurs due to the desorption of moisture at elevated temperatures [113].

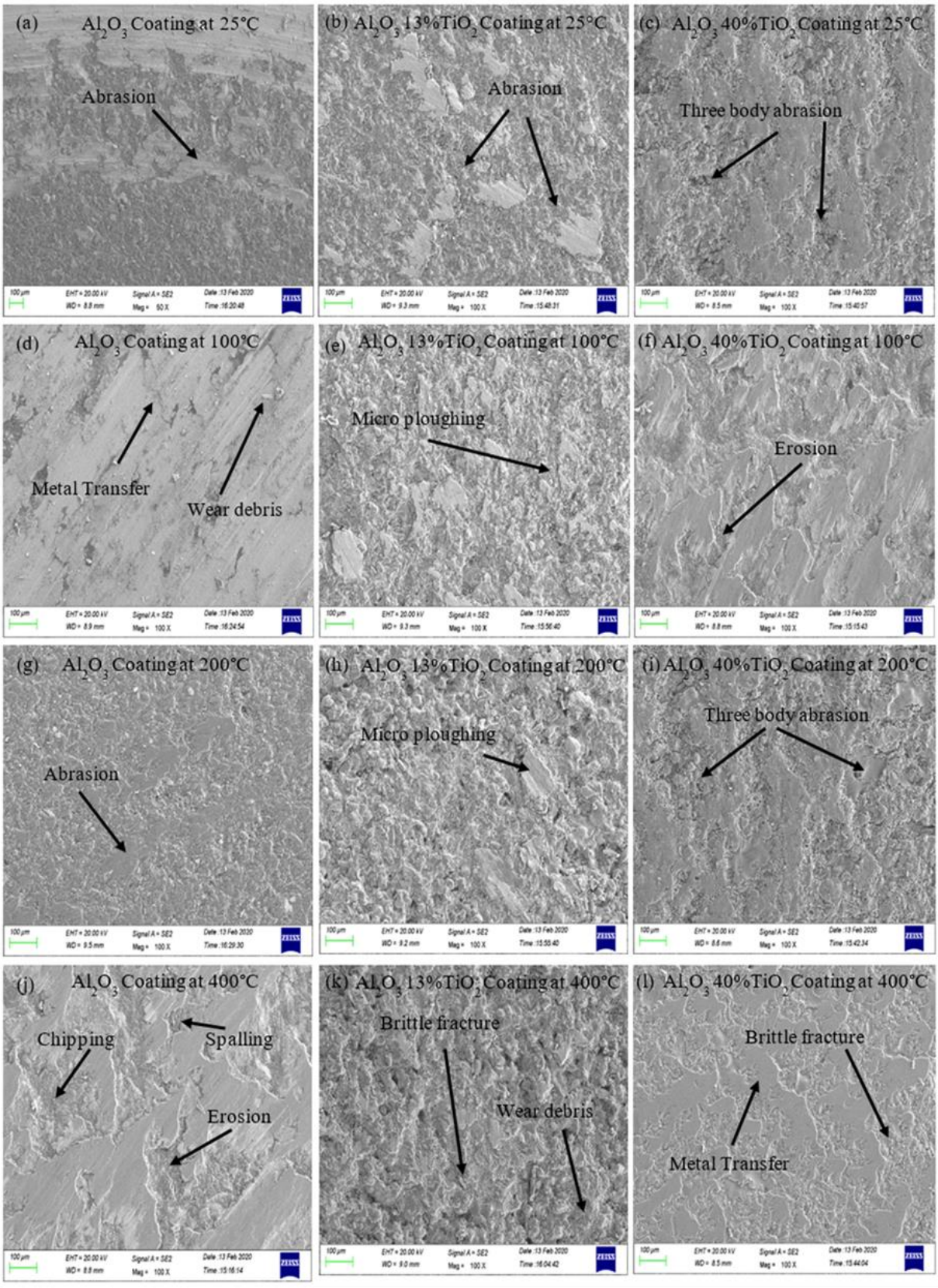

Figure 4.8 Wear mechanism of the deposited coatings at different temperatures

4.3 THERMAL CONDUCTIVITY

To analyse the heat transfer in a disc, longitudinal heat flow is assumed to be the dominant mechanism. In contrast, radial and tangential heat loss is neglected due to the disc's small thickness. The Fourier law, described by Equation (8), is employed to determine the amount of heat (Q) transferred, which is proportional to the thermal conductivity (K) and the temperature gradient (dT/dx) in the flow direction[114], [115].

$$Q = KA\,(dT/dx) \tag{8}$$

Equation (6) is also expressed in terms of thermal resistance to equation (9),

$$Q = \Delta T/R \tag{9}$$

The thermal resistance (R) to heat flow in a plate is determined by the ratio of its thickness (L) to the product of its cross-sectional area perpendicular to heat flow (A) and the thermal conductivity (K). The temperature difference (ΔT) between the two surfaces of the plate is also taken into account, and convective and radiative heat losses are ignored due to slight heat loss. For a composite material consisting of a substrate and a coating, the thermal resistance of the composite is equal to the sum of the thermal resistances of the substrate and the coating. To calculate the thermal resistance of the composite, an electrical model is utilized that provides the heat transfer rate produced by multiplying the instantaneous potential difference and current values measured by the setup. The required temperature difference is achieved by measuring the temperature of the top and bottom surfaces of the coating.

J-type thermocouples are employed to measure the respective temperatures of a coated substrate (Al_2O_3 coating) in the system. In addition, the thermal resistance of the substrate is determined by using the formula R(substrate) = L/KA, where the thickness (L) is 3 mm, area (A) is 0.00785 m^2, and the thermal conductivity (K_1) is 16.3 W/m-K of the substrate [116] The calculated value of the resistance of the substrate is found to be 0.0237 K/W.

Subsequently, by using the formula Q = ΔT /R, where Q is the heat flux, ΔT is the temperature difference, and R is the thermal resistance, calculations for Q and ΔT are performed. Based on the obtained values, the composite thermal resistance R(composite) is determined to be 0.0431 K/W.

Furthermore, the value of the thermal resistance of coating R(coating) is computed as 0.010615 K/W by subtracting the thermal resistance of the substrate from the composite thermal resistance. After obtaining the value of R(coating), the thermal conductivity of the coating can be computed using the formula K = L/ [A x R(coating)], which yields a value of 2.85 W/m-K. Similarly, these calculations were done for the other two different coatings.

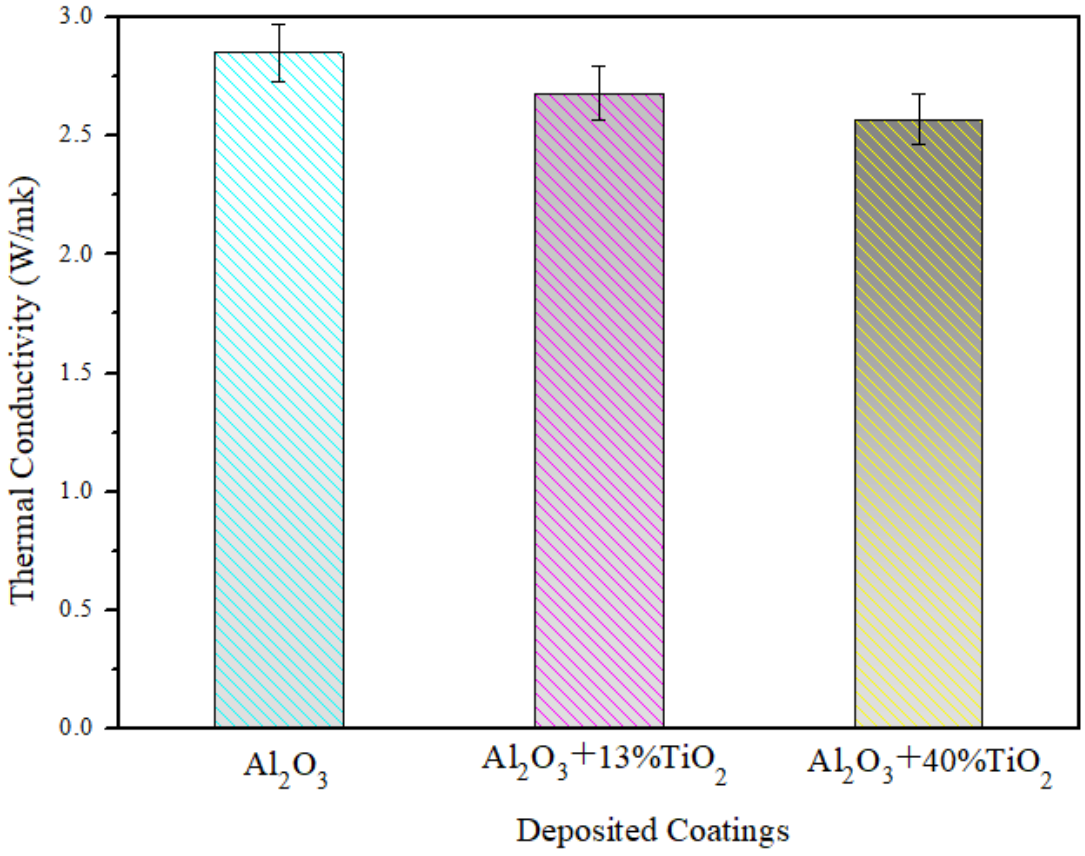

Figure 4.9 Thermal conductivity of deposited coatings

The thermal conductivity of the three coatings - Al_2O_3-13% TiO_2, Al_2O_3-40% TiO_2, and pure Al_2O_3 were calculated in the experiment and are shown in Figure 4.9. The results indicate that

pure Al_2O_3 has the highest average thermal conductivity value of 2.85 W/m-K. This could be attributed to the fact that Al_2O_3 has a high crystal symmetry and a relatively low thermal boundary resistance, which enables it to conduct heat more effectively.

On the other hand, the addition of TiO_2 to Al_2O_3 can significantly affect its thermal conductivity. The average thermal conductivity of Al_2O_3-13% TiO_2 is found to be 2.68 W/m-K, which is slightly lower than that of pure Al_2O_3. This could be attributed to the fact that TiO_2 has a lower thermal conductivity than Al_2O_3. Additionally, the presence of TiO_2 may increase the number of thermal boundaries in the material, which can impede the flow of heat [117]. Furthermore, the average thermal conductivity of Al_2O_3-40% TiO_2 is observed to be 2.57 W/m-K, which is significantly lower than that of both pure Al_2O_3 and Al_2O_3-13% TiO_2. This decrease in thermal conductivity could be due to the high concentration of TiO_2, which may result in an increased number of thermal boundaries and reduced heat flow.

The results of this study can have significant implications for practical applications, especially in the field of thermal management. For instance, the high thermal conductivity of pure Al_2O_3 could make it a suitable choice for applications that require efficient heat dissipation, such as heat sinks for electronic devices. Meanwhile, the lower thermal conductivity values of the TiO_2-containing coatings may make them more appropriate for applications where a lower thermal conductivity is desired, such as in insulation materials or thermal barriers [118], [119].

4.4 ELECTROCHEMICAL CORROSION RATE

The study aimed to investigate the corrosion behaviour of alumina-based coatings on SS substrates. The purpose of the investigation was to evaluate the effectiveness of the coatings in resisting corrosion, which is an important factor in determining the durability of metal substrates. The electrochemical corrosion test was performed on three different alumina-based

coatings deposited on the SS substrate in 3.5 wt.% NaCl solution. The coatings were Al_2O_3, Al_2O_3-13%TiO_2, and Al_2O_3-40%TiO_2.

To conduct an electrochemical corrosion test, a sample of coated substrate and electrodes were prepared and placed in a glass cell in a way that the sample and electrodes were sufficiently immersed in the solution facing towards each other at the same level. This setup ensured that the electrochemical reaction occurred only at the interface between the sample and solution interface. Before starting the experiment, an OCP (open circuit potential) plot was taken for 30 minutes to stabilize the sample in the provided corrosion medium. This was done to establish the baseline potential of the sample and to ensure that the sample was not affected by external factors such as surface contamination or variations in the composition of the solution.

After the sample was stabilized, a Tafel plot was generated at a scan rate of 1 mV/s. A Tafel plot is a graphical representation of the polarization curve, which shows the relationship between the current density and the potential of the sample. The Tafel plot was then fitted using Tafel fit in EC Lab software to determine the electrochemical parameters, such as the corrosion potential (Ecorr.) and corrosion current (Icorr.).

The electrochemical parameters, Ecorr. and Icorr. were calculated using filtering the polarization curve. These parameters were then used in equation Q to determine the corrosion rate of the coated sample. The equation used to calculate the corrosion rate was CR (mmpy)= (0.00327*Icorr. *EW) / d, where Icorr. is the corrosion current density ($\mu A/cm^2$), EW is the equivalent weight (g), and d is the density of the sample (g/cm3). To ensure the reproducibility of results, a fresh 300ml electrolyte solution was prepared for each test study, using a 3.5 wt.% NaCl solution. Each study was performed at least three times, and the average value of the

corrosion rate was calculated from these experiments. This approach helps to ensure that the results are reliable and can be used for further analysis and comparison with other studies.

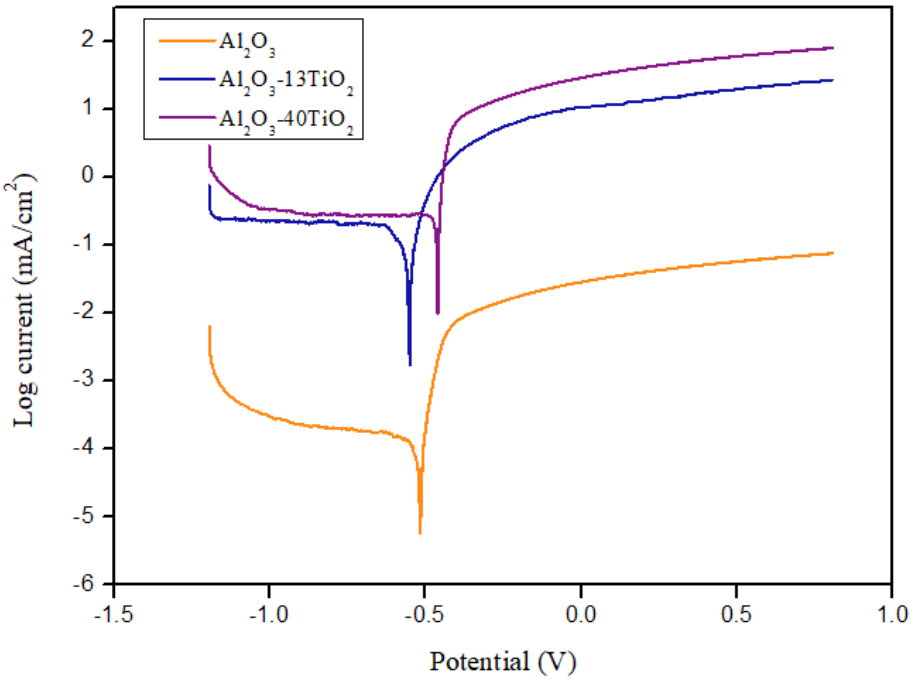

Figure 4.10 Tafel plot of three different coatings

Tafel plots were generated for each coating, and the corrosion rate was evaluated using Tafel fitting in EC lab software. The corrosion rates for each coating were presented in Table 4.1, while Figure 4.10 showed the effect of the coatings on the corrosion behaviour. The results showed that the coating with 40% TiO_2 had the lowest corrosion rate compared to the pure Al_2O_3 and Al_2O_3-13%TiO_2 coatings. The coated sample with 40% TiO_2 showed the lowest I corr. compared to the other coatings. It was observed that the corrosion current density (I corr.) decreased as the TiO_2 content in the coating composition increased. This suggests that the coating with 40% TiO_2 possesses more corrosion-resistant characteristics that resist the movement of ions and provide passivation. The formation of a passive layer over the surface acts as a protective layer that prevents the loss of ions and provides the desired corrosion resistance characteristics to the substrate [120]–[122].

Table 4.1 Corrosion rate of deposited coatings

S. No.	Coatings	Ecorr. (mV)	I corr. ($\mu A/cm^2$)	Corrosion rate (mm/year)
1	Al_2O_3	510.325	15.943	0.259
2	Al_2O_3-13%TiO_2	504.126	10.754	0.149
3	Al_2O_3-40%TiO_2	519.242	8.670	0.116

The results of the current study suggest that the addition of TiO_2 to the alumina-based coating improves its corrosion resistance properties. The study also highlights the importance of conducting electrochemical corrosion testing to evaluate the effectiveness of coatings in resisting corrosion. The electrochemical corrosion test is a valuable tool for evaluating the performance of coatings under different environmental conditions. The test provides information on the corrosion behaviour of the coatings, such as their corrosion rate and corrosion current density. This information can be used to optimize the composition and properties of coatings to improve their corrosion resistance.

CHAPTER 5 CONCLUSIONS AND FUTURE SCOPES

5.1 CONCLUSIONS

In the present study, Al_2O_3-TiO_2-based ceramic coatings were successfully coated by the thermally flame spray process. The objective of this research is to compare the different coatings and obtain the best wear-resistant coating for high-temperature applications. The wear behaviour of different coatings was studied at four levels of temperatures (25 °C, 100 °C, 200 °C and 400 °C). Subsequently, coated samples were characterized based on morphological analysis and various mechanical properties. The thermal behaviour and corrosion rate of the deposited coatings were investigated. The findings in this research have drawn the following conclusions.

- The thermally flame spray coating exhibits a relatively dense lamellar microstructure with laminar splats, minor micro-cracks, partially melted region and few pores in the microstructure. The thickness of the deposited coatings ranges from 148- 152 µm.
- The EDS analysis showed that the coatings' chemical composition was consistent with the intended composition. The coatings contained aluminium, oxygen, and titanium, with the titanium content increasing as the TiO_2 content in the coating composition increased. The even distribution of the powder materials on the surface of the coatings was confirmed by EDS analysis and elemental mapping.
- The Al_2O_3+40%TiO_2 has shown the least microhardness value. The average microhardness value for Al_2O_3 coating is 913.30HV, Al_2O_3-13%TiO_2 coating is 900.15 HV, and for 40%TiO_2 coating is 742.17 HV. The surface roughness of the deposited coatings was obtained. The measured values are 5.3 µm for Al_2O_3, 6.3 µm for Al_2O_3-13% TiO_2 and 6 µm for Al_2O_3-40% TiO_2.

- The specific wear rate of Al_2O_3, Al_2O_3 -13%(TiO_2) and Al_2O_3 -40%(TiO_2) coatings determined were more in the initial stage, which decreases to a steady state in the latter. The specific wear rate decreases with the increase in the temperature at a constant load and sliding distance. Whereas For Al_2O_3 coating, the wear coefficient suddenly increases at 400 ^oC due to chippings or spalling from the substrate. This is because of the deformation and ploughing that causes the large detachment of coating particles from the substrate at high temperatures.
- The friction coefficient of deposited three alumina-based is decreasing with increasing temperature. The decrease in the friction coefficient is governed by tribochemical reactions between alumina-based coatings and counter-body. There is a reduction in the sticking tendency of wear debris with increasing temperature, and the formation of oxides is favoured as the contact layer.
- The main type of wear in Al_2O_3-based coatings sliding against stainless steel counter body is a brittle fracture and abrasive behaviour. Whereas the wear mechanism in Al_2O_3 with varying percentages of TiO_2 coating wears scars, wear tracks with a flattened surface, minor cracks and severe abrasion. The fatigue-induced surface cracks and consequent spallation arise due to the plastic deformation of the coating.
- At high temperatures, the coatings show a brittle fracture during sliding wear on the worn surface of the deposited coating at a temperature varying from 25 °C to 400 °C.
- Pure Al_2O_3 exhibits the highest average thermal conductivity of 2.85 W/m-K, attributed to its high crystal symmetry and low thermal boundary resistance. The addition of TiO_2 decreases the thermal conductivity, with Al_2O_3-13% TiO_2 having a slightly lower value of 2.68 W/m-K due to increased thermal boundaries. Al_2O_3-40% TiO_2 shows a significant decrease to 2.57 W/m-K mainly due to an increase in the percentage of TiO_2 concentration in the coating, which further increases the thermal boundaries and reduces heat flow.

- The study evaluated the corrosion behaviour of three different alumina-based coatings on SS substrates using electrochemical corrosion testing in 3.5 wt.% NaCl solution. The results showed that the coating with 40% TiO_2 had the lowest corrosion rate and corrosion current density compared to the pure Al_2O_3 and Al_2O_3-13%TiO_2 coatings. The study highlights the importance of conducting electrochemical corrosion testing to evaluate the effectiveness of coatings in resisting corrosion. The results of the study suggest that the addition of TiO_2 to the alumina-based coating improves its corrosion resistance properties, consistent with previous studies.
- Among the three alumina-based coatings, the Al_2O_3-40% TiO_2 coating exhibits superior wear and corrosion resistance properties, along with a low coefficient of friction, when compared to the Al_2O_3-13% TiO_2 coating and pure Al_2O_3 coating. Additionally, it possesses low thermal conductivity, making it well-suited for thermal insulation applications.
- The Al_2O_3-40% TiO_2 coating demonstrates not only high wear and corrosion resistance properties but also low thermal conductivity, making it suitable for both wear & corrosion protection and thermal insulation applications. This combination of properties allows it to provide adequate insulation against heat transfer while also protecting the underlying substrate from wear and corrosion. Therefore, it is an ideal choice for applications where both thermal insulation and protective coating properties are required, such as in high-temperature environments or equipment exposed to harsh corrosive conditions, such as exhaust systems & engine components in the automotive industry, pipelines & storage tanks in oil and gas industry, power generation facilities like thermal power plants, nuclear reactor and boilers.

5.2 FUTURE SCOPES

The results documented in the present research are significant. However, recommendations for further work are as follows:

1. Wear behaviour of the same composition of the coating can be investigated at cryogenic conditions. The wear behaviour of coatings under extremely low temperatures can provide important insights about its stability in cold environments
2. The high-temperature erosion behaviour of the coatings for the same composition can be investigated.
3. The effect of coatings of the same composition on microstructural and vibration for thermal barrier applications can be investigated. This investigation can show the impact of the coatings on the structural integrity and vibrational characteristics of materials in high-temperature environments.
4. The damping coefficient of the same deposited coatings can be studied.

REFERENCES

[1] Y. Meng, J. Xu, Z. Jin, B. Prakash, and Y. Hu, "A review of recent advances in tribology," *Frict. 2020 82*, vol. 8, no. 2, pp. 221–300, Apr. 2020, doi: 10.1007/S40544-020-0367-2.

[2] A. Zhecheva, W. Sha, S. Malinov, and A. Long, "Enhancing the microstructure and properties of titanium alloys through nitriding and other surface engineering methods," *Surf. Coatings Technol.*, vol. 200, no. 7, pp. 2192–2207, Dec. 2005, doi: 10.1016/J.SURFCOAT.2004.07.115.

[3] S. Saber-Samandari and C. C. Berndt, "IFTHSE Global 21: Heat treatment and surface engineering in the twenty-first century: Part 10 - Thermal spray coatings: A technology review," *Int. Heat Treat. Surf. Eng.*, vol. 4, no. 1, pp. 7–13, Mar. 2010, doi: 10.1179/174951410X12572442577381.

[4] A. Ralls, P. Kumar, M. Misra, and P. L. Menezes, "Material Design and Surface Engineering for Bio-implants," *JOM*, vol. 72, no. 2, pp. 684–696, Feb. 2020, doi: 10.1007/S11837-019-03687-2/FIGURES/5.

[5] A. Dhanola and H. C. Garg, "Tribological challenges and advancements in wind turbine bearings: A review," *Eng. Fail. Anal.*, vol. 118, no. September, p. 104885, 2020, doi: 10.1016/j.engfailanal.2020.104885.

[6] B. Mao, A. Siddaiah, Y. Liao, and P. L. Menezes, "Laser surface texturing and related techniques for enhancing tribological performance of engineering materials: A review," *J. Manuf. Process.*, vol. 53, no. December 2019, pp. 153–173, 2020, doi: 10.1016/j.jmapro.2020.02.009.

[7] H. J. Spies, "Surface engineering of aluminium and titanium alloys: An overview," *Surf. Eng.*, vol. 26, no. 1–2, pp. 126–134, Feb. 2010, doi: 10.1179/174329409X451146.

[8] W. Zhai *et al.*, "Recent Progress on Wear-Resistant Materials: Designs, Properties, and Applications," *Adv. Sci.*, vol. 8, no. 11, pp. 1–29, 2021, doi: 10.1002/advs.202003739.

[9] M. Morra *et al.*, "Surface engineering of titanium by collagen immobilization. Surface characterization and in vitro and in vivo studies," *Biomaterials*, vol. 24, no. 25, pp. 4639–4654, Nov. 2003, doi: 10.1016/S0142-9612(03)00360-0.

[10] C. Muratore, J. J. Hu, and A. A. Voevodin, "Tribological coatings for lubrication over multiple thermal cycles," *Surf. Coatings Technol.*, vol. 203, no. 8, pp. 957–962, Jan. 2009, doi: 10.1016/j.surfcoat.2008.08.073.

[11] M. Abbas and M. Shafiee, "An overview of maintenance management strategies for corroded steel structures in extreme marine environments," *Marine Structures*, vol. 71. Elsevier, p. 102718, May 01, 2020. doi: 10.1016/j.marstruc.2020.102718.

[12] P. Sundberg and M. Karppinen, “Organic and inorganic-organic thin film structures by molecular layer deposition: A review,” *Beilstein Journal of Nanotechnology*, vol. 5, no. 1. Beilstein-Institut, pp. 1104–1136, Jul. 22, 2014. doi: 10.3762/bjnano.5.123.

[13] C. Vinoth Kumar, G. Rajyalakshmi, and J. Kartha, “Insights on Anti-corrosion Coating of Magnesium Alloy: A Review,” *J. Bio- Tribo-Corrosion 2022 91*, vol. 9, no. 1, pp. 1–21, Nov. 2022, doi: 10.1007/S40735-022-00732-7.

[14] D. K. Devarajan, B. Rangasamy, and K. K. Amirtharaj Mosas, “State-of-the-Art Developments in Advanced Hard Ceramic Coatings Using PVD Techniques for High-Temperature Tribological Applications,” *Ceramics*, vol. 6, no. 1, pp. 301–329, 2023, doi: 10.3390/ceramics6010019.

[15] G. Karadimas and K. Salonitis, “Ceramic Matrix Composites for Aero Engine Applications—A Review,” *Appl. Sci. 2023, Vol. 13, Page 3017*, vol. 13, no. 5, p. 3017, Feb. 2023, doi: 10.3390/APP13053017.

[16] A. Lynam, A. R. Romero, F. Xu, R. W. Wellman, and T. Hussain, “Thermal Spraying of Ultra-High Temperature Ceramics: A Review on Processing Routes and Performance,” *J. Therm. Spray Technol. 2022 314*, vol. 31, no. 4, pp. 745–779, Apr. 2022, doi: 10.1007/S11666-022-01381-5.

[17] E. N. Kablov and S. A. Muboyadzhyan, “Heat-resistant coatings for the high-pressure turbine blades of promising GTEs,” *Russ. Metall.*, vol. 2012, no. 1, pp. 1–7, Jan. 2012, doi: 10.1134/S0036029512010089/METRICS.

[18] K. N. Lee, D. S. Fox, and N. P. Bansal, “Rare earth silicate environmental barrier coatings for SiC/SiC composites and Si3N4 ceramics,” *J. Eur. Ceram. Soc.*, vol. 25, no. 10, pp. 1705–1715, Jan. 2005, doi: 10.1016/J.JEURCERAMSOC.2004.12.013.

[19] S. A. Galedari, A. Mahdavi, F. Azarmi, Y. Huang, and A. McDonald, “A Comprehensive Review of Corrosion Resistance of Thermally-Sprayed and Thermally-Diffused Protective Coatings on Steel Structures,” *J. Therm. Spray Technol. 2019 284*, vol. 28, no. 4, pp. 645–677, Mar. 2019, doi: 10.1007/S11666-019-00855-3.

[20] H. Herman and S. Sampath, “Thermal spray coatings,” *Metall. Ceram. Prot. Coatings*, pp. 261–289, 1996, doi: 10.1007/978-94-009-1501-5_10.

[21] P. Fauchais, “Current status and future directions of thermal spray coatings and techniques,” *Futur. Dev. Therm. Spray Coatings Types, Des. Manuf. Appl.*, pp. 17–49, Jan. 2015, doi: 10.1016/B978-0-85709-769-9.00002-6.

[22] A. A. Abubakar, A. F. M. Arif, K. S. Al-Athel, S. S. Akhtar, and J. Mostaghimi, “Modeling Residual Stress Development in Thermal Spray Coatings: Current Status and Way Forward,” *J. Therm. Spray Technol. 2017 266*, vol. 26, no. 6, pp. 1115–1145, Jul. 2017, doi: 10.1007/S11666-017-0590-1.

[23] A. N. Lombardi, L. C. Casteletti, and G. E. Totten, “Thermal Spray Technologies: An Overview,” *Encycl. Tribol.*, pp. 3607–3617, 2013, doi: 10.1007/978-0-387-92897-5_684.

[24] S. Amin, H. Panchal, and A. Professor, “A Review on Thermal Spray Coating Processes,” *Int. J. Curr. Trends Eng. Res. Sci. J. Impact Factor*, vol. 2, no. 4, pp. 556–563, 2016, [Online]. Available: http://www.ijcter.com

[25] D. Kumar, Q. Murtaza, and P. Singh, “Comparative Investigation on Thermally Sprayed Al2O3, Al2O3-13%(TiO2) and Al2O3-40%(TiO2) Composite Coatings from Room to 400 °C Temperature,” 2021, [Online]. Available: https://doi.org/10.21203/rs.3.rs-566802/v1

[26] G. Sundararajan, D. S. Rao, G. Sivakumar, and S. V. Joshi, “Detonation Spray Coatings,” *Encycl. Tribol.*, pp. 736–742, 2013, doi: 10.1007/978-0-387-92897-5_704.

[27] L. Wang, L. Zhang, Q. Huang, C. Zhang, and L. Zhang, “Characteristics and Thermal Shock Resistance of HVOF-Sprayed TiAlNb Coatings,” *J. Therm. Spray Technol.*, vol. 29, no. 7, pp. 1752–1762, Oct. 2020, doi: 10.1007/S11666-020-01061-2/FIGURES/12.

[28] A. Vardelle, C. Moreau, N. J. Themelis, and C. Chazelas, “A Perspective on Plasma Spray Technology,” *Plasma Chem. Plasma Process.*, vol. 35, no. 3, pp. 491–509, Apr. 2015, doi: 10.1007/S11090-014-9600-Y/FIGURES/7.

[29] Z. Zhang *et al.*, “Plasma spray of Ti2AlC MAX phase powders: Effects of process parameters on coatings’ properties,” *Surf. Coatings Technol.*, vol. 325, pp. 429–436, Sep. 2017, doi: 10.1016/J.SURFCOAT.2017.07.006.

[30] S. Kumar and K. Panneerselvam, “Two-body Abrasive Wear Behavior of Nylon 6 and Glass Fiber Reinforced (GFR) Nylon 6 Composite,” *Procedia Technol.*, vol. 25, pp. 1129–1136, Jan. 2016, doi: 10.1016/J.PROTCY.2016.08.228.

[31] J. T. Terwey, M. A. Fourati, F. Pape, and G. Poll, “Energy-Based Modelling of Adhesive Wear in the Mixed Lubrication Regime,” *Lubr. 2020, Vol. 8, Page 16*, vol. 8, no. 2, p. 16, Feb. 2020, doi: 10.3390/LUBRICANTS8020016.

[32] V. Shibe and V. Chawla, “A Review of Surface Modification Techniques in Enhancing the Erosion Resistance of Engineering Components,” *Int. J. Res. Mech. Eng. Technol.*, vol. 4, no. 2, pp. 2249–5762, 2014, [Online]. Available: https://www.researchgate.net/publication/319207272

[33] M. Lin *et al.*, “Surface characteristics underpinning fretting wear performance of heavily loaded duplex chameleon/PEO coatings on Al,” *Tribol. Int.*, vol. 154, p. 106723, Feb. 2021, doi: 10.1016/J.TRIBOINT.2020.106723.

[34] A. Tsujimoto *et al.*, “Wear of resin composites: Current insights into underlying

mechanisms, evaluation methods and influential factors," *Jpn. Dent. Sci. Rev.*, vol. 54, no. 2, pp. 76–87, May 2018, doi: 10.1016/J.JDSR.2017.11.002.

[35] W. Chi, S. Sampath, and H. Wang, "Ambient and high-temperature thermal conductivity of thermal sprayed coatings," *Proc. Int. Therm. Spray Conf.*, vol. 15, no. 4, pp. 773–778, 2006, doi: 10.1361/105996306X146730/METRICS.

[36] Y. Huang *et al.*, "Effect of different types of pores on thermal conductivity of YSZ thermal barrier coatings," *Coatings*, vol. 9, no. 2, pp. 1–10, 2019, doi: 10.3390/COATINGS9020138.

[37] S. Wee *et al.*, "Review on mechanical thermal properties of superalloys and thermal barrier coating used in gas turbines," *Appl. Sci.*, vol. 10, no. 16, 2020, doi: 10.3390/APP10165476.

[38] M. Zielińska, M. Yavorska, M. Poreba, and J. Sieniawski, "Thermal properties of cast nickel based superalloys," *Arch. Mater. Sci. Eng.*, vol. 44, no. 1, pp. 35–38, 2010.

[39] N. Burger, A. Laachachi, M. Ferriol, M. Lutz, V. Toniazzo, and D. Ruch, "Review of thermal conductivity in composites: Mechanisms, parameters and theory," *Prog. Polym. Sci.*, vol. 61, pp. 1–28, 2016, doi: 10.1016/j.progpolymsci.2016.05.001.

[40] Y. Guo, K. Ruan, G. Wang, and J. Gu, "Advances and mechanisms in polymer composites toward thermal conduction and electromagnetic wave absorption," *Sci. Bull.*, vol. 68, no. 11, pp. 1195–1212, 2023, doi: 10.1016/j.scib.2023.04.036.

[41] L. T. Popoola, A. S. Grema, G. K. Latinwo, B. Gutti, and A. S. Balogun, "Corrosion problems during oil and gas production and its mitigation," *Int. J. Ind. Chem.*, vol. 4, no. 1, pp. 1–15, Dec. 2013, doi: 10.1186/2228-5547-4-35/FIGURES/20.

[42] X. Yang, M. Liu, Z. Liu, C. Du, and X. Li, "Failure analysis of a 304 stainless steel heat exchanger in liquid sulfur recovery units," *Eng. Fail. Anal.*, vol. 116, no. January, p. 104729, 2020, doi: 10.1016/j.engfailanal.2020.104729.

[43] M. H. Wood, A. V. Arellano, L. Van Wijk, and 26331.Wood European Commission Joint Research Centre, report no. EUR, *Corrosion-Related Accidents in Petroleum Refineries: Lessons learned from accidents in EU and OECD countries*. 2013. doi: 10.2788/379.

[44] A. H. Al-Moubaraki and I. B. Obot, "Corrosion challenges in petroleum refinery operations: Sources, mechanisms, mitigation, and future outlook," *J. Saudi Chem. Soc.*, vol. 25, no. 12, p. 101370, 2021, doi: 10.1016/j.jscs.2021.101370.

[45] A. Kadhim, A. A. Al-Amiery, R. Alazawi, M. K. S. Al-Ghezi, and R. H. Abass, "Corrosion inhibitors. A review," *Int. J. Corros. Scale Inhib.*, vol. 10, no. 1, pp. 54–67, 2021, doi: 10.17675/2305-6894-2021-10-1-3.

[46] G. S. Frankel, “Fundamentals of corrosion kinetics,” *Springer Ser. Mater. Sci.*, vol. 233, p. 17, May 2016, doi: 10.1007/978-94-017-7540-3_2/COVER.

[47] Joseph R. Davis, *Corrosion: Understanding the Basics - Google Books*. 2000. Accessed: Jun. 23, 2023. [Online]. Available: https://books.google.co.in/books?hl=en&lr=&id=D0nAMorpSIYC&oi=fnd&pg=PR1&dq=TYPES+OF+CORROSION+ASM&ots=yhyHnd7u_e&sig=OMzl_0r997vt5Sih8Bu8z9NSRjs#v=onepage&q=TYPES OF CORROSION ASM&f=false

[48] D. H. Xia *et al.*, “Electrochemical measurements used for assessment of corrosion and protection of metallic materials in the field: A critical review,” *J. Mater. Sci. Technol.*, vol. 112, pp. 151–183, 2022, doi: 10.1016/j.jmst.2021.11.004.

[49] C. U. Hardwicke and Y. C. Lau, “Advances in thermal spray coatings for gas turbines and energy generation: A review,” *J. Therm. Spray Technol.*, vol. 22, no. 5, pp. 564–576, Jun. 2013, doi: 10.1007/S11666-013-9904-0/FIGURES/11.

[50] R. R. Boyer, J. D. Cotton, M. Mohaghegh, and R. E. Schafrik, “Materials considerations for aerospace applications,” *MRS Bull.*, vol. 40, no. 12, pp. 1055–1065, 2015, doi: 10.1557/mrs.2015.278.

[51] P. Sengupta and I. Manna, “Advanced High-Temperature Structural Materials in Petrochemical, Metallurgical, Power, and Aerospace Sectors—An Overview,” *Futur. Landsc. Struct. Mater. India*, pp. 79–131, 2022, doi: 10.1007/978-981-16-8523-1_5/COVER.

[52] J. A. Ali, A. M. Kalhury, A. N. Sabir, R. N. Ahmed, N. H. Ali, and A. D. Abdullah, “A state-of-the-art review of the application of nanotechnology in the oil and gas industry with a focus on drilling engineering,” *J. Pet. Sci. Eng.*, vol. 191, p. 107118, Aug. 2020, doi: 10.1016/J.PETROL.2020.107118.

[53] Z. Wang, S. Shuai, Z. Li, and W. Yu, “A Review of Energy Loss Reduction Technologies for Internal Combustion Engines to Improve Brake Thermal Efficiency,” *Energies 2021, Vol. 14, Page 6656*, vol. 14, no. 20, p. 6656, Oct. 2021, doi: 10.3390/EN14206656.

[54] S. C. Vlădescu *et al.*, “Exploiting the Synergy between Concentrated Polymer Brushes and Laser Surface Texturing to Achieve Durable Superlubricity,” *ACS Appl. Mater. Interfaces*, vol. 14, no. 13, pp. 15818–15829, 2022, doi: 10.1021/acsami.2c00725.

[55] S. Singh, C. C. Berndt, R. K. Singh Raman, H. Singh, and A. S. M. Ang, “Applications and Developments of Thermal Spray Coatings for the Iron and Steel Industry,” *Materials (Basel).*, vol. 16, no. 2, pp. 1–27, 2023, doi: 10.3390/ma16020516.

[56] M. Chinnasamy, R. Rathanasamy, S. K. Pal, and S. K. Palaniappan, “Effectiveness of cryogenic treatment on cutting tool inserts: A review,” *Int. J. Refract. Met. Hard*

Mater., vol. 108, no. April, p. 105946, 2022, doi: 10.1016/j.ijrmhm.2022.105946.

[57] K. Friedrich, "Polymer composites for tribological applications," *Adv. Ind. Eng. Polym. Res.*, vol. 1, no. 1, pp. 3–39, Oct. 2018, doi: 10.1016/J.AIEPR.2018.05.001.

[58] C. I. Idumah, C. M. Obele, E. O. Emmanuel, and A. Hassan, "Recently Emerging Nanotechnological Advancements in Polymer Nanocomposite Coatings for Anti-corrosion, Anti-fouling and Self-healing," *Surfaces and Interfaces*, vol. 21, p. 100734, Dec. 2020, doi: 10.1016/J.SURFIN.2020.100734.

[59] Y. Bai, H. Zhang, Y. Shao, H. Zhang, and J. Zhu, "Recent Progresses of Superhydrophobic Coatings in Different Application Fields: An Overview," *Coatings 2021, Vol. 11, Page 116*, vol. 11, no. 2, p. 116, Jan. 2021, doi: 10.3390/COATINGS11020116.

[60] V. P. Singh, A. Sil, and R. Jayaganthan, "A study on sliding and erosive wear behaviour of atmospheric plasma sprayed conventional and nanostructured alumina coatings," *Mater. Des.*, vol. 32, no. 2, pp. 584–591, Feb. 2011, doi: 10.1016/J.MATDES.2010.08.019.

[61] K. A. Habib, J. J. Saura, C. Ferrer, M. S. Damra, E. Giménez, and L. Cabedo, "Comparison of flame sprayed Al2O3/TiO2 coatings: Their microstructure, mechanical properties and tribology behavior," *Surf. Coatings Technol.*, vol. 201, no. 3–4, pp. 1436–1443, 2006, doi: 10.1016/j.surfcoat.2006.02.011.

[62] G. Di Girolamo, A. Brentari, C. Blasi, and E. Serra, "Microstructure and mechanical properties of plasma sprayed alumina-based coatings," *Ceram. Int.*, vol. 40, no. 8, pp. 12861–12867, Sep. 2014, doi: 10.1016/J.CERAMINT.2014.04.143.

[63] S. T. Aruna, N. Balaji, J. Shedthi, and V. K. W. Grips, "Effect of critical plasma spray parameters on the microstructure, microhardness and wear and corrosion resistance of plasma sprayed alumina coatings," *Surf. Coatings Technol.*, vol. 208, pp. 92–100, 2012, doi: 10.1016/j.surfcoat.2012.08.016.

[64] H. S. Grewal, H. Singh, and A. Agrawal, "Microstructural and mechanical characterization of thermal sprayed nickel–alumina composite coatings," *Surf. Coatings Technol.*, vol. 216, pp. 78–92, Feb. 2013, doi: 10.1016/J.SURFCOAT.2012.11.029.

[65] J. Rauch, G. Bolelli, A. Killinger, R. Gadow, V. Cannillo, and L. Lusvarghi, "Advances in High Velocity Suspension Flame Spraying (HVSFS)," *Surf. Coatings Technol.*, vol. 203, no. 15, pp. 2131–2138, 2009, doi: 10.1016/j.surfcoat.2008.12.002.

[66] G. Bolelli *et al.*, "Wear behaviour of high velocity suspension flame sprayed (HVSFS) Al2O3 coatings produced using micron- and nano-sized powder suspensions," *Surf. Coatings Technol.*, vol. 204, no. 16–17, pp. 2657–2668, 2010, doi:

10.1016/j.surfcoat.2010.02.018.

[67] G. Bolelli *et al.*, “Properties of Al2O3 coatings by High Velocity Suspension Flame Spraying (HVSFS): Effects of injection systems and torch design,” *Surf. Coatings Technol.*, vol. 270, pp. 175–189, 2015, doi: 10.1016/j.surfcoat.2015.03.005.

[68] J. W. Murray, A. S. M. Ang, Z. Pala, E. C. Shaw, and T. Hussain, “Suspension High Velocity Oxy-Fuel (SHVOF)-Sprayed Alumina Coatings: Microstructure, Nanoindentation and Wear,” *J. Therm. Spray Technol.*, vol. 25, no. 8, pp. 1700–1710, 2016, doi: 10.1007/s11666-016-0462-0.

[69] J. A. Wahab *et al.*, “Effects of micro-grooves on tribological behaviour of plasma-sprayed alumina-13%titania coatings,” *Ceram. Int.*, vol. 43, no. 8, pp. 6410–6416, 2017, doi: 10.1016/j.ceramint.2017.02.052.

[70] Z. Zou, Y. Wang, F. Zhou, L. Wang, S. Liu, and Y. Wang, “Tribological property of plasma-sprayed Al 2 O 3 -13wt%TiO 2 coatings onto resin-based composites,” *Appl. Surf. Sci.*, vol. 431, pp. 75–80, 2018, doi: 10.1016/j.apsusc.2017.05.239.

[71] S. Mehar, S. G. Sapate, N. Vashishtha, and P. Bagde, “Effect of Y2O3 addition on tribological properties of plasma sprayed Al2O3-13% TiO2 coating,” *Ceram. Int.*, vol. 46, no. 8, pp. 11799–11810, 2020, doi: 10.1016/j.ceramint.2020.01.214.

[72] A. A. Abdel-Samad, A. M. M. El-Bahloul, E. Lugscheider, and S. A. Rassoul, “Comparative study on thermally sprayed alumina based ceramic coatings,” *J. Mater. Sci.*, vol. 35, no. 12, pp. 3127–3130, 2000, doi: 10.1023/A:1004824104162.

[73] A. Rico, P. Poza, and J. Rodríguez, “High temperature tribological behavior of nanostructured and conventional plasma sprayed alumina-titania coatings,” *Vacuum*, vol. 88, no. 1, pp. 149–154, 2013, doi: 10.1016/j.vacuum.2012.01.008.

[74] X. Lin, Y. Zeng, C. Ding, and P. Zhang, “Effects of temperature on tribological properties of nanostructured and conventional Al2O3-3 wt.% TiO2 coatings,” *Wear*, vol. 256, no. 11–12, pp. 1018–1025, 2004, doi: 10.1016/S0043-1648(03)00541-6.

[75] X. Shen, X. Nie, H. Hu, and J. Tjong, “Effects of coating thickness on thermal conductivities of alumina coatings and alumina/aluminum hybrid materials prepared using plasma electrolytic oxidation,” *Surf. Coatings Technol.*, vol. 207, pp. 96–101, Aug. 2012, doi: 10.1016/J.SURFCOAT.2012.06.009.

[76] A. Ganvir *et al.*, “Influence of Microstructure on Thermal Properties of Axial Suspension Plasma-Sprayed YSZ Thermal Barrier Coatings,” *J. Therm. Spray Technol.*, vol. 25, no. 1–2, pp. 202–212, Jan. 2016, doi: 10.1007/S11666-015-0355-7/FIGURES/12.

[77] Z. Wang, A. Kulkarni, S. Deshpande, T. Nakamura, and H. Herman, “Effects of pores

and interfaces on effective properties of plasma sprayed zirconia coatings," *Acta Mater.*, vol. 51, no. 18, pp. 5319–5334, Oct. 2003, doi: 10.1016/S1359-6454(03)00390-2.

[78] F. Cernuschi, S. Ahmaniemi, P. Vuoristo, and T. Mäntylä, "Modelling of thermal conductivity of porous materials: application to thick thermal barrier coatings," *J. Eur. Ceram. Soc.*, vol. 24, no. 9, pp. 2657–2667, Aug. 2004, doi: 10.1016/J.JEURCERAMSOC.2003.09.012.

[79] Y. Wang, H. Liu, X. Ling, and Y. Weng, "Effects of pore microstructure on the effective thermal conductivity of thermal barrier coatings," *Appl. Therm. Eng.*, vol. 102, pp. 234–242, Jun. 2016, doi: 10.1016/J.APPLTHERMALENG.2016.03.174.

[80] J. R. Nicholls, K. J. Lawson, A. Johnstone, and D. S. Rickerby, "Methods to reduce the thermal conductivity of EB-PVD TBCs," *Surf. Coatings Technol.*, vol. 151–152, pp. 383–391, Mar. 2002, doi: 10.1016/S0257-8972(01)01651-6.

[81] S. Raghavan, H. Wang, R. B. Dinwiddie, W. D. Porter, and M. J. Mayo, "The effect of grain size, porosity and yttria content on the thermal conductivity of nanocrystalline zirconia," *Scr. Mater.*, vol. 39, no. 8, pp. 1119–1125, Sep. 1998, doi: 10.1016/S1359-6462(98)00290-5.

[82] N. Markocsan, P. Nylén, J. Wigren, X. H. Li, and A. Tricoire, "Effect of thermal aging on microstructure and functional properties of zirconia-base thermal barrier coatings," *J. Therm. Spray Technol.*, vol. 18, no. 2, pp. 201–208, Mar. 2009, doi: 10.1007/S11666-009-9313-6/FIGURES/10.

[83] Y. Huang *et al.*, "Effect of Different Types of Pores on Thermal Conductivity of YSZ Thermal Barrier Coatings," *Coatings 2019, Vol. 9, Page 138*, vol. 9, no. 2, p. 138, Feb. 2019, doi: 10.3390/COATINGS9020138.

[84] N. Chen *et al.*, "Quantitative Analysis of the Relationship Between Microstructures and Thermal Conductivity for YSZ Coatings," *J. Therm. Spray Technol.*, vol. 26, no. 4, pp. 745–754, Apr. 2017, doi: 10.1007/S11666-017-0542-9/TABLES/5.

[85] K. S. Ravichandran, K. An, R. E. Dutton, and S. L. Semiatin, "Thermal Conductivity of Plasma-Sprayed Monolithic and Multilayer Coatings of Alumina and Yttria-Stabilized Zirconia," *J. Am. Ceram. Soc.*, vol. 82, no. 3, pp. 673–682, Mar. 1999, doi: 10.1111/J.1151-2916.1999.TB01816.X.

[86] F. Cernuschi *et al.*, "Microstructural characterization of porous thermal barrier coatings by IR gas porosimetry and sintering forecasts," *Acta Mater.*, vol. 61, no. 1, pp. 248–262, Jan. 2013, doi: 10.1016/J.ACTAMAT.2012.09.055.

[87] I. Sevostianov and M. Kachanov, "Plasma-sprayed ceramic coatings: anisotropic elastic and conductive properties in relation to the microstructure; cross-property

correlations," *Mater. Sci. Eng. A*, vol. 297, no. 1–2, pp. 235–243, Jan. 2001, doi: 10.1016/S0921-5093(00)01022-4.

[88] A. K. Rivai and M. Takahashi, "Compatibility of surface-coated steels, refractory metals and ceramics to high temperature lead–bismuth eutectic," *Prog. Nucl. Energy*, vol. 50, no. 2–6, pp. 560–566, Mar. 2008, doi: 10.1016/J.PNUCENE.2007.11.081.

[89] E. Celik, I. Ozdemir, E. Avci, and Y. Tsunekawa, "Corrosion behaviour of plasma sprayed coatings," *Surf. Coatings Technol.*, vol. 193, no. 1–3, pp. 297–302, Apr. 2005, doi: 10.1016/J.SURFCOAT.2004.08.143.

[90] A. U. Ammar, M. Shahid, M. K. Ahmed, M. Khan, A. Khalid, and Z. A. Khan, "Electrochemical Study of Polymer and Ceramic-Based Nanocomposite Coatings for Corrosion Protection of Cast Iron Pipeline," *Mater. 2018, Vol. 11, Page 332*, vol. 11, no. 3, p. 332, Feb. 2018, doi: 10.3390/MA11030332.

[91] V. A. Andrei *et al.*, "Aluminum Oxide Ceramic Coatings on 316l Austenitic Steel Obtained by Plasma Electrolysis Oxidation Using a Pulsed Unipolar Power Supply," *Coatings 2020, Vol. 10, Page 318*, vol. 10, no. 4, p. 318, Mar. 2020, doi: 10.3390/COATINGS10040318.

[92] P. Deepa and R. Padmalatha, "Corrosion behaviour of 6063 aluminium alloy in acidic and in alkaline media," *Arab. J. Chem.*, vol. 10, pp. S2234–S2244, May 2017, doi: 10.1016/J.ARABJC.2013.07.059.

[93] G. X. Shen, Y. C. Chen, and C. J. Lin, "Corrosion protection of 316 L stainless steel by a TiO2 nanoparticle coating prepared by sol–gel method," *Thin Solid Films*, vol. 489, no. 1–2, pp. 130–136, Oct. 2005, doi: 10.1016/J.TSF.2005.05.016.

[94] H. Vasudev, L. Thakur, H. Singh, and A. Bansal, "A study on processing and hot corrosion behaviour of HVOF sprayed Inconel718-nano Al2O3 coatings," *Mater. Today Commun.*, vol. 25, p. 101626, Dec. 2020, doi: 10.1016/J.MTCOMM.2020.101626.

[95] Z. Wei, S. Hong, Z. Wei, N. Hu, G. Ying, and Y. Wu, "Comparison on long-term corrosion performance of WC-CoCr and Al2O3-TiO2 ceramic coatings in sulphide-containing 3.5 wt% NaCl solution," *Int. J. Refract. Met. Hard Mater.*, vol. 107, p. 105906, Sep. 2022, doi: 10.1016/J.IJRMHM.2022.105906.

[96] K. Holmberg and A. Mathews, "Coatings tribology: a concept, critical aspects and future directions," *Thin Solid Films*, vol. 253, no. 1–2, pp. 173–178, 1994, doi: 10.1016/0040-6090(94)90315-8.

[97] D. Kumar, S. M. Pandey, Q. Murtaza, P. Singh, and R. S. Walia, "Tribological Analysis of Increasing Percentage of CrC Content in Composite Coating by Atmospheric Plasma Spray Technique," pp. 99–113, 2021, doi: 10.1007/978-981-15-4550-4_6.

[98] S. K. Singh, S. Chattopadhyaya, A. Pramanik, S. Kumar, and A. K. Basak, “Tribological behaviour of chromium nitride coating,” *Int. J. Appl. Eng. Res.*, vol. 13, no. 6, pp. 23–25, 2018, [Online]. Available: http://www.ripublication.com

[99] J. Rong, K. Yang, H. Zhao, C. Liu, Y. Zhuang, and S. Tao, “Tribological performance of plasma sprayed Al2O3–Y2O3 composite coatings,” *Surf. Coatings Technol.*, vol. 302, pp. 487–494, 2016, doi: 10.1016/j.surfcoat.2016.06.053.

[100] T. Senda, J. Drennan, and R. McPherson, “Sliding Wear of Oxide Ceramics at Elevated Temperatures,” *Journal of the American Ceramic Society*, vol. 78, no. 11. pp. 3018–3024, 1995. doi: 10.1111/j.1151-2916.1995.tb09077.x.

[101] T. Senda, E. Yasuda, M. Kaji, and R. C. Bradt, “Effect of grain size on the sliding wear and friction of alumina at elevated temperatures,” *J. Am. Ceram. Soc.*, vol. 82, no. 6, pp. 1505–1511, 1999, doi: 10.1111/j.1151-2916.1999.tb01948.x.

[102] X. H. Cui, Y. S. Mao, M. X. Wei, and S. Q. Wang, “Wear Characteristics of Ti-6Al-4V Alloy at 20-400°C,” *Tribol. Trans.*, vol. 55, no. 2, pp. 185–190, 2012, doi: 10.1080/10402004.2011.647387.

[103] A. R. Riahi and A. T. Alpas, “The role of tribo-layers on the sliding wear behavior of graphitic aluminum matrix composites,” *Wear*, vol. 250–251, no. PART 2, pp. 1396–1407, 2001, doi: 10.1016/s0043-1648(01)00796-7.

[104] Ł. Leszek, M. Michalak, and M. Walczak, “Influence of 13 wt % TiO2 content in alumina-titania powders on microstructure , sliding wear and cavitation erosion resistance of APS sprayed coatings Surface & Coatings Technology Influence of 13 wt % TiO 2 content in alumina-titania powders on microstr,” no. February, 2021, doi: 10.1016/j.surfcoat.2021.126979.

[105] M. Szala, L. Łatka, M. Awtoniuk, M. Winnicki, and M. Michalak, “Neural modelling of aps thermal spray process parameters for optimizing the hardness, porosity and cavitation erosion resistance of al2o3-13 wt% tio2 coatings,” *Processes*, vol. 8, no. 12, pp. 1–15, 2020, doi: 10.3390/pr8121544.

[106] R. Heise and V. L. Popov, “Adhesive contribution to the coefficient of friction between rough surfaces,” *Tribol. Lett.*, vol. 39, no. 3, pp. 247–250, Sep. 2010, doi: 10.1007/S11249-010-9617-1/FIGURES/3.

[107] A. Ravikiran, V. S. Nagarajan, S. K. Biswas, and B. N. P. Bai, “Effect of Speed and Pressure on Dry Sliding Interactions of Alumina against Steel,” *J. Am. Ceram. Soc.*, vol. 78, no. 2, pp. 356–364, 1995, doi: 10.1111/j.1151-2916.1995.tb08808.x.

[108] P. Andersson and A. Blomberg, “Alumina in unlubricated sliding point, line and plane contacts,” *Wear*, vol. 170, no. 2, pp. 191–198, 1993, doi: 10.1016/0043-1648(93)90240-M.

[109] O. P. Oladijo, A. P. I. Popoola, M. Booi, J. Fayomi, and L. L. Collieus, “Corrosion and mechanical behaviour Of Al2o3.Tio2 composites produced by spark plasma sintering,” *South African J. Chem. Eng.*, vol. 33, no. May, pp. 58–66, 2020, doi: 10.1016/j.sajce.2020.05.001.

[110] L. Lu, Z. Ma, F. C. Wang, and Y. B. Liu, “Friction and wear behaviors of Al2O3-13 wt%TiO 2 coatings,” *Rare Met.*, vol. 32, no. 1, pp. 87–92, 2013, doi: 10.1007/s12598-013-0008-2.

[111] P. V. Deshpande *et al.*, “Lubricated sliding wear behaviour of Al2O3-13TiO 2 coatings,” *Surf. Eng.*, vol. 29, no. 6, pp. 447–454, 2013, doi: 10.1179/1743294413Y.0000000135.

[112] M. Öge, Y. Kucuk, M. S. Gok, and A. C. Karaoglanli, “Comparison of dry sliding wear behavior of plasma sprayed FeCr slag coating with Cr2O3 and Al2O3-13TiO2 coatings,” *Int. J. Appl. Ceram. Technol.*, vol. 16, no. 6, pp. 2283–2298, 2019, doi: 10.1111/ijac.13273.

[113] and K. C. V.V. Narulkar , S. Prakash, “Effects of Temperature on Tribological Properties of Al2 O3 -TiO2 Coating,” *Def. Sci. J.*, vol. 58, no. 4, pp. 582–587, 2008, doi: https://doi.org/10.14429/dsj.58.1680.

[114] C. Thiagarajan, M. Prabhahar, S. Prakash, J. Senthil, and M. Saravana Kumar, “Heat transfer analysis and optimization of engine cylinder liner using different materials,” *Mater. Today Proc.*, vol. 33, pp. 778–783, Jan. 2020, doi: 10.1016/J.MATPR.2020.06.173.

[115] K. Jeyajothi and P. Kalaichelvi, “Augmentation of Heat Transfer and Investigation of Fluid Flow Characteristics of an Impinging Air Jet on to a Flat Plate,” *Arab. J. Sci. Eng.*, vol. 44, no. 6, pp. 5289–5299, Jun. 2019, doi: 10.1007/S13369-018-3511-9/METRICS.

[116] H. Yao *et al.*, “Thermal transport property correlated with microstructural evolution of Fe-based amorphous alloy,” *Acta Mater.*, vol. 200, pp. 793–802, Nov. 2020, doi: 10.1016/J.ACTAMAT.2020.09.072.

[117] S. Wu, T. Yan, Z. Kuai, and W. Pan, “Thermal conductivity enhancement on phase change materials for thermal energy storage: A review,” *Energy Storage Mater.*, vol. 25, pp. 251–295, Mar. 2020, doi: 10.1016/J.ENSM.2019.10.010.

[118] A. Manap, S. Mahalingam, R. Vaithylingam, and H. Abdullah, “Mechanical, thermal and morphological properties of thermoplastic polyurethane composite reinforced by multi-walled carbon nanotube and titanium dioxide hybrid fillers,” *Polym. Bull.*, vol. 78, no. 10, pp. 5815–5832, Oct. 2021, doi: 10.1007/S00289-020-03393-Z/FIGURES/10.

[119] P. S. Saluja and G. Gupta, “Preparation and Thermal Behaviour of Polyester Composite Filled with TiO 2,” *Int. Res. J. Eng. Technol.*, vol. 4, no. 4, pp. 3135–3141, 2017, [Online]. Available: https://www.irjet.net/archives/V4/i4/IRJET-V4I4753.pdf

[120] J. F. Pagotto, F. J. Recio, A. J. Motheo, and P. Herrasti, “Multilayers of PAni/n-TiO2 and PAni on carbon steel and welded carbon steel for corrosion protection,” *Surf. Coatings Technol.*, vol. 289, pp. 23–28, Mar. 2016, doi: 10.1016/J.SURFCOAT.2016.01.046.

[121] A. Krishnan, B. Joseph, K. M. Bhaskar, M. S. Suma, and S. M. A. Shibli, “Unfolding the anticorrosive characteristics of TiO2–WO3 mixed oxide reinforced polyaniline composite coated mild steel in alkaline environment,” *Polym. Compos.*, vol. 40, no. 6, pp. 2400–2409, Jun. 2019, doi: 10.1002/PC.25103.

[122] F. Gao, J. Mu, Z. Bi, S. Wang, and Z. Li, “Recent advances of polyaniline composites in anticorrosive coatings: A review,” *Prog. Org. Coatings*, vol. 151, p. 106071, Feb. 2021, doi: 10.1016/J.PORGCOAT.2020.106071.

LIST OF PUBLICATIONS

In Journals

• **Deepak Kumar**, Qasim Murtaza, R. S. Walia, and Pushpendra Singh. "Comparative investigation on thermally sprayed Al_2O_3, Al_2O_3–13%(TiO_2) and Al_2O_3–40%(TiO_2) composite coatings from room to 400° C temperature." *Surface Topography: Metrology and Properties* 10, no. 1 (2022): 015043. *DOI 10.1088/2051-672X/ac5a75* **(SCIE, IF 2.7)**

• **Deepak Kumar**, R. S. Walia, Pushpendra Singh and Qasim Murtaza. "Tribological behaviour of thermally sprayed ceramic coating at high temperature." International Journal of Materials Research, 114, no. 9(2023). *DOI:10.1515/ijmr-2022-0318* (**SCIE, IF 0.8)**

• **Deepak Kumar**, Pushpendra Singh, Qasim Murtaza and R. S. Walia "Synergistic effect of Al_2O_3-40%TiO_2 coating on thermal conductivity and corrosion rate of SS 304 substrate" *Sadhana*, Springer 48, no. 4 (2023): 1-10. *https://doi.org/10.1007/s12046-023-02341-7* **(SCIE, IF 1.6)**

Deepak Kumar, Pushpendra Singh, R. S. Walia, and Qasim Murtaza, "Morphological and Vibration Analysis of thermally spraying Al_2O_3-40%TiO_2 Coating" *Material science and engineering* A, Elsevier (communicated)

International Conference

• "Microstructural and wear loss analysis of ceramic coating at high temperature deposited by flame spray process,", 6th International Conference on Advanced Production and Industrial Engineering, DTU, New Delhi, 18-19 June, 2021

• "Wear Analysis of Thermally Sprayed Al_2O_3-13%TiO2 Coating at High Temperature", 1st International Conference on Energy, Materials Sciences and Mechanical Engineering (EMSME - 2020), NIT Delhi, 30th October- 1st November, 2020